A Thesis for the Degree of
Doctor of Philosophy

Ultrasound Backscatter from Flowing Blood at Different Hematocrit Levels

Kweon-Ho Nam

Interdisciplinary Postgraduate Program in Biomedical Engineering
GRADUATE SCHOOL
CHEJU NATIONAL UNIVERSITY

2007. 8.

Ultrasound Backscatter from Flowing Blood at Different Hematocrit Levels

Kweon-Ho Nam
(Supervised by Professor Dong-Guk Paeng)

A thesis submitted in partial fulfillment of the requirement
for the degree of Doctor of Philosophy

2007. 8.

This thesis has been examined and approved.

Thesis director, Min Joo Choi, Prof. of Biomedical Engineering

---

Jun Hong Park, Prof. of Veterinary Medicine

Kwang-Man Lee, Prof. of Electronic Engineering

Young Ree Kim, Prof. of Laboratory Medicine

Dong-Guk Paeng, Prof. of Marine Industrial Engineering

Date

Interdisciplinary Postgraduate Program in Biomedical Engineering
GRADUATE SCHOOL
CHEJU NATIONAL UNIVERSITY

SUMMARY

It is well known that the scattering of ultrasound by blood is mainly attributed to red blood cells (RBCs) and that RBC aggregation is a major cause of the increased backscatter from blood. In this study, the effects of hemodynamics and hematocrit on ultrasonic backscatter were investigated using a mock flow loop with a stenosis and a rotational flow system.

RBC aggregation is known to be highly dependent on hemodynamic parameters such as shear rate, flow turbulence, and flow acceleration under pulsatile flow. The effects of these three hemodynamic parameters on RBC aggregation and echogenicity of porcine whole blood were investigated around an eccentric stenosis in a mock flow loop using a GE LOGIQ 700 expert system. A hyperechoic parabolic profile appeared downstream during the accelerating phase, suggesting that rouleaux formation may be enhanced by flow acceleration. The local increase of echogenicity and the hypoechoic "black hole" downstream is thought to be caused by the compound effect of flow turbulence and shear rate. In addition, the experimental results upstream of a stenosis showed that blood flow disturbed by a stenosis and weak backward flow affects the echogenicity and the distribution of RBC rouleaux. During diastole, the bright parabolic profiles and eddy-like flow patterns were shown in longitudinal images and the "bright ring" in cross-sectional images. These images could be reconstructed into 3-dimensional animation, providing a better understanding of dynamic changes of the rouleaux distribution upstream of a stenosis under pulsatile flow.

The blood samples from human, horse and rat in a cylindrical chamber were used for studying RBC aggregation. The flow in the chamber was controlled by a stirring magnet. Ultrasound backscattered power from blood was calculated from the backscattered signals measured by a 5 MHz focused transducer in a pulse-echo setup. The experimental results showed the differences in RBC aggregation tendency among the three mammalian species with an order of horse > human > rat. The ultrasound backscattered power decreased with stirring

speed in human and horse blood, but no variations were observed in rat blood. A sudden flow stoppage led to the slow increase of the backscattered power for human and horse blood. The enveloped echo images showed the radial and temporal variations of RBC aggregation in the cylindrical chamber. These observations from the different mammalian species may give a better understanding of the mechanism of RBC aggregation.

Ultrasonic backscatter from rat RBCs in autologous plasma and in 360 kDa polyvinylpyrrolidone (PVP 360) solution was measured as a function of hematocrit and shear rate. The variation of the backscattered power from rat blood could not be well determined because of the very low aggregation tendency of RBCs in rat blood. To enhance the aggregation level, rat plasma was replaced by polymer solution of PVP 360. At stirring conditions, the backscattered power rapidly increased to a plateau within 30 seconds. The magnitude of the mean backscattered power at plateau was in proportion to hematocrit at a range of 10 to 40 %. However, when the flow was suddenly stopped, the power slowly increased up to the maximal levels and the rate of power buildup nonlinearly increased with hematocrit. Using a simplified shearing system and small amount of RBC samples in aggregating media, the hematocrit and shear rate dependency of RBC aggregation was successfully demonstrated.

Finally, this simplified system was proposed to examine the effect of drugs on RBC aggregation. Rat RBCs in PVP 360 solution was employed for aggregation. Aggregation inhibitor, DIDS decreased RBC aggregation as a dose-dependent manner at both stasis and under shear forces. These results indicate that the present experimental setup is useful to study the relationship between drugs and RBC aggregation. In addition, it may contribute to elucidate the mechanism and pathophysiological roles of RBC aggregation.

Key words: Erythrocyte aggregation, Flow acceleration, Flow turbulence, Hematocrit, Shear rate, Ultrasound backscatter.

TABLE OF CONTENTS

LIST OF FIGURES

LIST OF TABLES

Chapter 1

INTRODUCTION

1.1. Background

1.1.1. RBC Aggregation

RBCs in plasma aggregate to form rouleaux and rouleaux networks under normal physiological conditions as a reversible process (Fig.1). This phenomenon continues to be of interest in the field of hemorheology since flow dynamics and flow resistance of blood are influenced by RBC aggregation. However, its pathophysiological impacts have not been fully resolved yet.

1.1.1.1. Mechanisms

The mechanisms of rouleaux formation and dissociation are very complex and not well understood. Two models have been proposed to explain the aggregation of RBCs, the bridging model and the depletion model (Rampling et al. 2004). In the bridging model, the formation of RBC aggregates results from the adsorption of plasmatic macromolecules at the surface of the RBC (Brooks et al. 1980; Chien 1981). In contrast, the depletion model suggests that RBC aggregation results from a lower localized macromolecule concentration near the cell membrane as compared with the suspending medium (Van Oss et al. 1990; Evans et al.1991). The exclusion of macromolecules near the RBC surface generates a reduction of the osmotic pressure in the gap between two nearby RBCs, creating an attractive force between them. These two models are in conflict and mutually exclusive. However, recent publications including the studies of RBC electrophoretic mobility have provided theoretical support for the depletion model (Donath et al. 1993; Armstrong et al. 1999; Baumler et al. 1996, 1999).

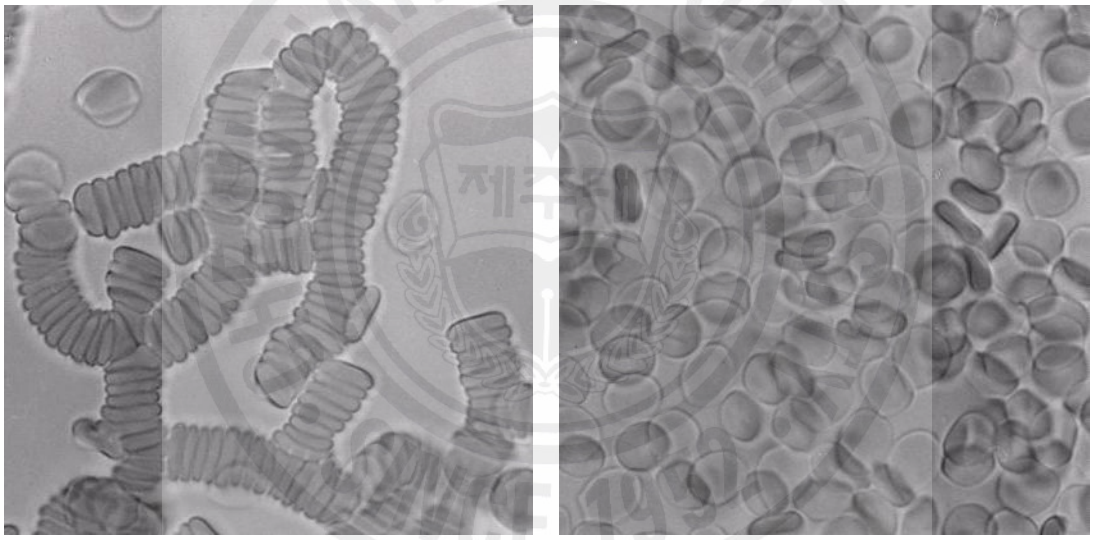

Fig. 1. Photomicrographs of human RBCs in plasma (left panel) and in saline (right panel). Magnification × 400 (Fatkin et al. 1997).

1.1.1.2. Factors

RBC aggregation does not occur if RBCs are suspended in isotonic salt solutions. Plasma proteins have been known to cause RBC aggregation (Rampling et al. 1984; Lowe 1993; Potron et al. 1994), and fibrinogen rather than globular proteins are mainly responsible for RBC aggregation. Previous studies about other macromolecules such as dextrans and some polymers have shown that the extent and rate of aggregate formation strongly depend on the type and concentration of polymers in the surrounding medium (Boynard and Leliere 1990; Nash et al. 1987; Neu and Meiselman 2002). More recent studies have shown that RBC cellular properties, such as RBC deformability, morphology, and surface charge, also play a very important role in the aggregation process (Rampling et al. 2004). The difference of cellular effects in aggregation tendency among different RBC samples can be measured in a defined polymer solution to exclude the various influences associated with autologous plasma.

The process of RBC aggregation can be considered as a result of a balance between aggregating and disaggregating forces that are affected by shear rate. Previous studies have suggested that the aggregation process involves three steps depending mainly on the shear stress, that is, the formation of short linear rouleaux which is composed of several RBCs, formation of long linear rouleaux, and the formation of complex 3-dimensional structures of branched rouleaux, whose occurrence is decreased with increasing shear stress (Shiga et al. 1983). Recent results by Paeng et al. (2004b, 2004c) suggested the possible effect of flow acceleration on the aggregation under pulsatile flow. According to the studies, it was hypothesized that blood flow acceleration is another factor that enhances the aggregation by increasing the probabilities of RBC collisions due to different inertia and compressional forces.

The non-linear relationship between hematocrit and RBC aggregation tendency has been reported in the several publications. According to those reports, it is clear that hematocrit plays an important role in RBC aggregation at a certain shear rate. However, the aggregation process

is also a function of shear rate. Since blood is a flowing substance in nature, shear rate should also be well controlled when we study the hematocrit dependency on RBC aggregation. It should be noted that the hematocrit dependency of ultrasonic backscatter from whole blood is quite different from that from RBC suspension where there is no RBC aggregate.

1.1.1.3. Differences in Mammalian Species

According to the reports on domestic fowls (Ohta et al. 1992) and frogs (Klose et al. 1972), no RBC aggregation was observed even at the lowest shear rate. These amphibian and bird have similar shape of an RBC that looks like an ellipsoid and RBCs do not have a nucleus. Such characteristics of RBCs are likely to face obstacles when they approach each other to aggregate due to their shapes and poor deformability. Therefore, it is assumed that the RBC aggregation may be a unique phenomenon that can be observed only in mammalian blood.

Windberger et al. (2003) reported that RBC aggregation was high in pig, dog, and cat and was intensively high in horse, whereas RBC aggregation in rat, cattle, sheep, rabbit, and mouse was low or underdetectable. RBC aggregation levels in pig, horse, sheep, and calf blood samples were also investigated and compared with that of normal human blood (Weng et al. 1996b). In that study, the adhesive forces and the index of structure of the aggregates in pig blood were close to those of human blood. The results for horse blood showed a very high level of aggregation kinetics and adhesive forces between RBCs. For sheep and calf blood, little RBC aggregation was found. They also showed that different human RBC aggregation levels could be simulated by diluting the concentration of plasma proteins in equine and porcine blood.

Comparative analyses of RBC membrane lipids have revealed species-specific differences in phospholipid composition (Roelofsen et al. 1981). The sodium dodecyl sulfate-polyacrylamide gel electrophoresis (SDS-PAGE) analysis of membrane proteins from horse, human, and rat RBC implies that significant differences may exist in the structure of

carbohydrate-rich proteins that are the main carriers of RBC negative surface charge (Baskurt et al. 1997). The two-phase partition coefficient for these three mammals suggested a difference in membrane surface charge with an order of rat > human > horse. Fibrinogen is known to be the major RBC aggregating factors in human. However, in other mammals, the fibrinogen concentrations are not always well correlated with the degree of RBC aggregation (Schneck 1988; Johnn et al. 1992; Ohta et al. 1992). Species differences might exist in the molecular weights of fibrinogen and other macromolecules which are important for RBC aggregation (Andrews et al. 1992). Variations in the RBC volume ratio, cell diameter, and mean corpuscular volume of mammalian species were reported. These variations may also cause differences in RBC aggregation among species. Popel et al. (1994) related the degree of aggregation in difference mammals to their exercise capacity, which showed that the athletic animals exhibited a higher tendency of RBC aggregation than the sedentary animals.

1.1.2. Scattering of Ultrasound by Blood

RBCs are the dominant ultrasonic scatterers in blood, because they constitute a great portion of the cellular components of blood. The dimension of RBC is much smaller than the ultrasonic wavelength for frequency ranges of most diagnostic imaging devices, so that an RBC can be considered as a Rayleigh scatterer. Since the acoustic mismatch between plasma and RBCs is very small, the Born approximation can be applied (Lucas and Twersky 1987; Shung and Thieme 1993). Then the backscattering cross section of a single RBC is given by

$$\sigma_{bs} = \frac{\pi^2 V_e^2}{\lambda^4}\left[\frac{\kappa_e - \kappa_0}{\kappa_0} - \frac{\rho_e - \rho_0}{\rho_e}\right]^2$$

where the V_e is the volume of a RBC, λ is the transmitted acoustic wavelength, κ is the

compressibility, ρ is the density, and the subscripts of e and 0 indicate RBC and the surrounding fluid media, respectively.

At low hematocrit range, the total backscattered power can be calculated by summation of the backscattered power from all RBCs. However, the scattering by blood is a complex phenomenon because of the high density of RBCs in blood. For a dense suspension of scatterers, uncorrelated positions of scatterers can no longer be assumed. Even under nonaggregating conditions, their positions are significantly correlated. Under this condition, the backscattered power is a function of the spatial arrangement of RBCs and is not simply proportional to the number of RBC.

Various attempts have been made to explain the relationship between the backscattered power from blood and the manner in which RBCs are packed. Until now, the scattering models typically can be divided into two categories of particle model and continuum approach (Angelsen 1980; Twersky 1987; Shung and Thieme 1993). In the particle model, the total scattering wave from an interrogated scattering medium is assumed to be the summation of all contributed scattering waves from each scatterer (Twersky 1975, 1978, 1987; Lucas and Twersky 1987; Bascom and Cobbold 1995). The continuum model recognizes that the scattering wave is determined by the density and compressibility fluctuation of the interrogated scattering medium as a source term in an inhomogeneous wave equation (Angelsen 1980).

The backscattering coefficient (BSC) is the average backscattered power per steradian from a unit volume of blood, insonated by a plane wave of unit intensity (Shung and Thieme 1993), which can be given by combining the packing factor (W) with backscattering cross section. Mo and Cobbold (1992) proposed a general particle scattering model where the BSC is expressed as follows,

$$BSC = \sigma_{bs}(H / V_e)W$$

where H is the hematocrit. The packing factor is a measure of the orderliness in the spatial arrangement of the particles. It expresses the acoustic interference between all echoes.

In the continuum model, BSC is defined by the variance in the number of scatterers in a voxel and the average backscattering cross section. The hybrid approach was developed by combining both particle and continuum model by Mo and Cobbold (1992). A plausible insight of the hybrid model is that it considers both the resolution of a transducer and the interaction among scatterers.

The particle approach with the concept of the packing factor to account for the effect of interactions among scatterers, which was first brought up by Twersky and his associates (Berger et al. 1991), was modified by Bascom and Cobbold (1995) as follows.

$$W_m = \frac{(1-H)^{m+1}}{[1+(m-1)H]^{m-1}}$$

The parameter m, which is referred to as the packing dimension, is related to the physical dimension and the packing symmetry of the scatterers. A geometrical interpretation is that scatterers with m=1, 2, and 3 are represented as an infinite plane, cylinder, and sphere, respectively. Practically, the packing factor approach is easier to implement than continuum model, so it has been frequently applied to verify the results from experimental measurements or simulations.

A nonlinear relationship between hematocrit and ultrasonic backscatter of RBC suspension was found experimentally and the results are in excellent agreement with the above theoretical models which predict a scattering maximum peak at a hematocrit around 13-20 % (Shung et al. 1976, 1984; Yuan and Shung 1988a, 1988b; Shung et al. 1992). The packing

dimension was validated by the results of backscattering measurements from RBC suspension under various flow conditions. The analysis showed that the packing dimension is lower under turbulent flow than under stationary condition or uniform flow (Shung et al. 1984). Although the experimental results and the theoretical models were well corresponded to each other, it is still unclear if the packing factor approximation is fully valid in the presence of RBC aggregates because the distance of correlation among the positions of the scatters can increase significantly in case of the aggregation. Moreover, since the RBC aggregation involves the formation of long straight chains of RBCs which can branch to form complex 3-dimensional networks (Shiga et al. 1983; Samsel and Perelson 1984; Murata and Secomb 1989), it is possible that the Rayleigh scattering theory (Shung and Thieme 1993; Fontaine et al. 1999) may no longer be applicable to model the backscattering of RBC aggregates (Lockwood et al. 1991). More recently, the results from RBC suspension with very high frequencies of 30-90 MHz (Maruvada et al. 2002) showed that the frequency dependence was significantly lower than the fourth power relationship predicted by the Rayleigh theory because the wavelength in the very high frequencies is comparable to the size of a RBC.

1.2. Specific Aims

The object of the present research is primarily placed on the studies of the ultrasonic backscatter due to the RBC aggregation from blood. There are three specific aims in this research.

The first aim is to elucidate the hemodynamic effects of the echogenic variation by blood flow disturbance. Most of the previous studies regarding this subject have been performed with RBC suspension in saline, so that the effects of RBC aggregation were not considered. Even though those approaches can provide scientifically meaningful information, it is essential that

the influence of RBC aggregation on echogenicity should be considered together, because RBCs in whole blood form aggregates as a reversible process. In order to investigate the effects of flow disturbance, pulsatile flow was generated in a flow loop with an artificial stenosis. The variations of echogenicity around a stenosis were measured with a commercial scanner and analyzed in terms of flow turbulence, acceleration, and shear rate.

The second aim is to establish a simple experimental setup for the measurement of RBC aggregation by ultrasonic backscatter. Up to now, the majority of the previous studies by ultrasound have used a mock flow loop model to simulate the RBC aggregation in human blood vessels. Indeed, those systems are suitable to study the impacts of hemodynamics on RBC aggregation, but they require a lot of blood volume and are not easily applicable to the repetitive experiments to ensure a statistical confidence using blood of small animals or human. In order to simplify the shearing system, a rotational flow system that has been used for RBC suspension study was modified. The modification of rat RBC with aggregating media was applied to obtain the experimental blood at our convenience. The usefulness of this experimental setup was verified by using an aggregating inhibitor and the comparison of different levels of aggregation among mammalian species, so that we can ensure the feasibility of this system for characterization of RBC aggregation.

Finally, we tried to elucidate hematocrit and shear rate dependency of RBC aggregation using this simplified experimental setup by rotational flow and rat RBCs in polymer solution. It has been known that the RBC aggregation is a function of hematocrit. However, there has been a discrepancy in hematocrit dependency among the previous reports, which may be due to the different experimental conditions, such as the measurement method and the shearing system. The methodological disagreement between photometry and ultrasound is still unresolved. Therefore, the extensive study for hematocrit and shear rate (including stasis) dependency may provide a clue to explain the unsolved problem.

1.3. Thesis Outlines

There are five chapters additional to the chapter of introduction.

Chapter 2 shows the influence of flow disturbance on ultrasonic backscatter. The ultrasonic measurements from porcine blood were performed by a commercial scanner. The effects of hemodynamic parameters such as flow turbulence, acceleration, and shear rate on echogenicity and RBC aggregation were investigated downstream and upstream of a stenosis in a mock flow loop.

Chapter 3 is dedicated to the investigation of the difference of RBC aggregation among mammalian species by ultrasound. Human, horse, and rat blood were employed as testing mammals because these three species have distinct differences in their RBC aggregation characteristics. The method for the backscattering measurements including the experimental setup is described in detail in this chapter.

Chapter 4 demonstrates that the rotational flow as a shearing system is a good tool to study rat RBC aggregation in aggregating media. In this chapter, shear rate and hematocrit dependency of rat RBC aggregation were determined by ultrasonic backscatter.

Chapter 5 presents the pharmacological applications for RBC aggregation and the usefulness of the rotational flow with rat RBCs in polymer solution. In this chapter, we demonstrated that the backscattered power decreased with the concentration of an aggregation inhibitor.

Chapter 6 summarizes and concludes the findings in this research.

Chapter 2

ULTRASONIC OBSERVATION OF BLOOD DISTURBANCE IN A STENOSED TUBE

2.1. Introduction

Ultrasound as a real time imaging technique has been used to visualize blood flow and to study hematology and hemodynamics (Shung et al. 1984; Paeng and Shung 2003; Shung and Paeng 2003). Ultrasonic backscatter from blood has been known to be highly dependent on red cell aggregation, which is affected by hemodynamic parameters including shear rate and turbulence (Sigel et al. 1983; Shung et al. 1984) as well as non-hemodynamic parameters including fibrinogen concentration, hematocrit, and temperature (Yuan and Shung 1988a, 1988b). When echogenicity variation over a pulsatile cycle is analyzed, hemodynamic parameters are the dominant factors for a blood sample where non-hemodynamic parameters do not change appreciably. Under such a condition, the combined effects of shear rate and flow acceleration have been hypothesized to enhance the RBC aggregation and were verified based on the experimental studies in a mock flow loop (Cao et al. 2001; Paeng et al. 2001; Paeng and Shung 2003, Paeng et al. 2004b, 2004c).

There have been many studies carried out to investigate hemodynamics and hemorheology in a stenosed tube using ultrasound (Bascom et al. 1997; Cloutier et al. 1995, 1996, 2000). Most of the studies have been focused on turbulence induced by a stenosis and the effects of blood turbulence on the Doppler power or power Doppler imaging from RBC suspension. However, RBC suspension is not an ideal medium to study blood flow *in vivo* since red cells do not aggregate without mediating proteins in plasma. Moreover, Doppler power

measurements are restricted by the position of the sampling volume, and power Doppler imaging may not be sensitive enough to visualize blood flow and hemodynamics compared to B-mode images. In this study in a stenosed tube, porcine whole blood, which mimics human blood in many aspects, was used to examine the influence of hemodynamic parameters on B-mode echogenicity.

In the presence of a stenosis that can be formed by an atherosclerotic plaque in the blood vessel wall, it is known that the blood flow is disturbed and the distribution of RBC rouleaux is thus changed by hemodynamic conditions. In the post-stenotic region, ultrasonic echogenicity may reflect the complicated hemorheology including the effects of shear rate, flow turbulence, and acceleration on RBC aggregation under pulsatile flow. Since it is difficult to estimate the effects of these three hemodynamic parameters independently, the contribution of each parameter to ultrasonic echogenicity is not fully understood. This chapter is focused on analyzing how each hemodynamic parameter influences echogenicity variation from the experiments performed in a mock flow loop with an artificial eccentric stenosis under pulsatile flow.

Flow turbulence is known to increase ultrasonic backscatter. The rationale has been analyzed theoretically (Bascom and Cobbold 1995; Lucas and Twersky 1987; Mo and Cobbold 1992). The results show that the scattering from a packed distribution of small scatterers is related to fluctuation of the number and size of the scatterers in a volume rather than the number itself. The possibility of turbulence is greatly increased by the presence of a stenosis in the artery. Earlier experimental results suggested the enhancement of ultrasonic backscatter by turbulence (Yuan and Shung 1988; Shung et al. 1992). Later, Cloutier et al. (1995, 1996, 2000) demonstrated that flow turbulence in the post-stenotic region increased the Doppler power from RBC suspension. Bascom et al. (1997) used a photochromic dye technique to examine the flow turbulence and the nature of the flow field downstream of an asymmetric stenosis under both

steady and pulsatile flow conditions using human RBC suspension. They confirmed that the distal flow field downstream from the stenosis could be divided into four primary zones, namely stable jet, transition, turbulence, and relaminarization zones.

Shear rate has been suggested as the most important hemodynamic parameter that affects RBC aggregation. Since Sigel et al. (1983) first showed that ultrasonic backscatter was dependent on shear rate, many studies have been published to confirm this observation. There have been several studies performed under pulsatile flow at different speeds and flow-cycle repetition rates to elucidate hemodynamic effects on RBC aggregation using ultrasound (Cao et al. 2001; Paeng et al. 2001; Paeng et al. 2004b). Several phenomena are well explained by a shear-rate analysis, but others are not. The radial variation of echogenicity and the decrease of echogenicity with increasing mean speed can be attributed to shear rate, but the cyclic variation of echogenicity cannot be explained by shear rate alone. Therefore, it was first hypothesized and experimentally verified by them that flow acceleration is another factor that may cause enhancement of the aggregation resulted from the higher probability of red cell interaction due to the different inertia and compressional forces.

In addition, the “black hole” (BLH) phenomenon, a hypoechoic central hole with a surrounding hyperechoic ring in cross-sectional ultrasonic B-mode images of whole blood in the tube, was reported under steady flow (Yuan and Shung 1989). More studies followed for a better understanding of its mechanism under pulsatile flow (Cao et al. 2001; Paeng et al. 2001; Paeng et al. 2004b). The present experimental analysis will show the temporal and regional variation of the BLH phenomenon downstream from a stenosis, which may yield more insight of the BLH phenomenon. The previous experiments using an Aloka 280 scanner with a 7.5 MHz transducer (Paeng et al. 2004a) also showed that the bright parabolic profile was observed downstream of a stenosis during the accelerating period. This observation will be further examined in more detail for a better understanding of its origin.

The “bright ring” (BRR), an expanding and collapsing hyperechoic ring was observed in cross-sectional B-mode images in the previous studies (Paeng and Shung 2003, Paeng et al. 2004b, 2004c). The present study showed the BRR profiles in the cross-sectional views and the parabolic or eddy-like profiles in the longitudinal images upstream of a stenosis during diastole of each pulsatile cycle. The BRR and the parabolic profiles were reconstructed to form 3-dimensional animations, which have never been reported.

The aims of the first part in this chapter are to measure ultrasonic echogenicity from porcine whole blood, and to examine the effects of essential hemodynamic parameters on RBC aggregation and ultrasonic echogenicity downstream of a stenosis at different flow-cycle repetition rates, where shear rate, flow turbulence and acceleration can be considered together.

The second part of this chapter is focused on echogenicity variation upstream of a stenosis. That is because the weak backward flow during diastole and the sudden narrowness of blood vessels may induce disturbance of blood flow and the distribution of RBC rouleaux upstream of a stenosis. Until now, there have been several studies on how the backscattering would be changed downstream of a stenosis (Cloutier et al. 1995, 2000; Bascom et al. 1997; Paeng et al. 2004a), but there has been no exhaustive analysis upstream of a stenosis.

2.2. Materials and Methods

2.2.1. Blood Preparation

In this experiment, porcine blood was used instead of human blood because it is easier to obtain and has many hematological properties similar to those of human blood, including average RBC size, fibrinogen concentration, and RBC aggregation tendency (Yuan and Shung 1988a, 1988b). Fresh porcine blood was collected from a local slaughterhouse in 4 L bottles that were prepared with a solution consisting of 12 g ethylenediamine tetraacetic acid (EDTA)

dipotassium salt dissolved in 120 ml of saline for anticoagulation. RBCs and plasma were separated by centrifuging. The buffy layers were separated by centrifugation and the hematocrit was adjusted to 40 % by remixing the RBCs with the autologous plasma. RBC suspension was used to study the origin of the variation of echogenicity because rouleaux formation does not occur in the suspension. To prepare the RBC suspension, the plasma and buffy coat were removed and the red cells were washed twice with 0.9 % normal saline solution buffered to pH 7.4. Then, the washed concentrated RBCs were reconstituted with 0.85 % saline solution to 40 % hematocrit. To prevent crenation of the red cells, 0.5 % bovine albumin was added to the saline solution. The experiments were completed within 36 hours after collecting the blood. The detailed procedures for obtaining fresh porcine blood and preparing blood were also described in Paeng et al. (2001).

2.2.2. Flow Model

A schematic representation of the flow system for this study is illustrated in Fig. 2. To simulate an eccentric stenosis in an artery, a rubber ball (diameter = 1.5 cm) was inserted into a round hole in a rigid tube (inner diameter = 0.95 cm) and glued to it using silicone. The relative size of the ball and the round hole determined the percentage of stenosis, and 70 % of an eccentric stenosis was created for the experiments in this chapter. Three flow-cycle repetition rates of pulsatile flow [20, 40 and 60 bpm (beat per minute)] were generated using a piston pump (Harvard Apparatus, South Natick, MA). The flow parameters such as flow rate, Reynolds number, and Womersley number are presented in Table 1. One reservoir was used to remove bubbles and to store blood. A magnetic stirrer at the bottom of the reservoir prevented the blood from settling. The inlet length of a polystyrene tube (i.d. 9.5 mm, o.d. 11.1 mm, Nalgene, Rochester, NY) was 1 m, which ensured a fully developed laminar flow before the stenosis. A bifurcation of the tube was constructed and included in the flow loop so that the flow rate could

be controlled by opening and closing this bifurcation. The blood was circulated at least for 30 minutes to remove bubbles inside the loop and reach a room temperature of 25℃ before any measurements. The presence of the bubbles could be checked from B-mode images or visually in the top side of the tube. The mock flow loop used in this experiment was also described in detail by Paeng et al. (2001).

2.2.3. Ultrasound System and Data Analysis

A LOGIQ 700 Expert system (GE, Milwaukee, WI) with an M12L linear transducer was used to study backscattering from porcine blood in a stenosed tube. The transducer frequency was set to 13 MHz. Fundamental B-mode images, duplex images and color Doppler images were obtained and used to analyze echogenicity with flow speed. Longitudinal B-mode images along the tube were obtained from 1D to 6D (1 to 6 diameters of the tube) downstream. The transducer was placed parallel to the tube for longitudinal view and perpendicularly for cross-sectional imaging to observe the BRR phenomenon upstream. Video images were stored on videotapes and digitized at 30 frames/second using a video-editing system on a personal computer for further analysis. For better visualization of B-mode snapshots, the contrast in an image was increased by clipping of the darkest and lightest parts of the histogram from the original image. To increase the signal-to-noise ratio for better visualization of the echogenicity at 1, 2, 3 and 4D downstream of a stenosis, an ensemble average over 7 pulsatile cycles was taken, and then the temporal and regional variations of echogenicity were calculated. The echogenicity was normalized with respect to the maximum gray scale of 256. The velocity profile was computed from the Doppler spectrograms of duplex imaging. The Doppler spectrograms were taken at the center of the stenosed lumen, where the Doppler frequency was 6.2 MHz, pulse repetition rate was 6010 Hz, and sample spacing was 1 mm. The MATLAB® software was used to process the digitized video images.

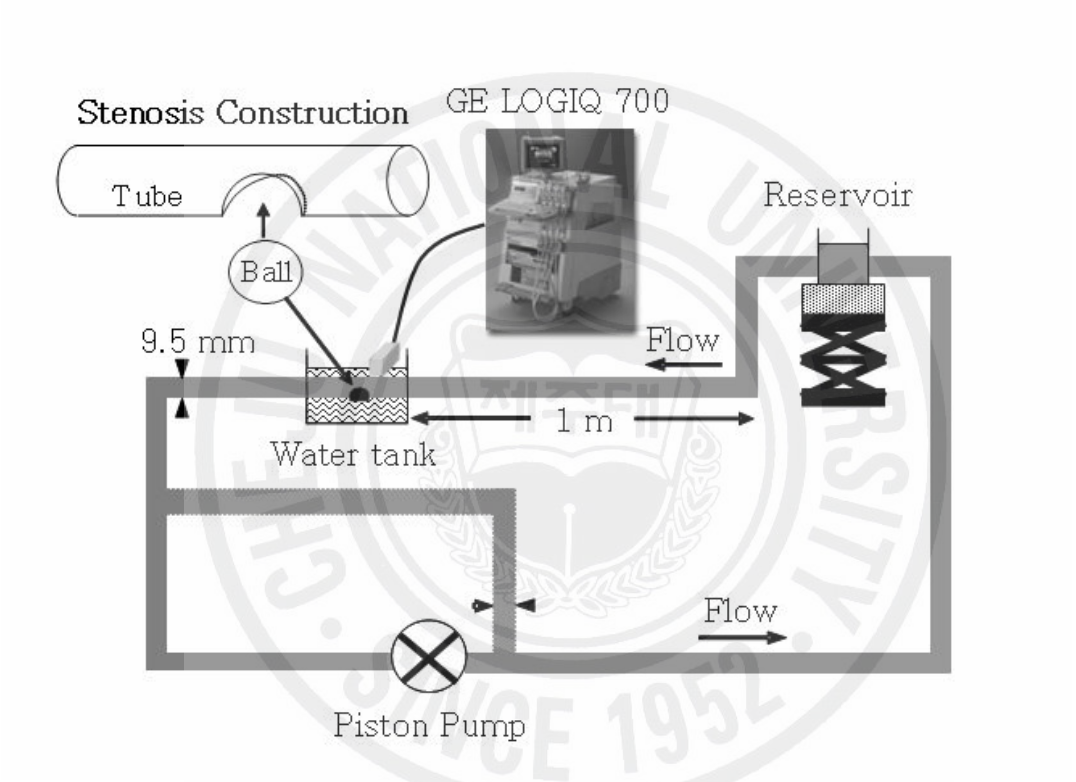

Fig. 2. Experimental setup for the flow loop model and construction of an eccentric stenosis.

Table 1. Flow parameters

Flow-cycle repetition rate (bpm)	20	40	60
Mean flow rate (ml/min)	70	170	290
Peak flow rate (ml/min)	221	533	911
Reynolds number (*Re*)	130	313	536
Womersley number (α)	3.53	4.99	6.11

The flow rates were calculated from the velocity profiles by Womersley's analysis (1995). *Re* is defined based on the tube inlet diameter and the instantaneous mean velocity at peak flow rate. The approxiamate values of *Re* and α were calculated with the kinematic viscosity of 0.038 cm^2/s (see appendix).

2.3. Downstream of an Eccentric Stenosis

2.3.1. Results

2.3.1.1. B-mode Snapshots at Accelerating Phase

Fig. 3 shows eight consecutive B-mode images at 1D to 3D (T1 ~ T4) and 4D to 6D (T5 ~ T8) downstream during systole at 40 bpm. These snapshot images were extracted from the digitized video files and the contrast was enhanced for better visualization. The bottom panel shows the velocity profile at the stenotic site, which was computed from the Doppler specrograms. The two vertical lines indicate the corresponding times of the first snapshot image (T1) and the last one (T8). As indicated by the arrows on the top of each panel, apparent shift of the echogenic profile can be seen along the blood flow direction. The approximate speed of this profile was calculated to be 20 cm/sec from T1 to T4. This profile was formed only across the throat of the stenosis and appeared to have a round shape near the stenosis. It expanded across the full diameter of the tube further downstream, becoming sharper and more irregular. This echogenic profile appeared at every accelerating phase and moved along the blood flow direction during systole. At 20 and 40 bpm, these profiles were apparent, but not at 60 bpm.

2.3.1.2. 'Black Hole' Phenomenon Downstream

The BLH phenomenon, a central echo-poor zone surrounded by a bright hyperechoic zone, was observed downstream of a stenosis. Fig. 4 (a) and (b) show the line plots of temporal mean echogenicity over a cycle across the tube diameter for 20 and 40 bpm, respectively, which were calculated from the ensemble average of 7 pulsatile cycles at 1, 2, 3, and 4D downstream of the stenosis. At four sites downstream from the stenosis, the BLH phenomenon was apparent for both 20 and 40 bpm. At both flow-cycle repetition rates, echogenicity at 3D downstream was lower than those of the other sites. Fig. 4 (c) shows the BLH 2D upstream of the stenosis during

systole at 20 bpm. The diameter of BLH upstream was much smaller than that downstream. The instantaneous echogenicity in the central hypoechoic zone and the surrounding hyperechoic ring is displayed as a function of normalized time over a cycle for 20 bpm at different positions (1D ~ 4D) in Fig. 5. The differences of the normalized echogenicity between the two lines show the contrast of the BLH. The variation of these differences was large at different positions during 0.3 ~ 0.5 of normalized time. Specifically, both echogenicity at the surrounding hyperechoic zone and the differences between the two lines were largest at 3D and smallest at 1D. However the variation over a cycle at 4D was minimal.

2.3.1.3. Cyclic and Local Variation of Echogenicity

Fig. 6 shows the cyclic and local variation of the echogenicity deviation from the temporal mean echogenicity by subtraction of the mean value in Fig. 4 from the instantaneous echogenicity at different positions downstream of the stenosis. All x-axes represent the normalized time over one pulsatile cycle for each flow-cycle repetition rate. The y-axes of the upper four panels represent the normalized tube diameter, and the gray scales show the echogenicity deviation from the temporal mean echogenicity. The middle panel shows the radial mean of echogenicity deviation over a tube diameter calculated from the upper four panels. The cyclic variation of echogenicity was found to be larger from 1D, reach a maximum at 3D, and be smallest at 4D downstream during late systole. This pattern of cyclic and local variation was observed both at 20 and 40 bpm, but not at 60 bpm. A profile that looked like a bright tail in 1D and 2D in the upper panels for 40 bpm was seen during 0.5 ~ 0.7 of normalized time. These bright tails were not seen at 20 bpm but were clearer at 60 bpm, though the results are not given in this paper. Fig. 7 shows the snap shots of the B-mode images downstream of the stenosis during diastole at 40 bpm. The time interval of each image is about 0.1 second from T1 to T4. Apparent shift of the echogenic profile which was oriented more obliquely, could be seen along

the reverse flow direction, which was also seen in Fig. 6 as a bright tail. The profile was observed for every cycle.

2.3.1.4. RBC Suspension Experiments

It is well known that the turbulence significantly increases the ultrasound echogenicity in RBC suspension (Yuan and Shung 1988; Shung et al. 1992; Cloutier et al. 1995). The experiment for RBC suspension was performed under oscillatory flow as well as pulsatile flow. Fig. 8 (a) shows the B-mode images from RBC suspension under oscillatory flow. Echogenicity was increased in the post-stenotic region, but decreased upstream during forward blood flow. During backward flow, this was reversed, and higher echogenicity was observed in the pre-stenotic region. Echogenicity from RBC suspension was observed to be out of phase between post- and pre-stenotic sites, which is well presented by the line plots of normalized echogenicity in Fig. 8 (b). The lines were calculated from averaging the radial echogenicity at 2D upstream and downstream as a function of normalized time over two oscillatory cycles. The normalized echogenicity from RBC suspension was smaller (0.18 ~ 0.25) than that from whole blood (0.4~0.6) as shown in Figs. 4 and 5, due to a lack of RBC rouleaux. Under pulsatile flow, the brighter echogenicity was observed only downstream of a stenosis at systole (data are not shown here).

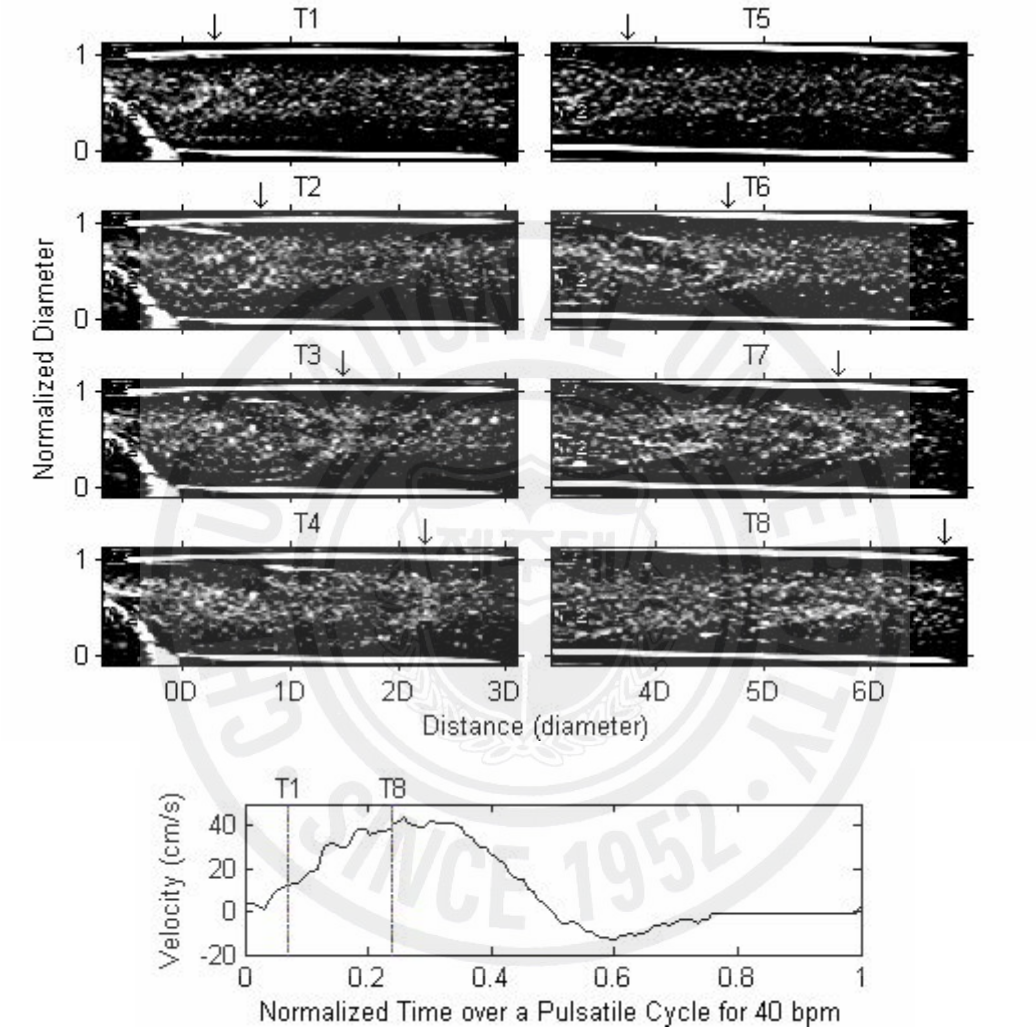

Fig. 3. Consecutive snap shots of B-mode images during accelerating phase of pulsatile flow (40 bpm) downstream of a stenosis. Arrows indicate the head of parabolic profiles moving down along the flow direction. A speed profile in cm/s was measured from the mean Doppler frequencies at the throat of the stenotic site.

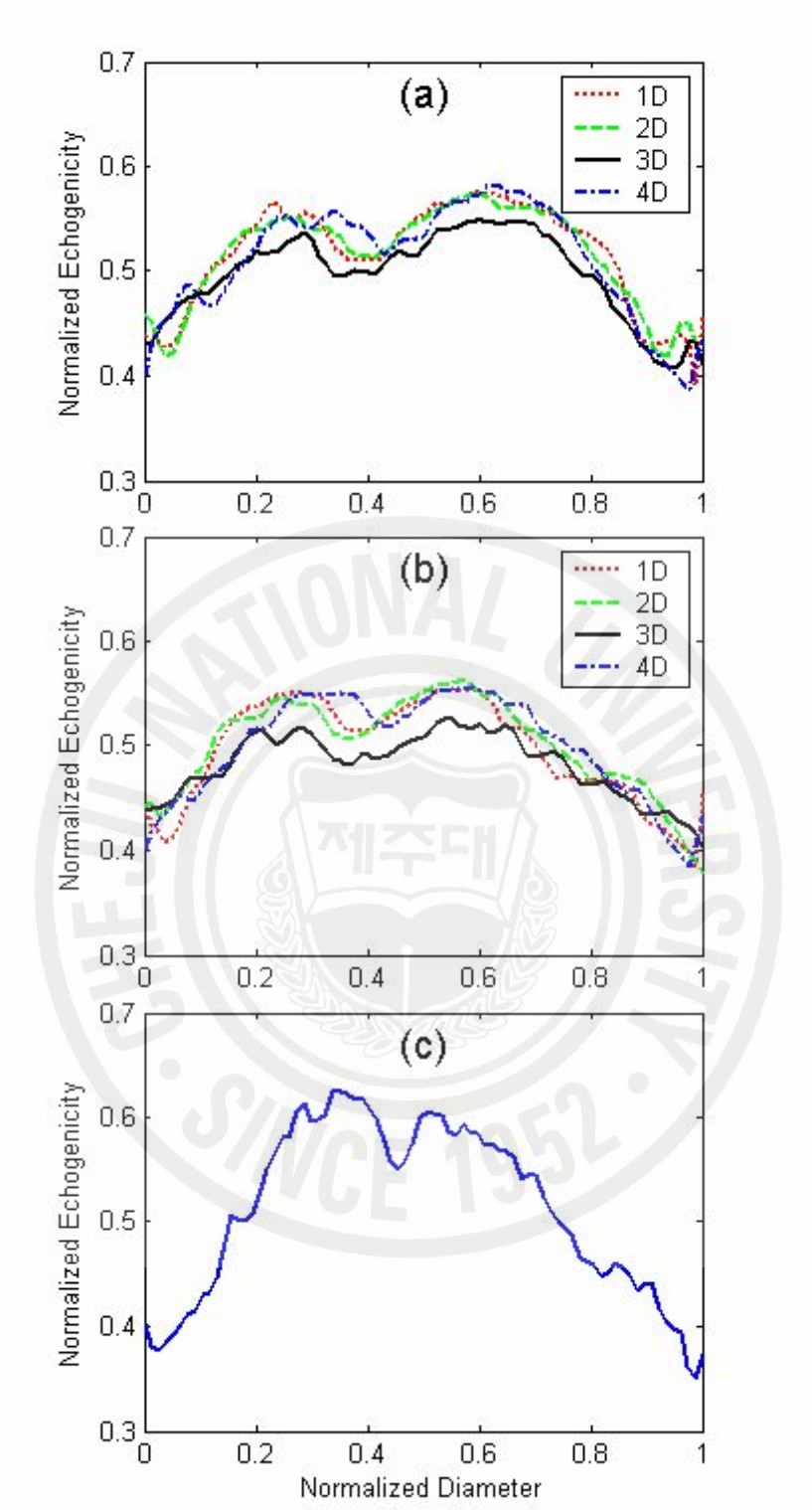

Fig. 4. The line plots of the temporal mean echogenicity over a pulsatile cycle for (a) 20 bpm and (b) 40 bpm at four sites of 1D to 4D downstream. (c) The line plot of echogenicity 2D upstream for 20 bpm.

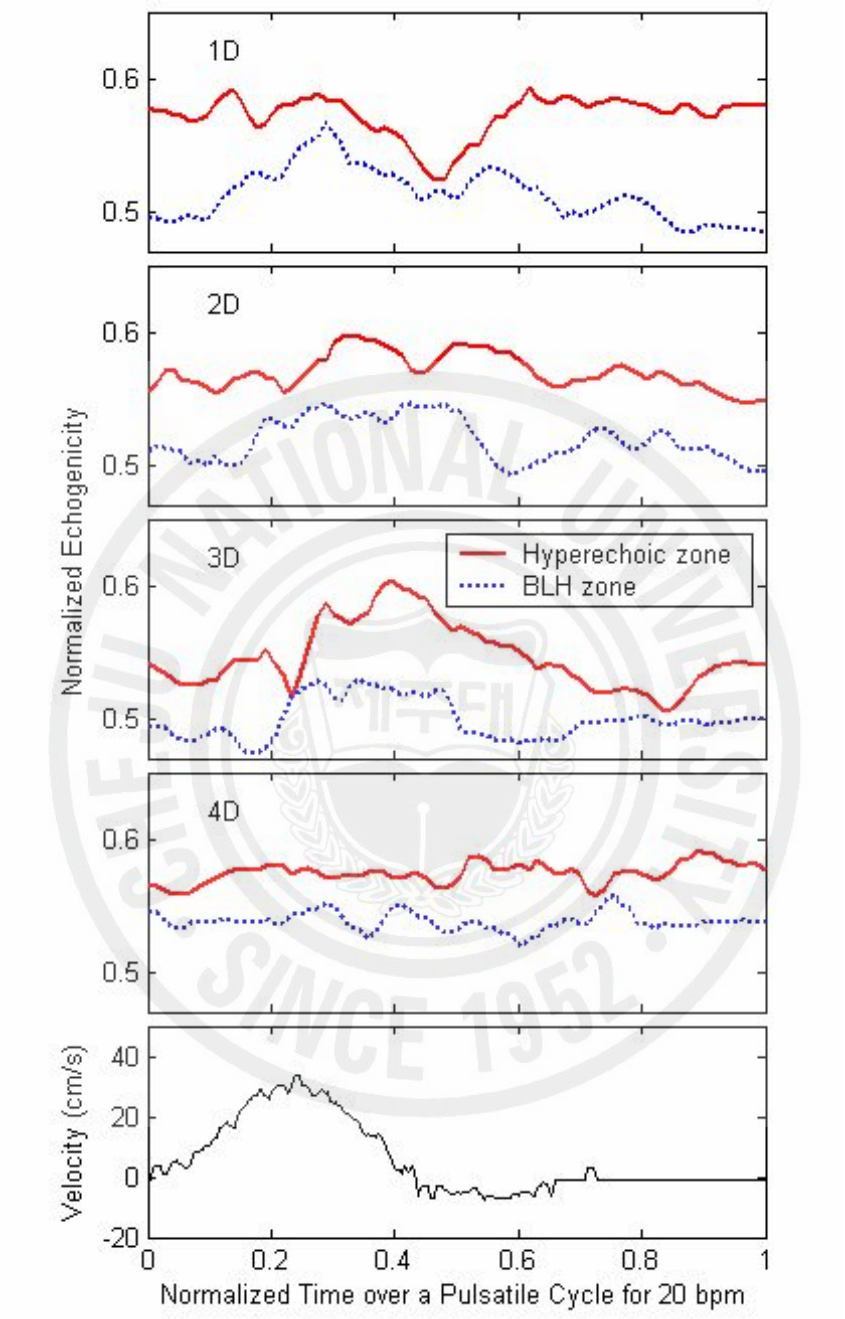

Fig. 5. The instantaneous echogenicity at the surrounding hyperechoic zone (solid line) and the BLH zone (dotted line) from 1D to 4D downstream for 20 bpm. The speed profile in cm/s was measured from the mean Doppler frequencies at the throat of the stenotic site.

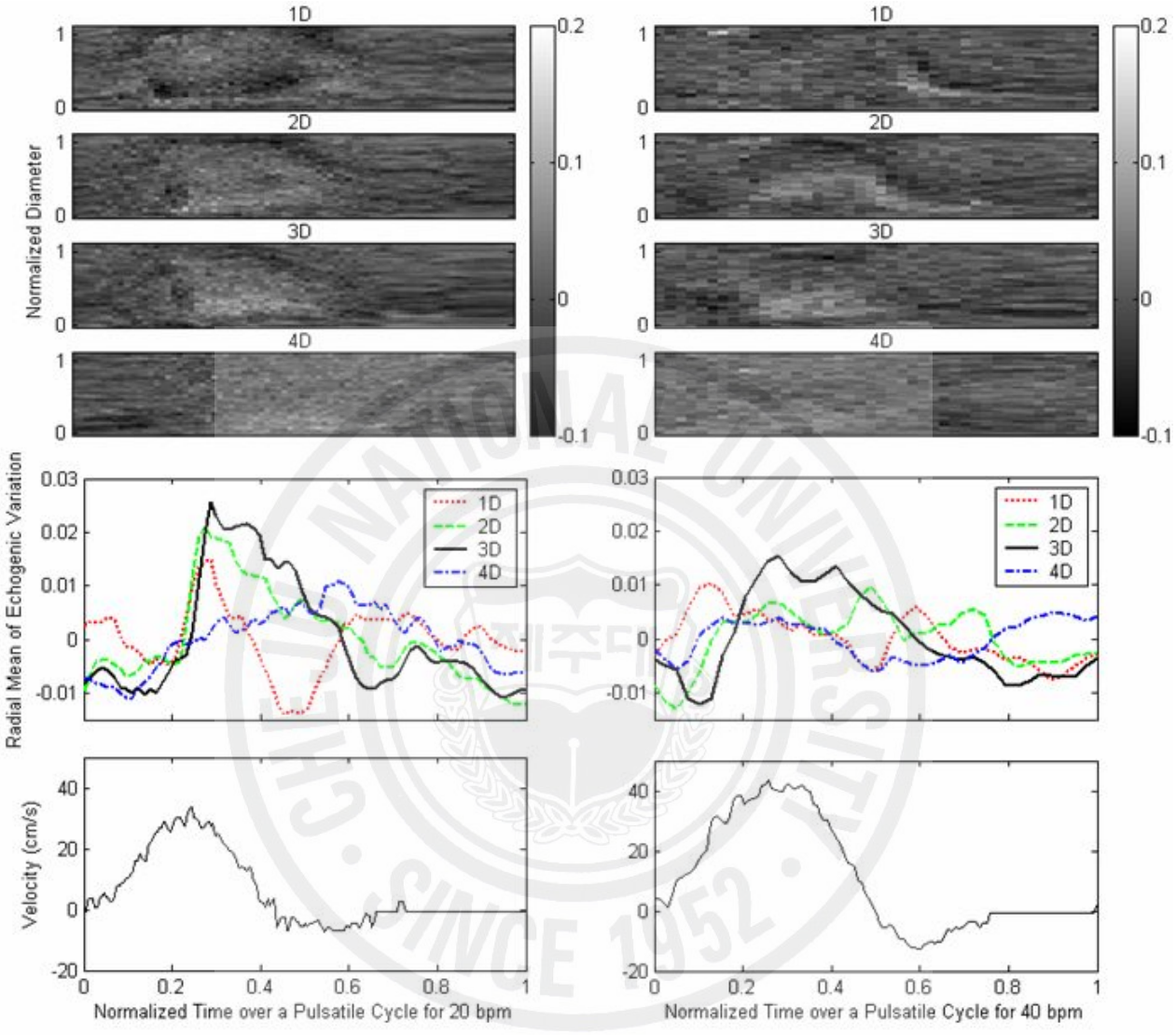

Fig. 6. The cyclic variation of the echogenicity deviation obtained by subtraction of the temporal mean echogenicity (as shown in Fig. 4) from the instantaneous echogenicity at different sites from 1D to 4D downstream of a stenosis under pulsatile flow for 20 and 40 bpm. The middle panel shows the radial mean of echogenicity deviation over a tube diameter calculated from the upper four panels. The speed profiles in cm/s were measured from the mean Doppler frequencies at the throat of the stenotic site.

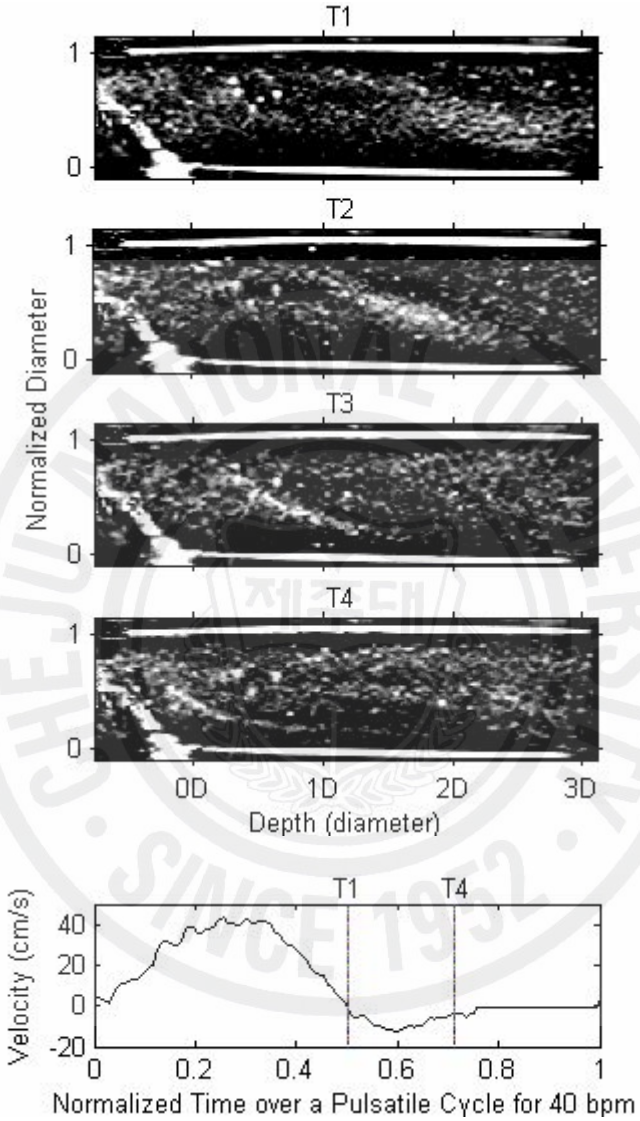

Fig. 7. Snap shots of B-mode images from whole porcine blood during diastole of pulsatile flow (40 bpm) downstream of a stenosis. The time interval of each image is about 0.1 second from T1 to T4. The speed profile in cm/s was measured from the mean Doppler frequencies at the throat of the stenotic site.

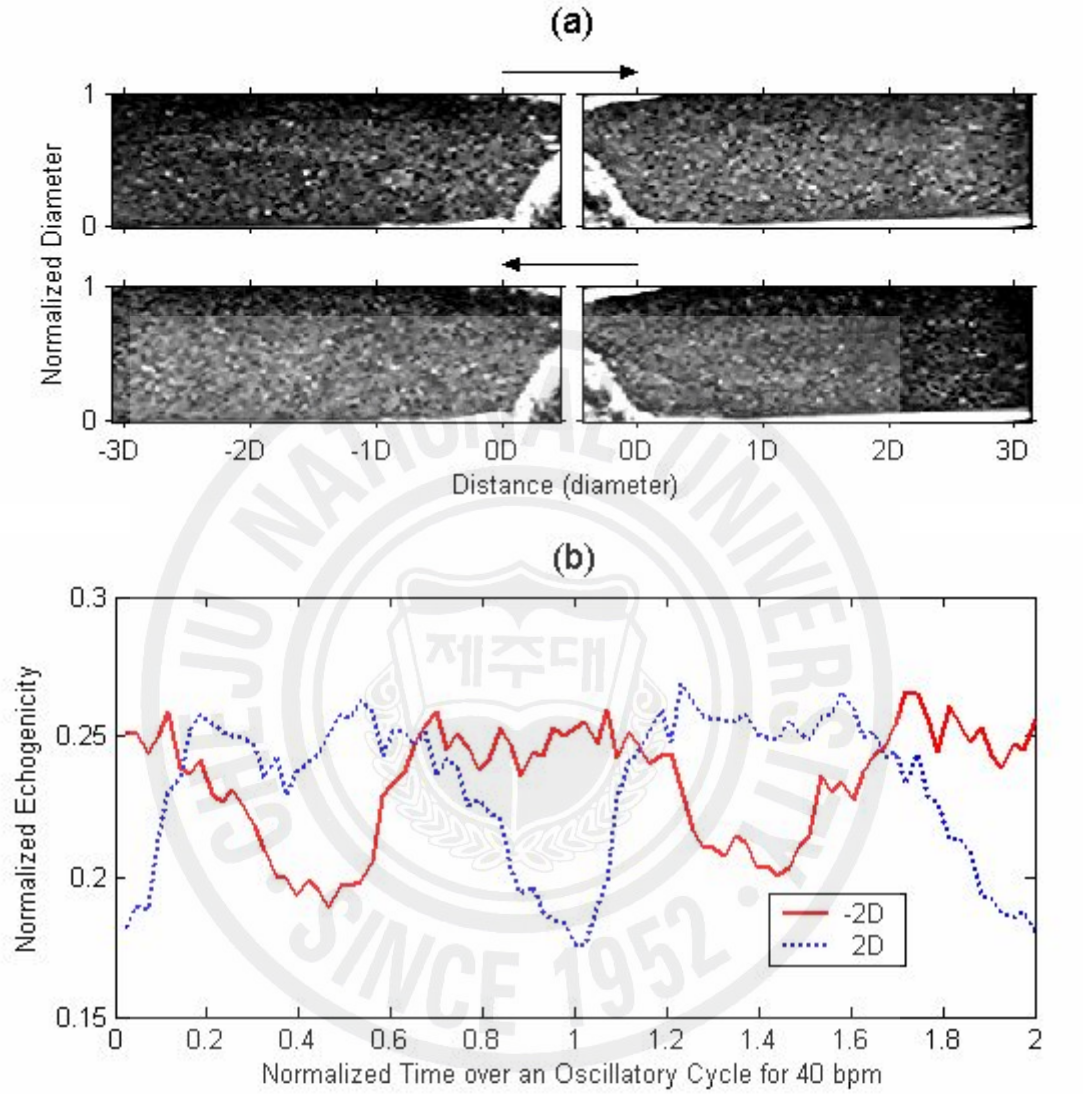

Fig. 8. (a) Snap shots of B-mode images from RBC suspension extracted from forward flow and backward flow under oscillatory flow of 40 bpm. The arrows indicate blood flow direction. (b) Radially averaged echogenicity 2D upstream and downstream over two oscillatory cycles.

2.3.2. Discussion

To investigate the characteristics of the echogenic variation downstream of a stenosis, ultrasound B-mode images from porcine whole blood in a mock flow loop were analyzed from the hemodynamic points of view, such as shear rate, flow turbulence, and flow acceleration. Several interesting phenomena, which were not previously reported, were observed.

2.3.2.1. Flow Acceleration

In the previous studies (Cao et al. 2001; Paeng et al. 2001; Paeng et al. 2004b), it was proposed that flow acceleration is another important factor affecting RBC aggregation in addition to shear rate. When the flow is accelerating, there are more chances for red cells to interact with each other to form larger rouleaux, resulting in greater scattering. Rouleaux of different sizes may experience different accelerations depending on their size and mass during early systole (Cao et al. 2001), which affect the chances for the collision of cells (Lim et al. 1997). Red cells may also come into contact with one another because of the compressional forces during acceleration. The experimental results in Fig. 3 show the formation of an echogenic parabolic profile during systole of every pulsatile cycle and its migration, which can be explained by the effects of flow acceleration. In addition to flow acceleration, flow turbulence may be another factor causing the echogenic profile, since blood flow was disturbed downstream of a severe stenosis. However, flow turbulence should decrease further downstream along the flow direction, while the bright parabolic profiles persisted even to 6D downstream. Therefore, flow turbulence could be ruled out to be the major reason responsible for these profiles, suggesting that flow acceleration is more likely to be the major cause of the bright parabolic profiles.

2.3.2.2. Flow Turbulence

Figs. 4 and 5 show the BLH phenomenon downstream of a stenosis. The formation of the BLH has been hypothesized to arise from the maximized red cell aggregation at an optimal shear rate, since the shear rate is smaller at the center and higher near the vessel wall than the optimal shear rate. Shehada et al. (1994) suggested that lower shear rate (<0.05 s^{-1}) should produce less aggregation at the center of the tube, while the maximum aggregation occurred at the surrounding area where shear rate was in the range of 0.05 ~ 2 s^{-1}. However, the BLH formations in the previous studies were observed under laminar flow conditions. In case of a post-stenotic flow field, turbulence might be generated so that the effect of turbulent flow should be also considered in addition to shear rate. Although the BLH observed under these circumstances is similar in nature to the previously reported BLH phenomenon under laminar flow, the mechanism of its formation and development may be different. This assumption may be supported by the broader BLH downstream in Fig. 4 (a) and (b) compared to the one upstream during systole in Fig. 4 (c). The temporal variation of the BLH over a cycle showed the different patterns at the different positions as shown in Fig. 5. The higher contrast of the BLH at 3D during 0.3~0.5 normalized time may be thought to be caused by locally maximized flow turbulence. The higher contrast of the BLH at 1D from diastole to early systole may be due to the higher backward flow during diastole and the higher accelerating jet flow during early systole near the throat of the stenosis. The fact that the BLH formed and remained over a pulsatile cycle under flow turbulence in the post-stenotic region was unexpected and requires further examination.

A large-eddy simulation (Mittal et al. 2001) by a computational modeling of turbulent arterial flows showed that the flow immediately downstream of the stenosis was transitional in nature, but the spectra indicated the presence of fully turbulent flow farther downstream. Three-dimentional numerical simulations by Mallinger and Drikakis (2002) also showed fluctuations of the velocity and wall shear stress farther downstream. These studies indicate that, when the

Reynolds number is higher than the critical value at a certain distance from the stenosis, turbulent flow may occur locally at the position far from the stenosis and become weaker further downstream along the flow direction. Fig. 9 shows the proposed scheme for formation of turbulent flow downstream of a stenosis. This may explain the sudden increase of echogenic variation 3D downstream in Figs. 5 and 6. Our experimental results and interpretation are consistent with the experimental investigation by Bascom et al. (1997) and Ahmed (1998). The maximum turbulence was observed around 5D downstream by Cloutier et al. (1996) using power Doppler imaging, which also supports our explanation for the result of localized flow turbulence far from the stenosis. According to Yellin (1966), systolic acceleration may be laminar regardless of the large value of the instantaneous Reynolds number, while deceleration probably produces disturbed flow, but not turbulent nor highly dissipative flow. This phenomenon is also well observed in Fig. 6, which shows higher echogenic variation during the decelerating period of systolic phase.

Up to now, there has not been any experimental observation indicating that flow turbulence increases ultrasound echogenicity in whole blood. Although a previous experiment using power Doppler angiography was done with whole blood at a concentric stenosis with an 80 % area reduction at 70 bpm and flow rate of 100 mL/min (Cloutier et al. 2000), no echogenic variation was detected downstream of the stenosis. The difference in these measurements might be due to the difference in flow velocity, flow-cycle repetition rate and the shape of the stenosis. The analysis of our experimental results shows that echogenicity could be increased due to the effect of turbulence in whole blood.

Turbulent flow significantly influences endothelial turnover that has been causally linked to the development of focal atherosclerosis (Berger and Jou 2000; Davies et al. 1986; Ku et al. 1985) and can contribute to the formation of thrombi (Asada and Sumiyoshi 1999; Johnson et al.

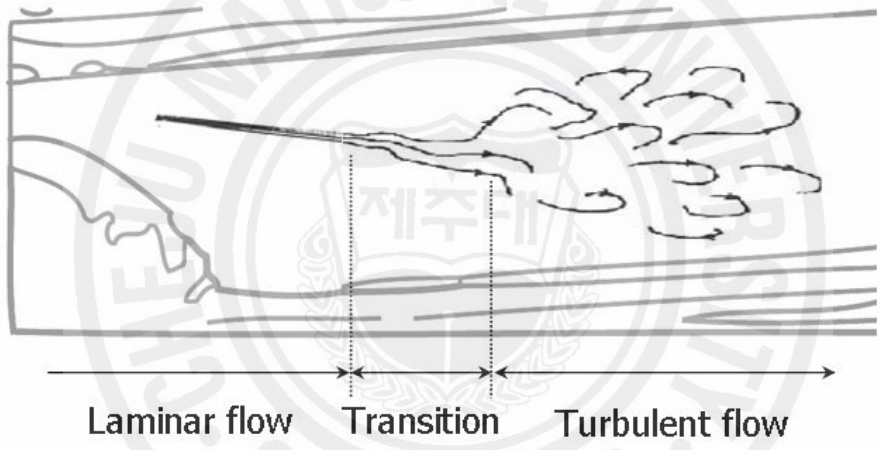

Fig. 9. A schematic diagram to show laminar and turbulent flow downstream of stenosis.

1993; Stein and Sabbah 1974). Therefore, the results from the present study suggest that an analysis of ultraosund echogenicity may be a potential tool for the detection of turbulence and turbulence intensity.

2.3.2.3. Echogenic Variation at Diastole

The bright streamline was observed to move with the boundary between the two disturbed flow zones downstream of the stenosis from our previous experiments on RBC suspension (Paeng et al. 2004a). According to Bascom et al. (1997), near the post-stenotic region, stable jet flow at the throat of the stenosis and low velocity on the stenosed side formed a dividing line that was observed during flow acceleration in RBC suspension. However, the bright oblique profile as shown in Fig. 7 in the present study was observed during weak backward flow at diastole in whole blood, and this is different from the bright streamline from RBC suspension. This phenomenon that shows the echogenic oblique profile seems to result from the regional RBC aggregation owing to the different acceleration and compressional forces between the stenosed side and the throat of the stenosis during backward flow.

2.3.2.4. Echogenic Variation in RBC Suspension

Because RBC aggregation cannot form in RBC suspension, the echogenic variations in Fig. 8 are small and most likely due to the presence of blood flow turbulence, in agreement with the report by Cloutier et al. (2000). In spite of the obvious echogenic variations in the RBC suspension, local variation of echogenicity was not observed, while it was shown in the whole blood experiments. This discrepancy might be due to the fact that turbulent flow may be formed more easily in RBC suspension because of its low viscosity. More studies are necessary to explain these differences.

2.3.2.5. Study Limitations

It should be noted that our results have inherent limitations due to the experimental setups. B-mode images of a commercialized ultrasound scanner are highly nonlinear so that our study is a qualitative analysis rather than quantitative analysis. The results cannot be quantitatively compared to other results without calibration. However, this does not mean that these results cannot be compared within our results and analyzed quantitatively, as long as all B-mode images were obtained under the same conditions using the same scanner. As a base line study, echogenicity from RBC suspension was measured within the range of flow speed up to 80 cm/s at the center of the tube under steady laminar flow and found to be similar. Our experiments were performed in *in vitro* mock flow loop, so the results might be different from those in *in vivo* blood. Human heart stroke rates are over 60 bpm, but our results were obtained from lower flow-cycle repetition rates. The blood flow velocity range was also lower in our experiments than that in some arteries. However, the possibility of the similar observation in human blood *in vivo* still exists, since the tendency of RBC aggregation is different in blood vessels *in vivo*. The cyclic variation of echogenicity from blood of human carotid arteries was observed with harmonic imaging at the high flow speeds (Paeng et al., 2003). Due to the low speed of blood flow in this study, turbulence might not occur during decelerating phase but flow disturbance might be present. The intensity of turbulence in whole blood due to a stenosis needs to be further investigated with a detailed velocity field for better understanding.

2.4. Upstream of an Eccentric Stenosis

2.4.1. Results and Discussion

2.4.1.1. B-mode and Duplex Image Snapshots Upstream

Fig. 10 displays typical B-mode images upstream of a stenosis during diastole at different stroke rates, where bright parabolic or eddy-like profiles are visually identified. The bright parabolic shape was well observed at the lowest stroke rate of 20 bpm, which appeared at an early diastolic period and then disappeared at the accelerating phase. The parabolic profile became larger and stronger as approaching towards the late stage of diastole. At 40 bpm, the echogenicity distribution was more complicated, showing eddy-like patterns. As the stroke rate rose to 60 bpm, the bright parabola became smaller compared to the cases with the lower stroke rates, and the contrast of echogenicity at this stroke rate was apparently reduced. Fig. 11 shows the duplex image at 40 bpm. The B-mode image was obtained at diastole. The Doppler spectrogram was taken from the center of the tube at a distance of 3D upstream from the stenosis. The eddy-like patterns of echogenicity were observed in the B-mode image during the period of a minor positive peak in Doppler spectrogram. When the stroke rate decreased to 20 bpm, this minor peak became weaker. It was found that B-mode images upstream of a stenosis repeatedly showed the bright parabolic profiles or the eddy-like flow patterns at diastole in every pulsatile cycle depending on stroke rates.

2.4.1.2. 'Black Hole' Phenomenon Upstream

Fig. 12 is the ultrasound image of averaging three consecutive snapshots taken at the time of the systolic peak at 20 bpm. The averaging process highlights the BLH phenomenon, a central echo-poor zone surrounded by a hyperechoic zone (Yuan and Shung 1988a, 1988b; Paeng et al. 2004b, 2004c), seen at the center of the tube along the flow direction. As shown in

the left panel of Fig. 12, the radial profile in which ten pixels within the two lines marked in the right panel were averaged along the axial direction also clearly manifests the BLH. The BLH phenomenon was quite apparent during systole at 20 bpm, but dimmed at higher stroke rates. In spite of the flow disturbance during diastole, the BLH appeared repeatedly at every pulsatile cycle. These would be the first observation of the BLH under the condition of a stenosis, even if there have been many studies on the BLH phenomenon since it was first reported by Yuan and Shung (1989).

2.4.1.3. 'Bright Ring' Phenomenon

To better understand the BRR and parabolic profile, a 3-dimensional image as shown in Fig. 13 (a) was reconstructed from a longitudinal imaging in Fig. 13 (b) and three cross-sectional imaging in Fig. 13 (c) at the different locations upstream of the stenosis during diastole at 20 bpm. In the longitudinal images, a parabolic profile was formed at diastole and disappeared at systole. This profile was stretched out over a distance of 3D upstream from the stenosis and maximized at diastole. In cross-sectional images, a bright ring was radially expanding from the tube center to the tube wall and then shrinking, periodically. These cross-sectional images were taken as video images from the three different sites at intervals of about 1 cm as marked by arrows in Fig. 13 (b). From these four different video images, it was possible to reconstruct a 3-dimensional image using MATLAB, showing the dynamic profiles of US echogenicity in 3-dimension.

Three-dimensional animation that cannot be shown here suggested that the BRR in the cross sectional images appeared as a parabolic or eddy-like profile in the longitudinal view and that the BRR and the parabolic profile were actually of the same phenomenon. Thus a better understanding of the BRR and parabolic profile was made possible by the 3-dimensional animation. Fig. 14 shows the snap shots of the animation over a pulsatile cycle. The contrast

between the bright profile and the surrounding region may be explained by the temporal and spatial variation of RBC rouleaux distribution caused by the compound effects of pulsatile flow and a stenosis. During systole, the size of rouleaux around the tube center is greater than that near the tube wall because of the smaller shear rate and flow acceleration. During diastole, the developed RBC rouleaux around the tube center upstream might be partially broken and pushed back due to the weak backward flow through the narrow lumen at stenotic region. Finally these rouleaux could be accumulated toward the flow margin or align themselves along the flow margin. Although these are similar to those observed from the pulsatile flow without a stenosis, its origin is different. This BRR arose from the blood flow disturbance caused by reversed blood flow, while the BRR in a straight tube without stenosis converged from the periphery to the center of the tube and eventually collapsed during a pulsatile cycle in the cross-sectional view, which might be caused by the combined effects of shear rate and acceleration.

The moving structures in these ultrasound B-mode images have little to do with the pattern of blood flow, but reflect the distribution of RBC rouleaux. In Fig. 15, the velocity field of blood flow extracted from the color Doppler images is shown and they are quite different from the temporal changes of RBC rouleaux as shown in Fig. 14. According to these color Doppler images at 20 bpm, the velocity profile during a cycle can be divided into the periods of positive flow, negative flow, and an intermediate stage. The flow speed at the center of tube was higher than near the tube wall during systole. During the period of negative flow, RBC rouleaux were disturbed to form parabolic profile, which was maintained during stasis. At the late stage of negative flow, the blood flow almost stopped, and the parabolic profile extended to 3D upstream. When the positive flow began at early systole, the parabolic profile was rapidly broken up.

2.4.1.4. Clinical Relevance

Clinically, Doppler ultrasound is used to detect the presence of stenoses by measuring the velocity waveform change between upstream and downstream (Fish 1990). It was also reported that the generation of turbulence downstream of a stenosis would have important implications for diagnostic procedure (Cloutier et al. 1995, 2000; Bascom et al. 1997). The present study makes use of a commercial ultrasound scanner to visualize blood flow *in vitro* experiments. It was clearly shown the regional and cyclic variation of echogenicity caused by RBC aggregates due to blood flow disturbance upstream of a stenosis. If the echogenicity variation in B-mode with Doppler spectrogram of a commercial scanner is observed *in vivo* on human arteries with or without stenosis including the bifurcations of arteries, it may be helpful for blood visualization and characterization of a stenosis. Although, the echogenic variations could be observed in a restricted region upstream close to the stenosis, the fact that blood flow disturbance can be occurred in the pre-stenotic region due to the weak backward flow may give a useful information in diagnosis of a stenosis, especially when an ultrasonic scanner is not fully accessible due to anatomical nature. In addition, the detection of the flow disturbance by B-mode imaging may also be useful to study the spatial and temporal distribution of RBC aggregates around the bifurcations of blood vessels (Berger et al. 2000) and atrioventricular system (Fatkin et al. 1997). However, its clinical implications are not known yet and further studies are required. Even though the echogenicity variation from blood in the vessel *in vivo* is rarely seen due to a high dynamic range between tissue and blood, it may be important to realize that echogenicity from blood is now more often seen through higher frequency transducers with a better sensitivity and other imaging modalities such as harmonic imaging.

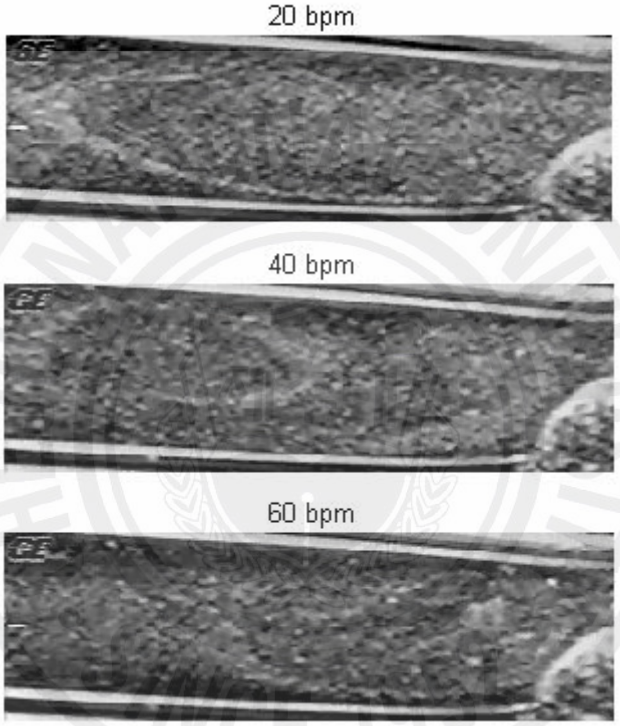

Fig. 10. Typical B-mode images of porcine blood upstream of a stenosis at diastole for three stroke rates of 20, 40 and 60 bpm.

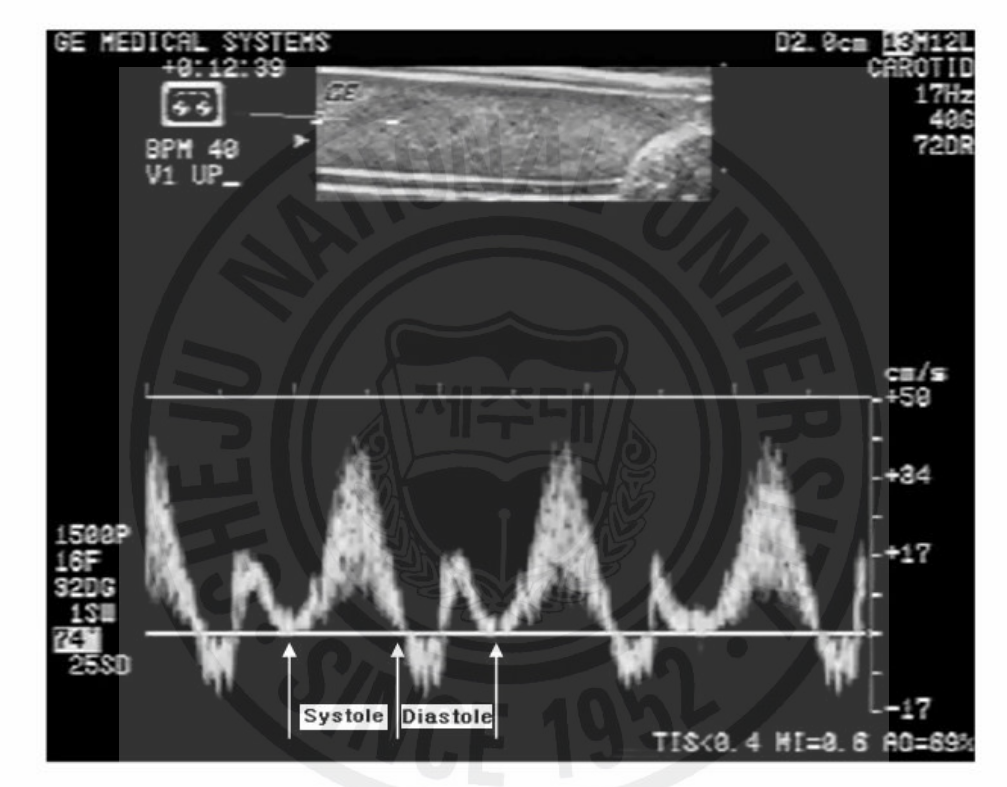

Fig. 11. A Duplex image of porcine blood flow upstream of a stenosis at diastolic phase of 40 bpm.

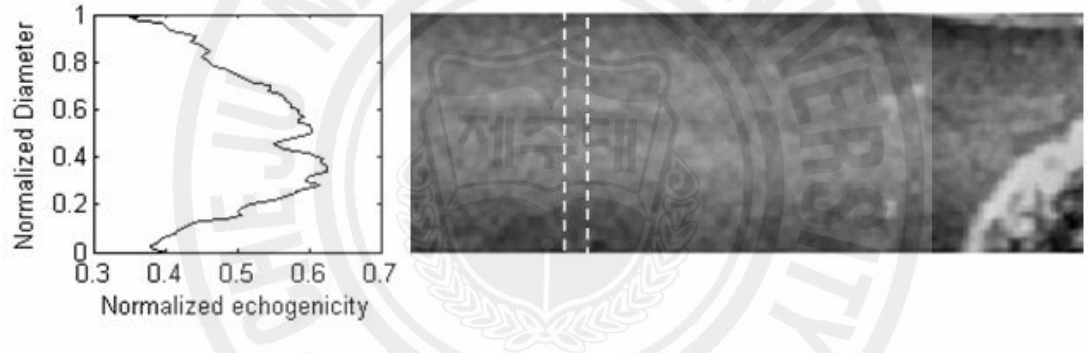

Fig. 12. B-mode image upstream of the stenosis at 20 bpm acquired at the time of peak systolic phase (right) and the normalized echogenicity profile in radial direction along the line marked on the image (left).

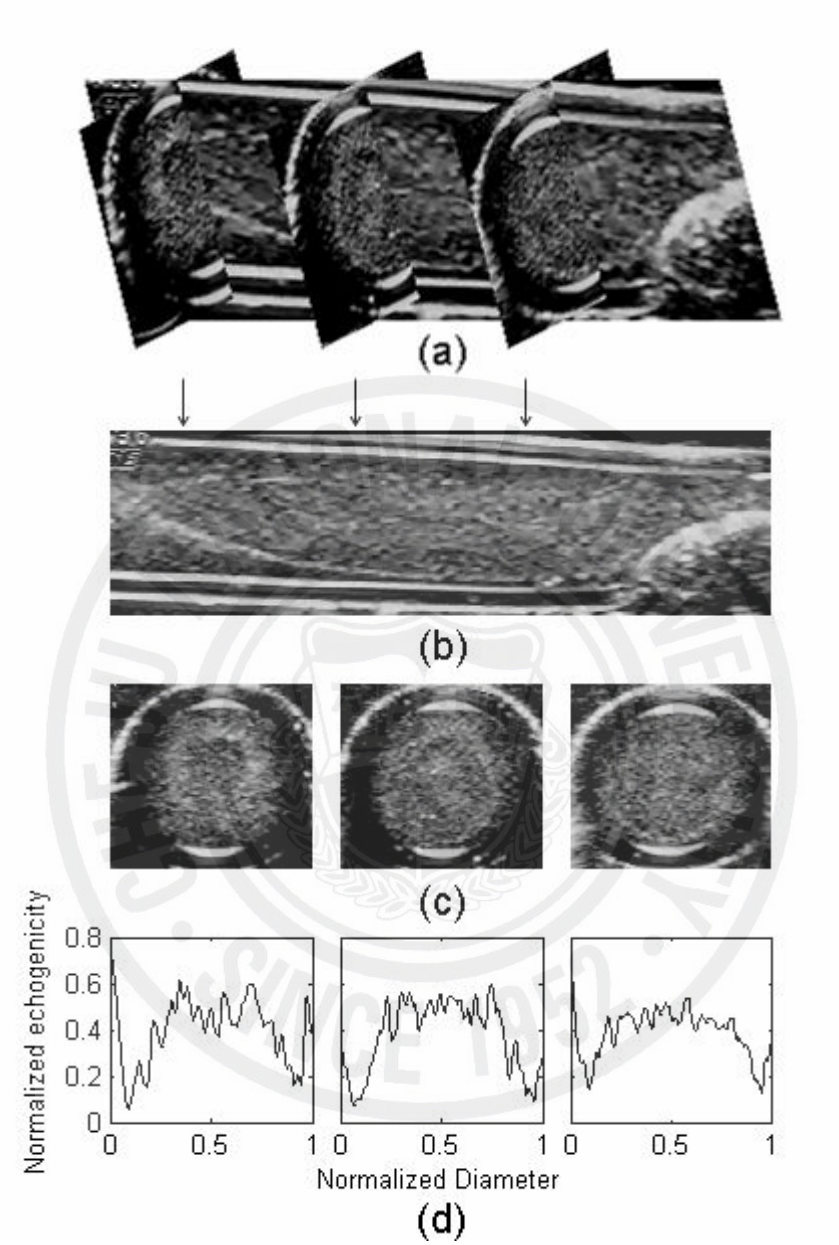

Fig. 13. (a) A reconstructed 3-dimensional ultrasound image of the BRR phenomenon upstream of a stenosis at diastole of 20 bpm from (b) a longitudinal B-mode image and (c) 3 cross-sectional images. (d) Normalized echogenicity over the diameter of the tube center corresponding to the images in (c). Arrows in (b) indicate the cross-sectional sites in (c).

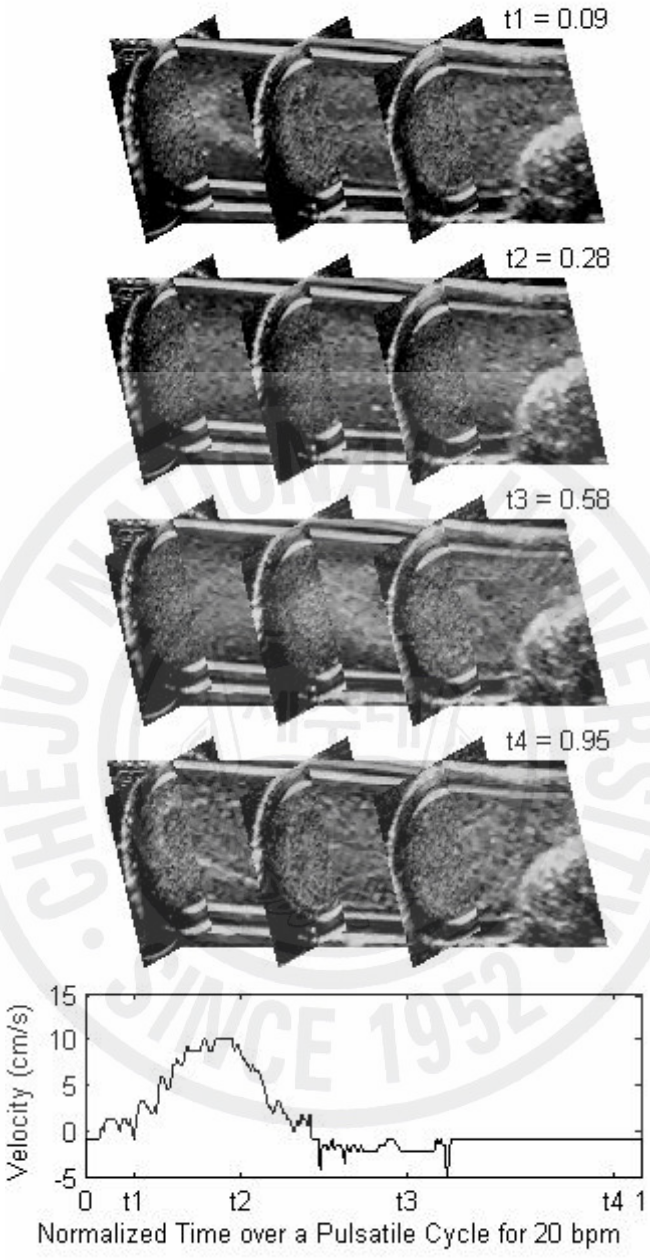

Fig. 14. Snap shots of ultrasound B-mode images extracted from the composite 3-dimensional animation over a pulsatile cycle. The figures on each image show the normalized time over a pulsatile cycle. In the bottom panel, the speed profile of the tube center was computed from the mean Doppler frequencies approximately 3D upstream of a stenosis.

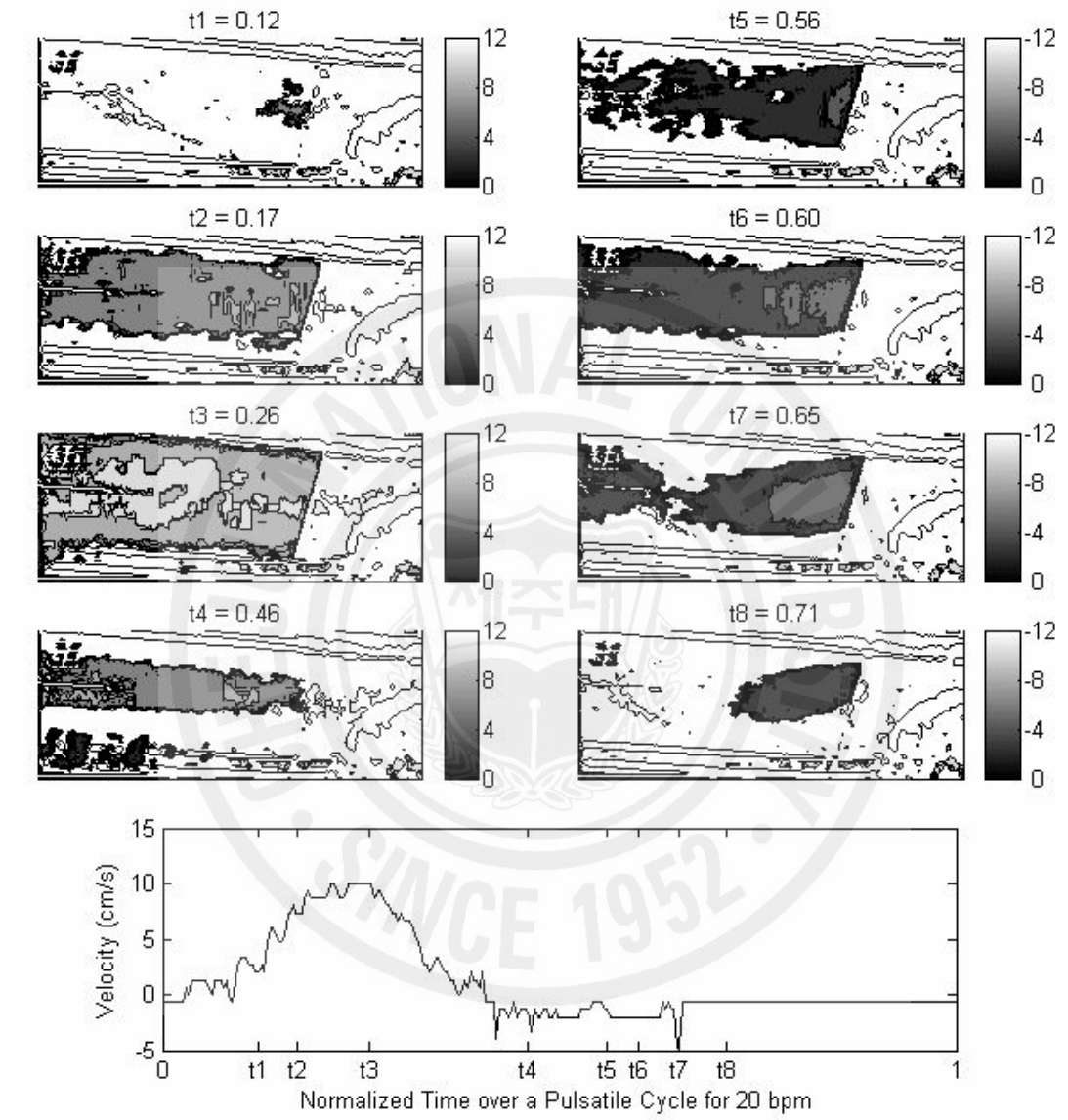

Fig. 15. Contour plots of color Doppler images over a pulsatile cycle. Red and blue colors of color Doppler imaging were converted to gray scale. The time was normalized by a period of one stoke. The negative values on contrast bars indicate the speed (cm/sec) for reverse flow.

2.5. Conclusions

A study was carried out to demonstrate the effects of hemodynamics on ultrasound echogenicity upstream and downstream of a stenosis using B-mode images. The present work has been focused on the variations of ultrasound echogenicity from porcine whole blood, which is different from the previous studies in which RBC suspensions were used. The analytical results from post-stenotic region suggest that the echogenic parabolic profiles are the results of flow acceleration in addition to shear rate. The BLH phenomenon and the sudden increase of echogenic variation 3D from the stenosis may be attributed to the complicated interactions between hemodynamic parameters including shear rate and flow turbulence. The hemodynamic changes due to weak backward flow upstream of an eccentric stenosis induced the disturbance of blood flow and RBC rouleaux. The 3-dimensional animation upstream of a stenosis was reconstructed using an image processing tool, providing a better understanding of the BRR phenomenon in cross sectional view and the parabolic profile in longitudinal view. The present study along with several previously published papers (Paeng et al. 2003, 2004a, 2004b, 2004c) that demonstrate ultrasound visualization of blood flow and RBC rouleaux is potentially a useful tool for a better understanding of the hemodynamics near a stenosis.

Chapter 3

ULTRASOUND BACKSCATTERING FROM RBC AGGREGATION OF HUMAN, HORSE, AND RAT BLOOD UNDER ROTATIONAL FLOW IN A CYLINDRICAL CHAMBER

3.1. Introduction

RBC aggregation and disaggregation are dynamic and reversible process in flowing blood. RBCs aggregate to form a stack of coins referred to as a rouleau, which is mediated by the macromolecules including fibrinogen in plasma. It was known that excessive RBC aggregation can decrease tissue perfusion, resulting in ischemic cardiovascular diseases, and can disturb flow by the increased blood viscosity, particularly in microcirculatory flow (Baskurt and Meiselman 2003). In various diseases and physiological states, such as diabetes (Schmid-Schobein and Volger 1976), hypertension (Razavian et al. 1992), hypercholesterolemia (Hadengue et al. 1996), sepsis (Baskurt et al. 1997), inflammation (Ziberman et al. 2005), myocardial infarction (Neumann et al. 1991), thrombosis (Chabanel et al. 1994), obesity (Poggi et al. 1994) and malignancies (Khan et al. 1995; Fatkin et al. 1997), greater RBC aggregation has been observed. It has thus been assumed that the increased RBC aggregation may play an important role in those diseases. However, despite a lot of the previous investigations, a complete understanding of its physiological and pathological mechanism of the RBC aggregation has not yet been fully established.

Although many studies have reported the RBC aggregation characteristics both in normal and in pathological human blood, relatively little information is available on other mammalian species. In spite of being similar in basic structure and in physiological functions in all

mammals, RBC aggregabilities differ extensively among various species (Ohta et al. 1992; Weng et al. 1996b; Baskurt et al. 1997; Windberger et al. 2003). The physiological significance of these variations among mammalian species has not yet been established. Because the hematological factors such as plasma proteins, cell shape, deformability, and surface electrical charge differ among mammalian species, the comparative studies of RBC aggregation with hematology from the different mammals can give us useful information regarding the mechanisms of rouleaux formation and its physiological roles. Furthermore, these researches can be applicable to studying human hematological diseases regarding RBC aggregation. Therefore, the accurate measurement system for RBC aggregation is of critical importance.

Several methods such as a microscopic examination including image analysis in a flow chamber (Chen et al. 1994), erythrocytes sedimentation rate (ESR) (Fabry 1987), viscometry (Lacombe and Lelievre 1987), photometry (Weng et al. 1996b; Baskurt et al. 1997; Windberger et al. 2003) and ultrasound backscattering, have been used to quantify the degree of RBC aggregation. Measuring the intensity of the transmitted and reflected light under the defined shearing conditions has been widely used to assess the different aspects of RBC aggregation. The optical methods provide aggregation indices (aggregation time and aggregation index at 10 seconds after flow stoppage), and shear rate values necessary to break rouleaux (dissociation threshold). However, there are some limitations in its applications because of the light opacity in blood (Shung and Paeng 2003). The gap between the two coaxial cylinders that contain the blood sample should be within a few millimeters to obtain an efficient light transmission. The narrow gap, however, does not provide the spatial information of RBC aggregation and is not freely applicable to various blood flow systems in laboratory as well as *in vivo* applications. ESR cannot apply to flowing or shearing blood but only to static blood, and it is also influenced by the plasma viscosity and several other factors. Viscometry is an indirect method so that it does not always agree with aggregation tendency. Microscopic methods are not quantitative in

nature.

It is well known that ultrasound backscattering of blood is caused by the presence of RBCs. Because of their small size (approximately 6~8 microns) compared to the ultrasound wavelength for up to 15 MHz, the scattering process is primarily Rayleigh scattering in nature. Sigel et al. (Sigel et al. 1983) first showed that the ultrasonic echogenicity was dependent on shear rate in flowing blood. They suggested that RBC aggregation was a major cause of the increased echogenicity from blood. Since then, many studies on ultrasonic scattering from blood have been carried out and confirmed the observation. Due to its ability to penetrate the tissue including blood compared to opacity of photometric methods, ultrasound appears to be a promising non-invasive tool for hemodynamic measurements including RBC aggregation.

The interest in this chapter is to propose an ultrasound method using a cylindrical chamber that is simple and requires smaller volume of blood samples than the conventional loop flow system. Shear rate to affect RBC rouleaux was varied in a cylindrical chamber where flow was controlled by a stirring magnet. Using A-mode ultrasound from rotational blood flow in a cylindrical chamber, the comparative tendency of RBC aggregabilities among human, horse and rat blood was investigated. These three mammalian species were chosen based on the distinct differences in their RBC aggregation characteristics. Horse RBCs have a strong aggregation tendency but rat RBCs very weak. Human blood is intermediate between these two extremes (Baskurt et al. 1997).

The measured ultrasound backscattering power showed the differences of RBC aggregability among the three mammals. This ultrasound setup using a cylindrical chamber was suggested as an alternative tool that may elucidate physiological and pathological roles of RBC aggregation, especially for small animals such as rat and guinea pig with artificial enhancement of RBC aggregation.

3.2. Materials and Methods

3.2.1. Blood Collection

Horse blood was withdrawn by jugular vein puncture from 2 year-old males of *Equus Caballus*. Rat blood was obtained from 9 ~ 12 week-old Sprague-Dawley rats (Charles River, Korea) by abdominal aorta puncture after laparotomy under intraperitoneal ketamine (100 mg/kg) and xylazine (10 mg/kg) anesthesia. Human blood samples were obtained from the healthy male volunteers with their age range of 26 to 39 years by venipuncture. All blood samples were anticoagulated with EDTA dipotassium salt (1.5 mg/ml blood as EDTA). The hematocrit was determined by reading RBC portions of capillary tubes after 5 minutes of centrifuging at 10000 revolutions per minute (rpm) with a microcentrifuge (Microspin, Hanil scientific industrial Co., Korea). The hematocrits in human, horse and rat blood were 45.2 ± 2.3, 38.2 ± 3.1 and 44.0 ± 1.3 %, respectively. All experiments were completed within 4 hours after collecting the blood.

3.2.2. Mixing Chamber

To obtain the backscattered ultrasonic signals from the blood samples both at stasis and under shear forces, a cylindrical chamber with 0.1 mm thick polyester membrane and 2 cm diameter was designed, which contains a small teflon-coated stirring magnet (diameter of 1.8 cm round type with a crucial projection on the top) at the bottom. The magnetic stirrer (PC-420, Corning, USA) was used to spin the magnet. The ultrasound transducer was mounted so as its focal zone to be placed at 0.5 cm above the top of the magnetic stirrer.

3.2.3. Experimental System

The experimental setup is shown in Fig. 16. A focused transducer (V326, Panametrics,

Waltham, MA, USA) with a center frequency of 5 MHz and 9.5 mm aperture diameter was used in the measurements. The beam profile of the transducer was measured by a planar scanning system (NTR, USA) containing a PVDF needle hydrophone (TNU001A, NTR) with a 30 dB preamplifier (HPA30, NTR) and an electric motor drive system. The relative acoustic intensity map in Fig. 17 shows -6 dB beam width of 2.5 mm at 60.5 mm focal point. The cylindrical blood container was positioned at 6.7 cm in front of the transducer. Both the ultrasound transducer and the blood container were immersed in distilled and degassed water. The temperature was constantly controlled to be 37 ℃ using thermostat (EH4, IKA, Germany). A pulser/receiver (5800, Panametrics, Waltham, MA, USA) was used to drive the transducer for transmitting and receiving ultrasonic signal. A National Instruments 100 MHz digitizer (NI PCI-5122, Austin, TX, USA) with the LABVIEW® system was used to collect the backscattered signal.

3.2.4. Measurement Protocol and Data Analysis

To investigate RBC aggregation tendency, 9 ml of fresh whole blood was placed into the cylindrical chamber. The blood was stirred in the container for at least 15 minutes before making any measurements to remove the bubbles inside the chamber and to allow the blood to reach 37 ℃ temperature. Stirring speed was altered in six steps of revolutions per second (rps) from high to low (4, 3, 2, 1.5, 1 and 0 rps). Blood samples were sheared for 30 seconds at high speed of 4 rps for the purpose of total dissociation of RBC aggregates. Then the flow was suddenly reduced or stopped to each stirring speed of 4, 3, 2, 1.5, 1 and 0 rps. The backscattered signal was digitized with a sampling frequency of 100 MHz. For 5 minutes, a total of 600 recordings of time domain ultrasound signals backscattered from the blood sample were collected. Each signal in the scattering window was consisted of 200 data points which corresponded to the 1.5 mm width of the blood sample for calculating backscattered power (Fig.

18. (a)). The backscattered power was computed in the time domain by summing the squared values of the signal over the time window given by,

$$\text{Backscattered Power} = 20 \times \log\left(\frac{V_{rms2}}{V_{rms1}}\right), \quad V_{rms} = \sqrt{\frac{1}{N}\sum_{i=1}^{N} V_i^{\,2}}$$

where N is the data points in scattering window and V is voltage. V_{rms1} and V_{rms2} represent the root mean square of voltage from the signals in water as a reference and from the blood sample, respectively. To reduce fluctuations in the mean ultrasound backscattered power curves, a 5 point-smoothing filter was used.

The enveloped echo images for monitoring the entire process of spatial and temporal RBC aggregation in the cylindrical tube were obtained from A-lines of the backscattered signals using the Hilbert transform. For a better visualization of these images, the brightness was converted into darkness. All data were processed on a personal computer using MATLAB® software. Measurements were performed on the blood samples from six different humans, horses and rats and the results were expressed as mean ± standard error (SE).

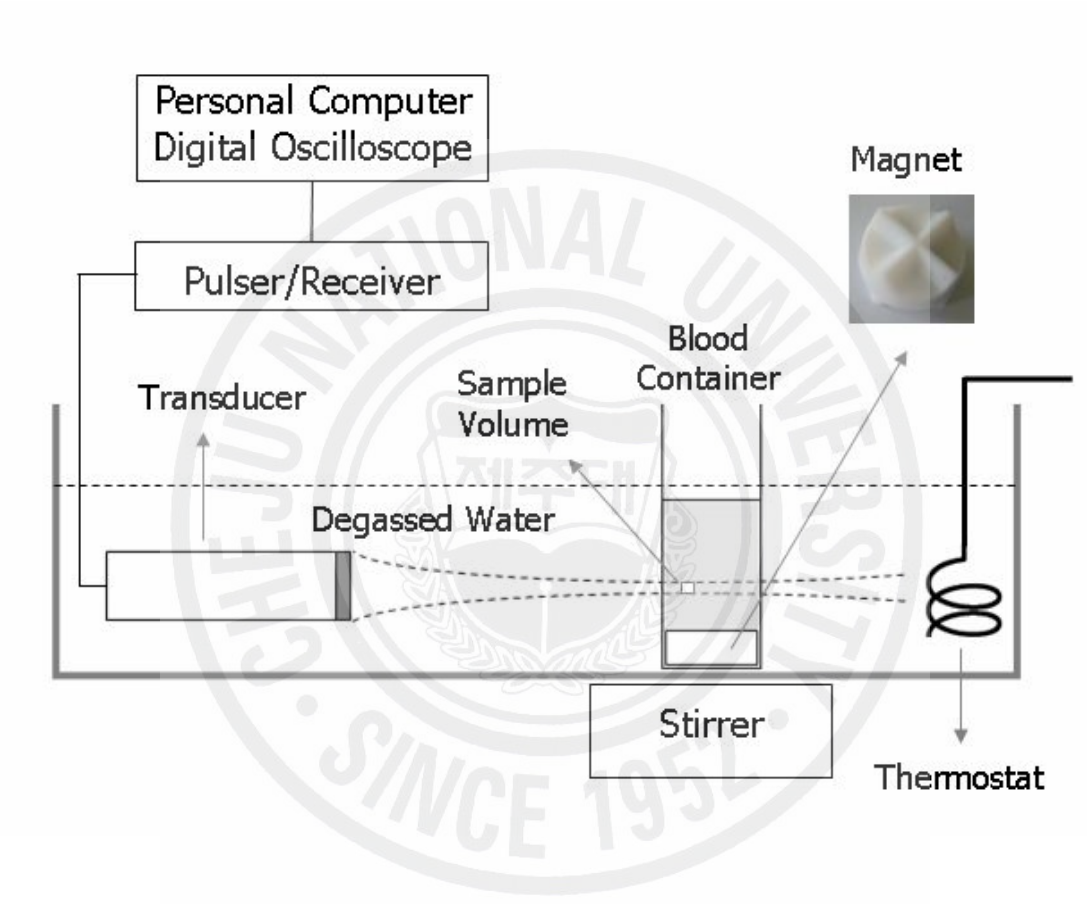

Fig. 16. Experimental system for the ultrasonic measurement from blood.

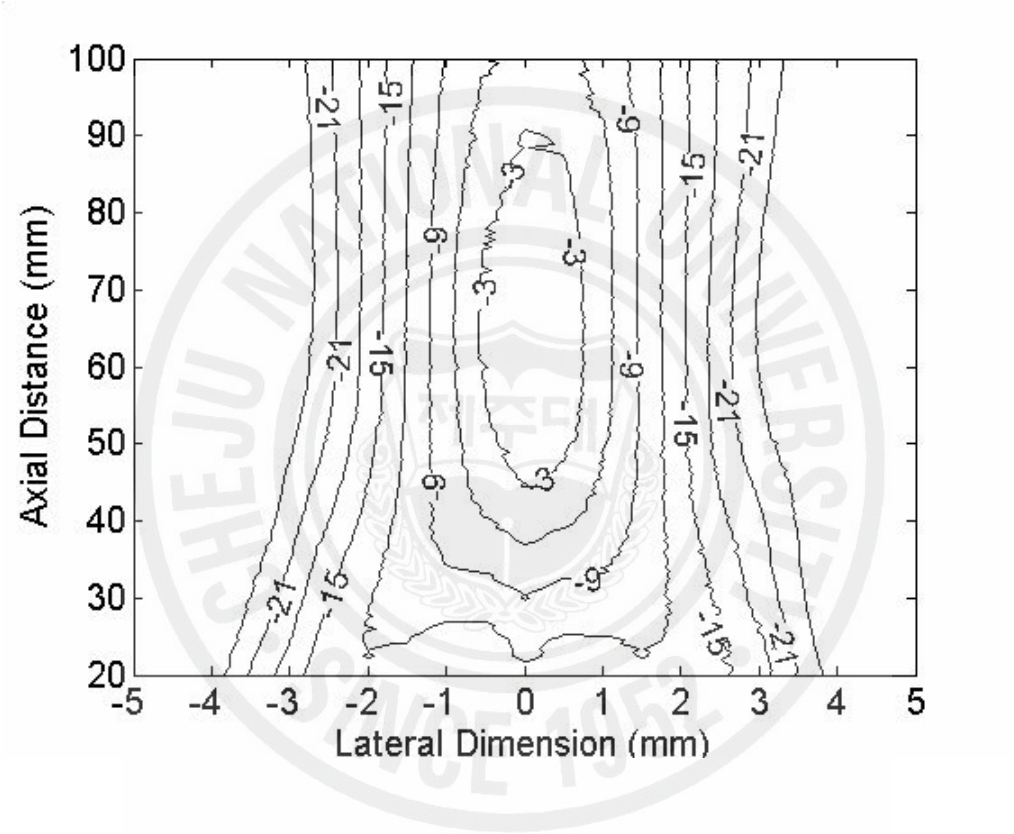

Fig. 17. A contour plot of the relative acoustic intensity for the transducer with 5 MHz center frequency and 9.5 mm aperture diameter. The numbers are in dB.

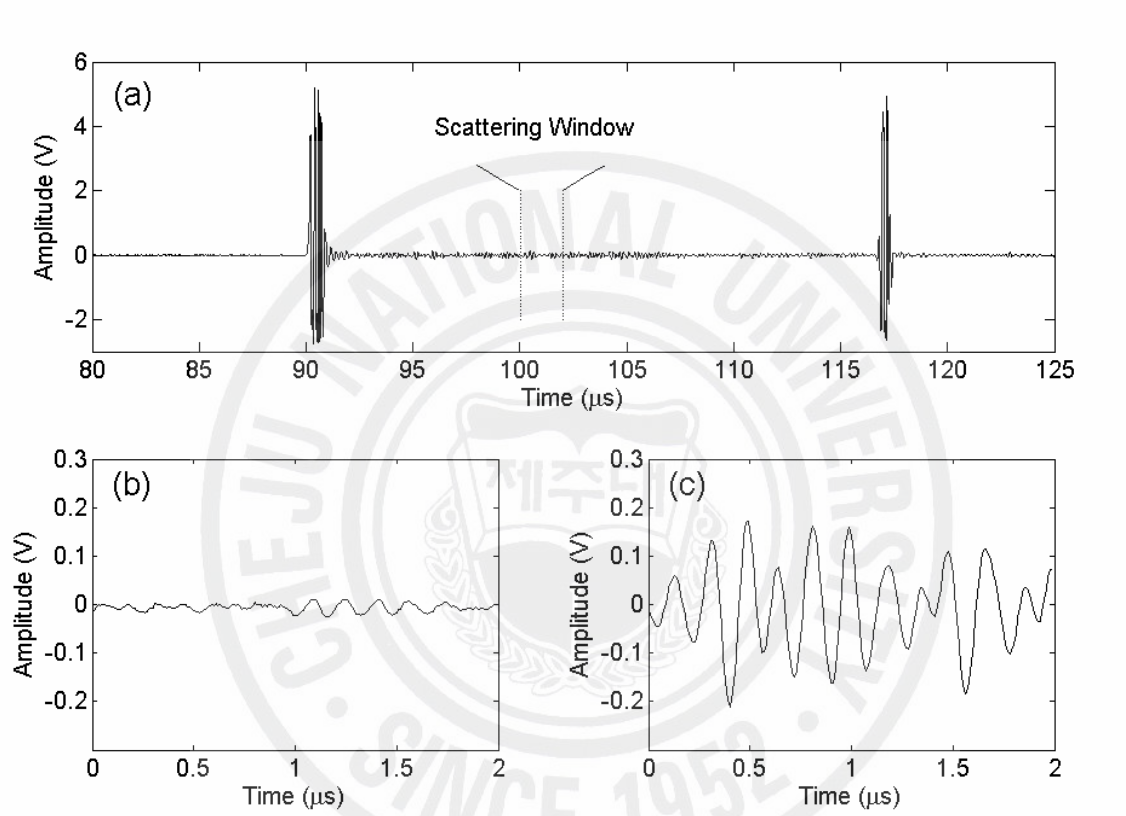

Fig. 18. Illustration of time characteristics of the backscattered signal (a), zoom images of the selected scattering window at stirring speed of 4 rps (b) and stasis (c) in horse whole blood.

3.3. Results

3.3.1. RF Signals

Fig. 18 (b) and (c) show the typical signals in the scattering window in Fig. 18 (a) from horse whole blood at 5 minutes after onset of the stirring with the rates of 4 rps and 1 rps, respectively. A remarkable increase in amplitude of the backscattered signal was seen at low shear rate of 1 rps condition.

3.3.2. M-mode Images

Fig. 19 shows the typical echo images that represent the spatial and temporal variations of RBC aggregations for horse blood, at six different stirring rates including stasis. All x-axes represent the time for 5 minutes, where the zero time represents the switching point from 4 rps to a reduced stirring rate. The y-axes represent the normalized diameter of the cylindrical chamber. The darkness of each pixel means the amplitudes of the backscattered signal envelope by Hilbert transform. At 3 rps, a clear dark zone is seen along the beam center. It was expanded toward the tube wall with lowering the stirring rate. This dark zone was started to appear at 10 to 20 seconds after sudden flow reduction and lasted for 5 minutes. The flow velocity in a cylindrical chamber varies from center to the tube wall along the radial direction. The shear force acting on a RBC aggregation at the far point from the center is higher than at the center, so that low shear rate around the tube center may cause higher RBC aggregation. The echogenic contrast between the dark zone and the surrounding region may be explained by the distribution of RBC rouleaux caused by radial variation of shear rate. As seen in this figure, the overall echogenicity increased with lowering stirring rate from 4 to 1 rps. However, this tendency was not applied to the stasis condition of zero rps. The sudden flow stoppage did not induce the remarkable increase of echogenicity.

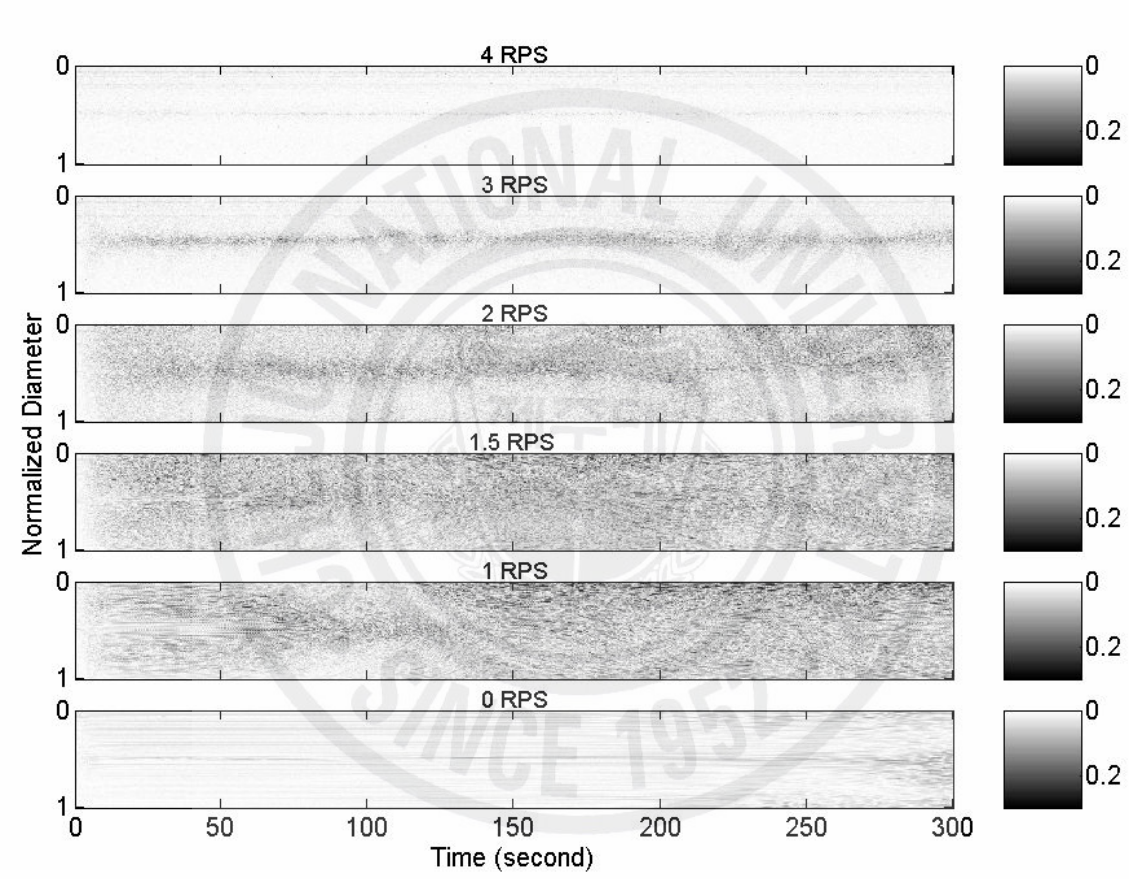

Fig. 19. Typical echo images from horse blood with various stirring rates for 5 minutes. The gray scale corresponds to the enveloped amplitude of backscattered signal.

3.3.3. Backscattered Power from Human, Horse, and Rat Blood

Fig. 20 presents the backscattered power variations at the different stirring rates for human, horse and rat whole blood as a function of time during the process of RBC aggregation. As seen in horse and human blood, the powers increased rapidly during the first 1 minute and reached a plateau. The time to reach a plateau was decreased by increasing the stirring rate. For all flow speeds, decreasing the stirring rate resulted in power increases. The backscattered power was markedly greater for horse blood under shearing condition compared with that for human blood. In contrast, rat blood exhibited no remarkable variations of the backscattered power for all stirring rate conditions. At the highest stirring rate of 4 rps, the backscattered powers from human, horse and rat blood were approximately 5, 7 and 1 dB, respectively. It is considered that the power differences at 4 rps may be due to the different hematocrits and RBC sizes, and the incomplete disaggregation of RBC rouleax among three mammals because the shear rate for total dissociation of RBC rouleaux depends on mammalian species. Fig. 21 shows the mean backscattered power for the last 1 minute of Fig. 20 as a function of stirring rate. In this figure, it was clearly indicated that the RBC aggregability depends on the mammalian species among human, horse and rat blood. It also decreased with stirring rate except in rat blood. The shear rate dependency in horse blood was higher than that in human blood.

The sudden flow stoppage in Fig. 22 did not induce a remarkable increase of the backscattered power in the three mammals. The powers increased slowly for 5 minutes in human and horse blood, but not in rat blood. The backscattered powers from human and horse blood for zero rps at 5 minutes were smaller than those from human for 1.5 rps and from horse blood for 3 rps, respectively. Therefore, the inverse proportion of aggregation tendency with stirring rate was not applicable to stasis condition.

3.4. Discussion

Using the 5 MHz focused transducer under rotational flow in a cylindrical chamber, the quantitative data of the backscattered power were obtained from human, horse and rat whole blood. The levels of ultrasonic backscattered power represented the differences of RBC aggregation of the mammalian species. The enveloped echo images showed the spatial and temporal variations of rouleaux distribution for whole blood in a cylindrical chamber.

It has been well known that shear rate is the most important hemodynamic parameter that affects RBC aggregation. For that reason, shearing systems are critical to investigate RBC aggregation phenomenon. Many researchers investigated the influence of shear rate on the ultrasonic backscattered power from blood. In those studies, the backscatter was examined in a mock flow loop by varying the average flow velocity. The loop flow system is similar to the physiological blood vessels and useful to study the effects of various blood flow on RBC aggregation. However, it needs large volume of blood to fill the flow loop, so has some difficulties to investigate the blood of small animals. Therefore, a cylindrical chamber for smaller blood volume was applied in the present study. Although the rotational flow system in a cylindrical chamber does not exactly represent physiological blood flow, the present experimental results of ultrasound backscattered power and echo images show that it is possible to compare the relative RBC aggregability among the various blood samples at both flowing and static conditions. Moreover, the circular flow pattern can be produced by the atrioventricular blood flow which is similar to the present shearing system. The previous studies using B-mode images from human blood also demonstrated the usefulness of a cylindrical mixing chamber in the measurement of blood echogenicity (Fatkin et al. 1997; Rastegar et al. 2003).

The mechanisms of rouleaux formation and its physiological and pathological roles in

human blood are not well understood. Although, fibrinogen level in plasma is known to be the major RBC aggregating factor in human blood, other macromolecules in plasma such as α2-macroglobulin, haptoglobulin, ceruloplasmin, C-reactive protein and serum amyloid A are considered as possible factors for influencing RBC aggregation (Weng et al. 1996a; Baskurt and Meiselman 2003). Especially, the ceruloplasmin concentration in horse blood was ten times higher than that in normal human blood (Okumura et al. 1991). The addition of ceruloplasmin to human blood also showed the significant increase in RBC aggregation (Weng et al. 1996a). Andrews et al. (1992) reported that the higher RBC aggregation in horse blood is partially ascribed to the higher molecular weight of horse fibrinogen. The cellular factors such as deformability, morphology, cell aging and surface charge can affect RBC aggregation (Rampling et al. 2004). The previous reports revealed that the three mammalian species have difference in RBC surface charge with the order of rat > human > horse (Baskurt et al. 1997). A higher negative charge on rat RBC membrane would be associated with low aggregation tendency by inducing electrostatic repulsive force. These results support the present experimental measurements of ultrasonic backscattered power from the three mammalian species.

Although our results of RBC aggregabilities among the three mammalian species agree with the previous reports measured by Myrenne aggregometer (Weng et al. 1996b; Baskurt et al. 1997; Windberger et al. 2003), Ohta et al. (1992) reported that similar RBC aggregation for rat and human blood was measured by photometry. It is assumed that this discrepancy may be related to the methodological differences in shearing blood and the optical detecting system. Therefore a better measurement system is essential to study RBC aggregation phenomenon.

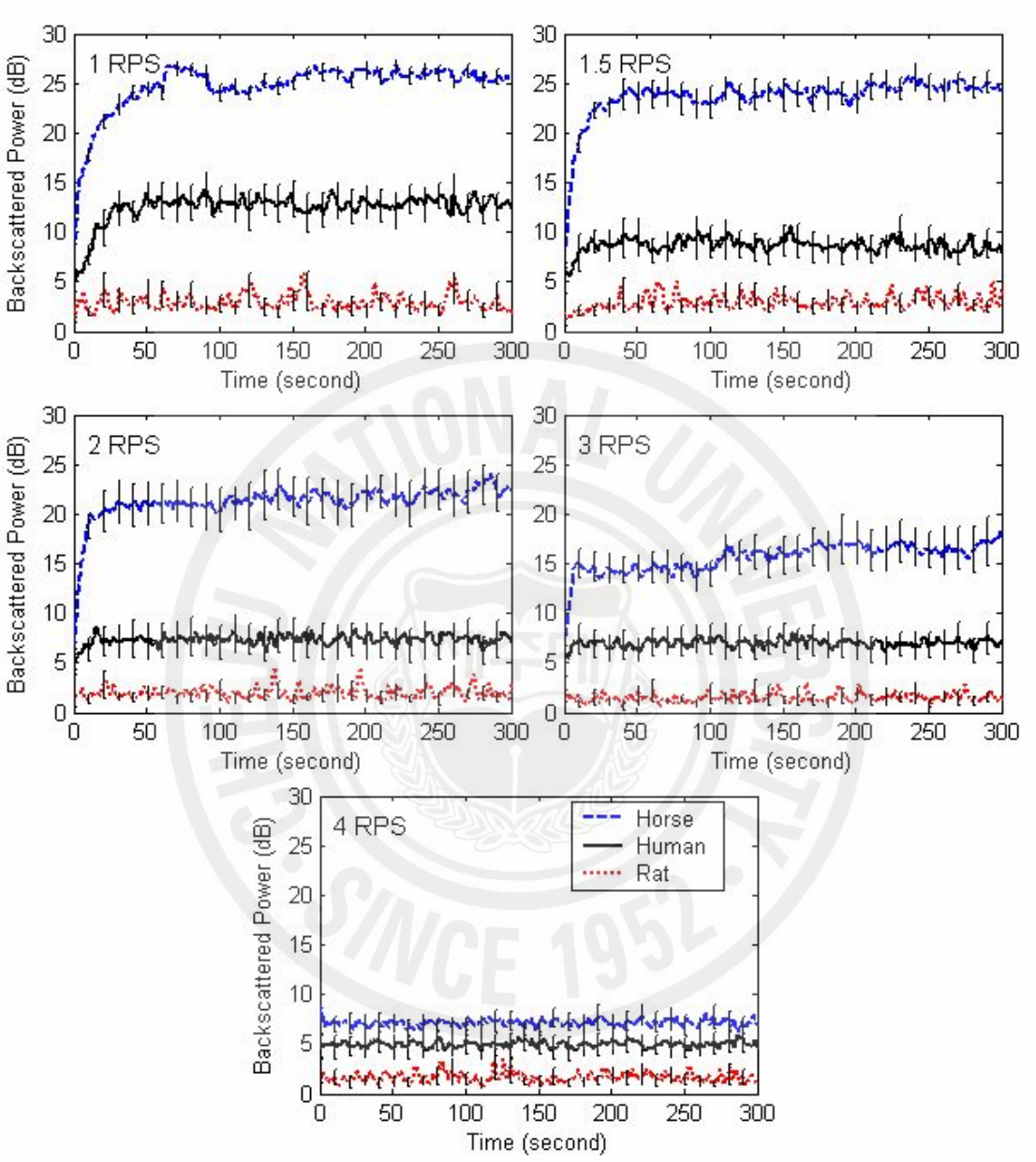

Fig. 20. The variation of ultrasound backscattered power following a sudden flow reduction from 4 rps to 1, 1.5, 2, 3 and 4 rps in human, horse and rat blood. Each plot represents the mean ± SE of six individuals. The SEs are only displayed for selected times in order to enhance the visualization of the graphs.

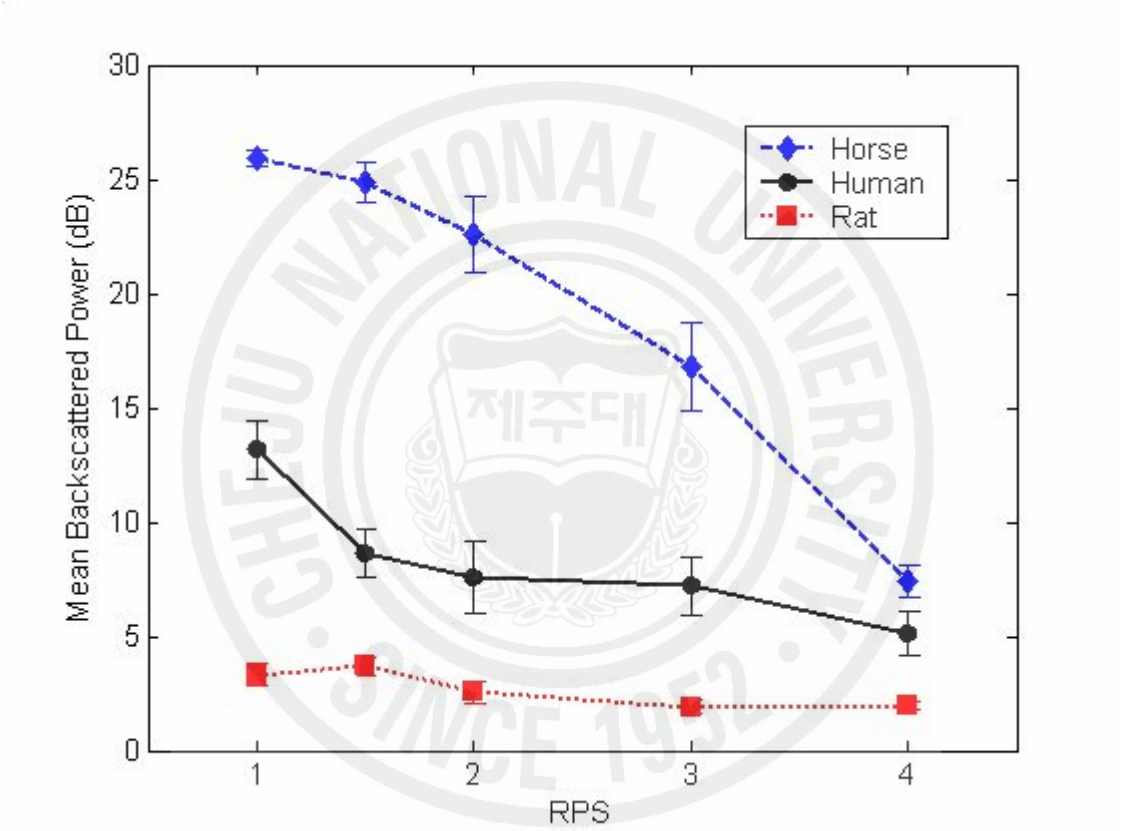

Fig. 21. Mean backscattered power as a function of stirring rate obtained by averaging of last 1 minute data in Fig. 20.

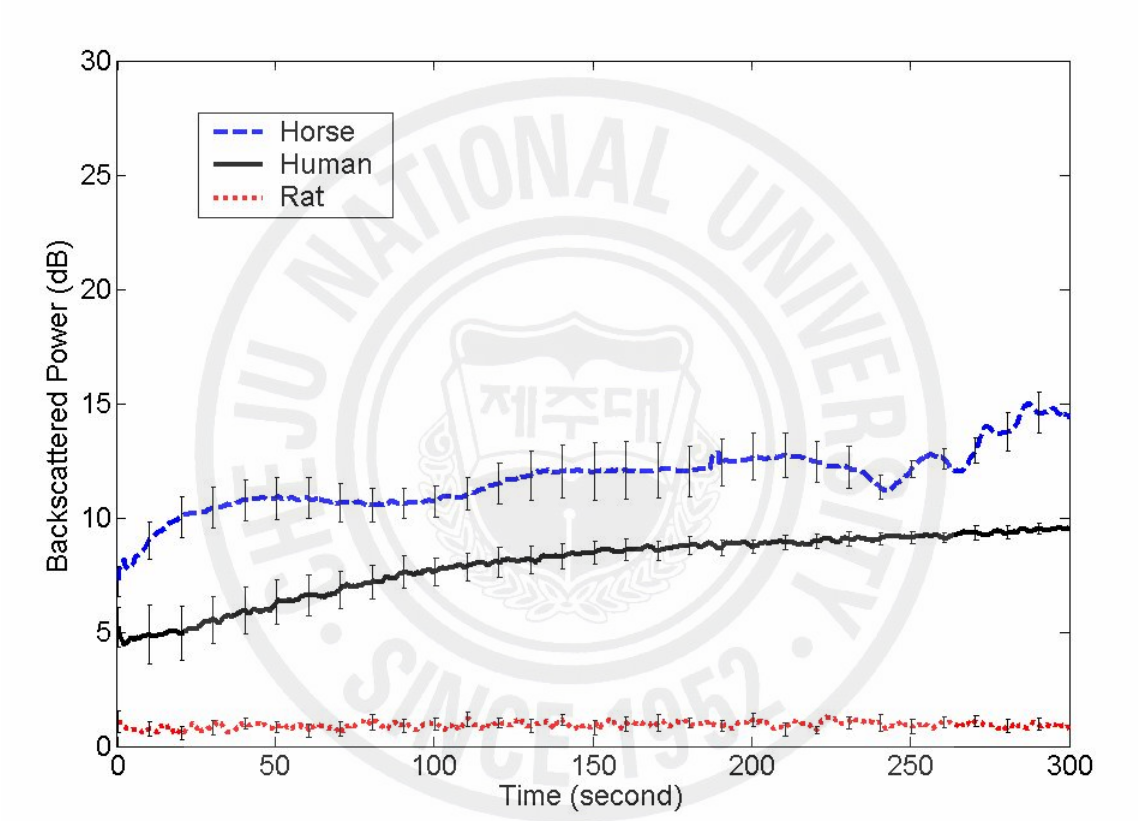

Fig. 22. The variation of ultrasound backscattered power following a sudden flow stoppage from 4 rps in human, horse and rat blood. Each plot represents the mean ± SE of six individuals. The SEs are only displayed for selected times in order to enhance the visualization of the graphs.

3.5. Conclusions

Using ultrasound backscatter measurement, the highest level of RBC aggregation was observed from horse blood followed by human and rat blood both at stasis and under shear forces. The present investigation of RBC aggregability from the various mammalian species can provide insight into the mechanisms of RBC aggregation. This measurement system of A-mode ultrasound in a cylindrical chamber with a stirring magnet is simple and requires relatively small amount of blood. It will also be useful to evaluate rat RBC aggregation in polymer solution which simulates hyper-aggregation in pathological states.

Chapter 4

EFFECTS OF HEMATOCRIT AND SHEAR RATE ON ULTRASONIC BACKSCATTER FROM RAT RBC IN AGGREGATING MEDIA

4.1. Introduction

In the last chapter, we have investigated ultrasonic backscatter from the mammalian blood of three species under rotational flow and suggested that the experimental setup may be useful to study RBC aggregation in small animals because it requires small quantity of blood (Nam et al. 2006). The study showed the differences in RBC aggregability among the three mammalian species in the order, horse > human > rat. The result was in agreement with the previous reports measured by Myrenne aggregometer (Baskurt et al. 1997; Windberger et al. 2003).

The aggregation characteristics of mammalian RBC exhibit a wide range among various species. Among them, porcine blood has a moderate aggregation tendency similar to human blood and can be obtained in large quantities required by the loop flow arrangement (Yuan and Shung 1988a), thereby many studies for RBC aggregation have been performed with porcine blood. However, there are some restrictions to obtain porcine blood from slaughterhouses and it is not easy to obtain it from many individuals to ensure a statistical confidence in experimental results.

Rats are widely used and well-documented as an experimental animal, and their blood can be easily obtained at our convenience. However, the aggregation of rat RBCs in plasma is very low or barely detectable due to the various factors in plasma (Windberger et al. 2003) and the higher electrostatic repulsion between rat RBCs than other mammalian RBCs (Baskurt et al.

1997). According to the recent report by Baskurt et al. (2000), the low RBC aggregability in rat blood could be successfully overcome by replacing the plasma with solutions of higher molecular weight polymers.

RBC aggregation is caused by the presence of a variety of macromolecules in plasma, especially fibrinogen. Similar aggregation can be mediated by artificial media such as solutions of dextran, PVP, poly (ethylene glycol) (PEG), poly-l-glutamic acid (P-L-Glu) (Rampling et al. 2004). Many investigators have reported the effects of polymer type, concentration, and molecular mass on RBC aggregation. Neu and Meiselman (2002) reviewed two typical aspects of polymer-induced RBC aggregation that include biphasic or bell-shaped response to polymer concentration and an increase of aggregation depending on molecular mass for a given polymer type. For human RBC, 3 % solution of dextran 70 has been commonly used as the standard suspending medium to test RBC aggregability. In case of rat RBC, the solutions of 0.75 % PVP 360 and 0.5 % dextran 500 were recommended as a standard aggregating media (Baskurt et al. 2000), since rat RBCs exhibit essentially no aggregation in dextran 70 solution at any range of concentration (Baskurt et al. 1997). The different response to polymer solutions between human and rat RBC can be partially explained by the model that combines electrostatic repulsion due to RBC surface charge with osmotic attractive forces due to polymer depletion near the RBC surface. That is because rat RBCs have higher negative charge on their surface than human RBCs, and depletion layer thickness and polymer penetration into the RBC glycocalyx can be varied by molecular mass of bulk phase polymer.

It is well established that the ultrasonic backscatter from RBCs suspended in saline initially increases with hematocrit, reaches a maximum in the range of 13-20 %, and decreases thereafter (Shung et al. 1984; Yuan and Shung 1988a; Mo et al. 1994; Wang and Shung 2001). Although the peak slightly shifted to the higher hematocrit due to turbulent flow by mesh screen in loop flow system and flow disturbance under stirring condition, the scattering peak did not

move beyond 20 % hematocrit.

For whole blood, where the backscattering is an index of RBC aggregation, the nonlinear relationship between the ultrasonic backscatter and hematocrit has been reported by a few investigators. In case of static conditions, the maximal aggregation was found to be varied over the hematocrit range of 15 to 50 % among the reports by different investigators. According to Deng et al. (1994), the aggregation intensity reached a plateau at 40 % hematocrit, where they used a light transmission technique and the cone-plate chamber as a shearing system. Donner et al. (1988) also reported direct correlation between hematocrit and RBC aggregation at hematocrit range of 30 to 50 % using light backscattering measurement and co-axial cylinder. On the other hand, the rate of echo intensity buildup was measured to be inversely related to hematocrit (Kim et al. 1989). This result is supported by the report from Sigel et al. (1981), where blood from anemic patients tends to form RBC rouleaux more readily than the normal blood does. In case of flowing condition that is available by ultrasound method, the linear relationship between the Doppler backscattered backscatter and hematocrit at the range of 5-40 % has been reported by Allard et al. (1996).

Up to now, the standardized experimental result as well as the mechanism for the hematocrit dependency on RBC aggregation in whole blood has not been fully established. In addition, the methodological discrepancy to measure RBC aggregation has been unresolved yet.

In this chapter, we tried to clarify the effects of hematocrit and shear rate on ultrasonic backscatter using rat RBCs suspended in aggregating media and the rotational flow as a shearing system.

4.2. Materials and Methods

4.2.1. Blood Preparation

Rat blood anticoagulated with EDTA was centrifuged at 3000 g for 15 min. The plasma was separated for resuspending the RBCs at different hematocrits. The buffy layers were removed by aspiration. To prepare RBC suspension in PVP 360 (Sigma-Aldrich, USA) solution, the RBCs were washed three times with isotonic phosphate buffered saline (PBS) with pH 7.4. Then, the washed concentrated RBCs were resuspended in plasma or in polymer solution containing 0.75 % PVP 360 in PBS at different hematocrit levels. All experiments were completed within 4 hours after collecting blood.

4.2.2. Flow System and Experimental Setup

The experimental setup was the same as described in Chapter 3, which contained the magnetic stirrer to spin the magnet, a cylindrical chamber (i.d. 14.5 mm, 0.1 mm thick polyester membrane) and a teflon-coated stirring magnet (diameter of 14 mm round type with a crucial projection on the top) at the bottom as shown in Fig. 16. To ensure the constant flow rate at the same sampling position, it should be noted that the magnetic stirrer fit the blood chamber.

Four ml of RBC sample was loaded into the chamber and the ultrasound transducer was mounted so as its focal center to be placed at 0.5 cm above the top of the magnetic stirrer.

4.2.3. Experimental Design and Analysis of RF Signal

The RBC samples resuspended in autologous plasma or PVP 360 solution at hematocrits of 5, 10, 20, 30 and 40 % were left in water bath for at least 15 minutes before making any measurements to allow blood temperature to reach 37 ℃. A series of experimental set for five hematocrits was able to be performed from each individual rat blood by serial addition of the packed RBCs and discarding the calculated volume of RBC sample in media.

Stirring speed was altered in six steps from 4 rps to stasis. The scattering window for calculating the backscattered power was selected between the tube center and the tube wall in

order to avoid multiple reflection from the tube wall and hyper-aggregation near the tube center. The backscattered power was calculated from the time domain signal by summing the squared values of the backscattered signal over the time window of 2 μs using ambient noise in water as a reference.

4.3. Results

Fig. 23 shows the backscattered power variation in autologous rat plasma as a function of time during the process of RBC aggregation. The centerlines at 300 seconds are the switching point from 4 or 1 rps to stasis. Upper panel represents the variation of the backscattered power following a sudden flow stoppage from 4 rps to stasis at five different hematocrt levels. For 5 minutes at 4 rps, the power increase was not observed as a function of time as well as hematocrit. After the flow stoppage, the magnitude of the backscattered power was not changed for about 3 minutes, and then it rapidly increased from 2 to 4 dB at 10 % hematocrit and from 2 to 3 dB at 5 % hematocrit, whereas no variations were observed at the hematocrit range of 20 to 40 %. At a stirring rate of 1 rps in lower panel, the backscattered power gradually increased from 2 to 3 dB and reached plateau after 2 minutes at 30 and 40 % hematocrit. After the flow was suddenly stopped, the power gradually decreased to the baseline, and in turn, increased to 4 and 5 dB at low hematocrit of 5 and 10 %, respectively. As seen in this result, at static conditions, the backscattered power was the highest at 10 % hematocrit at both prereduction stirring rate of 4 and 1 rps. At stirring rate of 1 rps, the power was higher at 30 and 40 % hematocrit. However, the power variations were less than 1 dB so that the exact tendency could not be well determined.

To enhance the aggregation level, rat plasma was replaced by 0.75 % PVP 360 solution. The results are shown in Fig. 24, where the effect of hematocrit and stirring rate on the

variations of the backscattered power was summarized. All zero times indicate the switching point from the prereduction stirring rate of 4 rps to the corresponding postreduction stirring rates. At higher stirring rate of 4 rps, no variation of the backscattered power was observed over 5 minutes, which was similar to those observed in Fig. 23 except for the slight increase in the baseline power. At the stirring rate of 1 to 3 rps, the power rapidly increased for the first 30 seconds and reached a plateau. The time to reach a plateau was increased by decreasing hematocrit. At 3 rps, there was an additional 11 dB increase in the backscattered power from zero to 5 minutes at 40 % hematocrit, and 3 to 4 dB at 5 to 30 % hematocrit. Between 1 and 2 rps, the backscattered power increased in inverse proportion to stirring rate at 5 to 40 % hematocrit.

The power variation as a function of time after a sudden flow stoppage is shown in Fig. 24 (f). At higher hematocrit levels of 30 and 40 %, the power increased steadily over 5 minutes up to 25 and 23 dB, respectively. At 10 % hematocrit, the fastest power increase up to 21 dB was observed within 2 minutes, followed by the power decrease due to the sedimentation of the majority of the RBC aggregates below the sampling point of RF signal, which was apparent to the naked eye. A similar tendency was observed at 5 and 20 % hematocrit, but the RBC sedimentation time was longer than that at 10 % hematocrit. As a result, the sudden flow stoppage caused less steep increase of the backscattered power than flowing conditions did, with the order of 10 > 20 > 5 > 30 ≥ 40 % hematocrit. Therefore, the aggregation tendency at shearing conditions that is proportionate to hematocrit was not applicable to the stasis condition. Rather, it showed a reverse correlation at the hematocrit range between 10 and 40 %. Fig. 25 and 26 show the variation of the backscattered power obtained by averaging of 100 - 120 seconds data in Fig. 24, as a function of stirring rate and hematocrit, respectively. From these integrated figures, the ultrasonic backscatter from RBC aggregation can be well explained as a function of hematocrit and shear rate.

Fig. 27 is the typical echo images that represent the radial and temporal variation of RBC aggregation in PVP 360 solution at various hematocrit levels and stirring rates. The echo images at 40 % hematocrit showed the similar profiles with those from horse blood in Chapter 3. Clear dark zones at higher hematocrit were seen along the tube center, which were expanded toward the tube wall with lowering the stirring rate. Overall echogenicities were gradually increased by hematocrit increase and flow reduction. In Fig. 27 (c) 0 rps, the echogenicity slightly increased after the sudden flow stoppage over 5 minutes. At 10 % hematocrit, the echogenicity was most quickly enhanced. The rate of echo buildup decreased with hematocrit at the range of 10 - 40 %. At 20 and 30 % hematocrit, the dark profile along the tube center that looked like a tail may be due to low shear rate near the tube center.

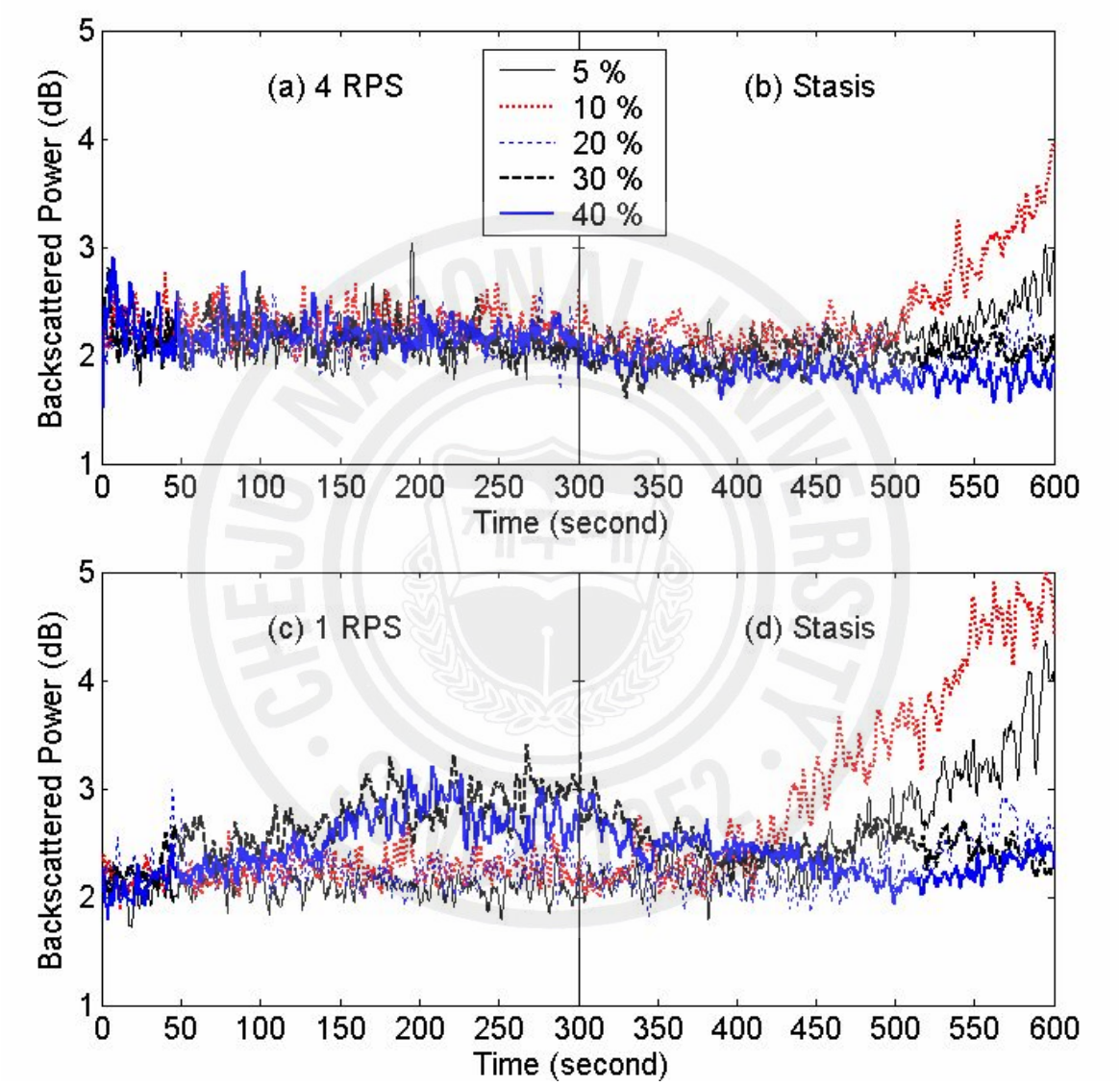

Fig. 23. The variation of backscattered power as a function of hematocrit from flowing and static rat RBCs in autologous plasma. The vertical lines at 300 seconds indicate the flow stoppage point. For each curve, averaging was performed over 10 experiments.

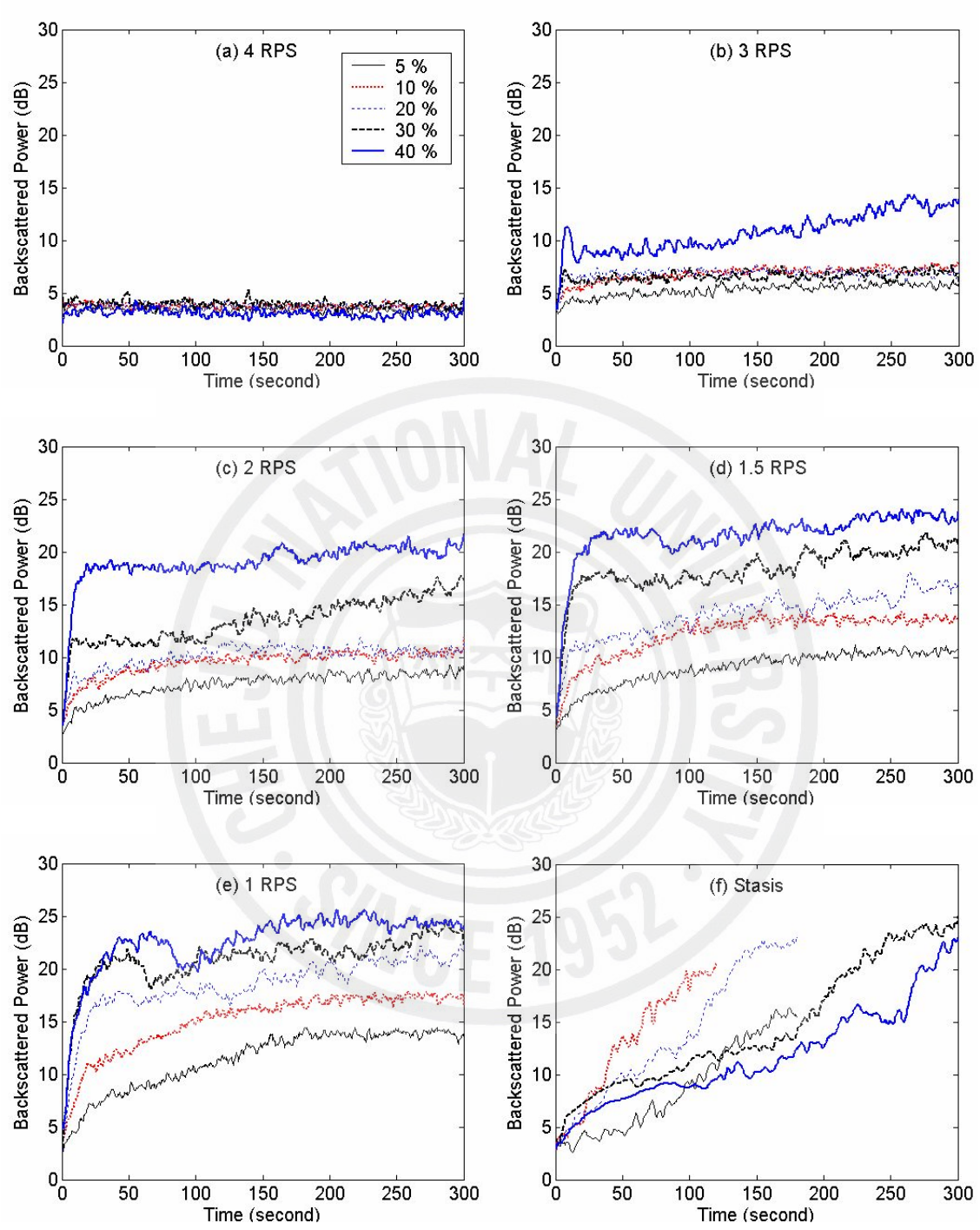

Fig. 24. The variation of backscattered power as a function of hematocrit for rat RBCs in 0.75 % PVP 360 solution. All zero times indicate the swiching point from 4 rps to sudden flow reduction or stoppage. For each curve, averaging was performed over 6 experiments.

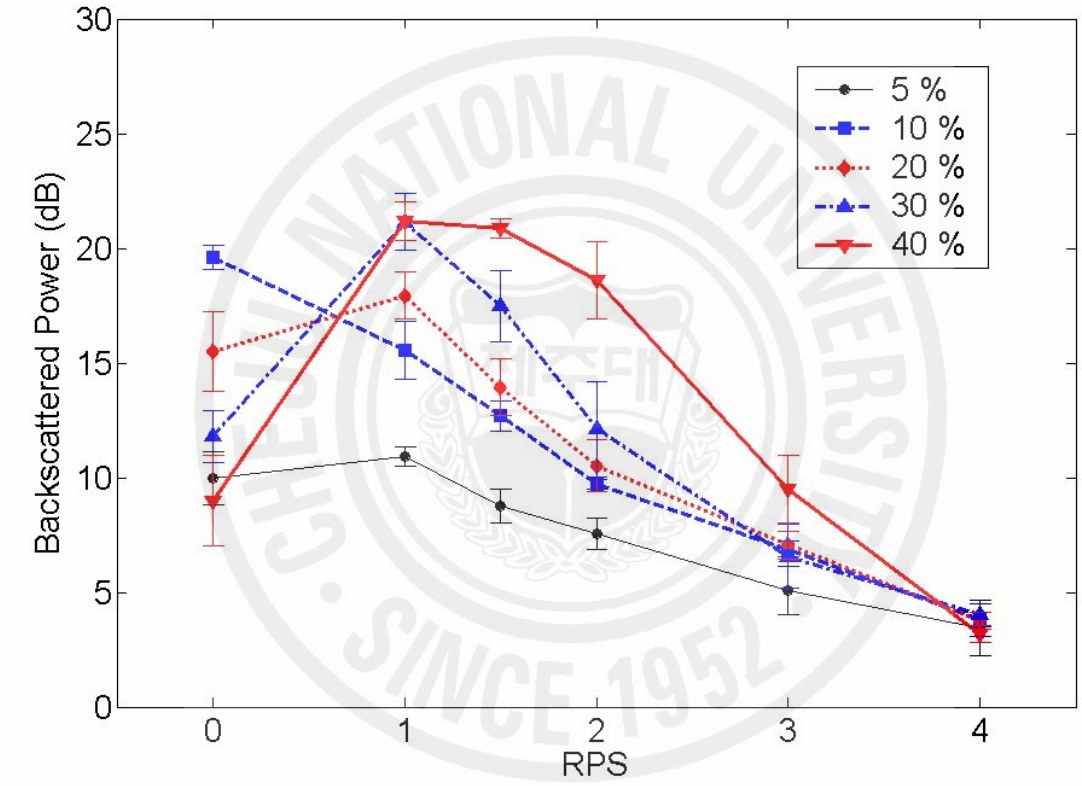

Fig. 25. Backscattered power as a function of stirring rate at hematocrit range between 5 and 40 %. Each plot represents the mean ± S.D. (n=6).

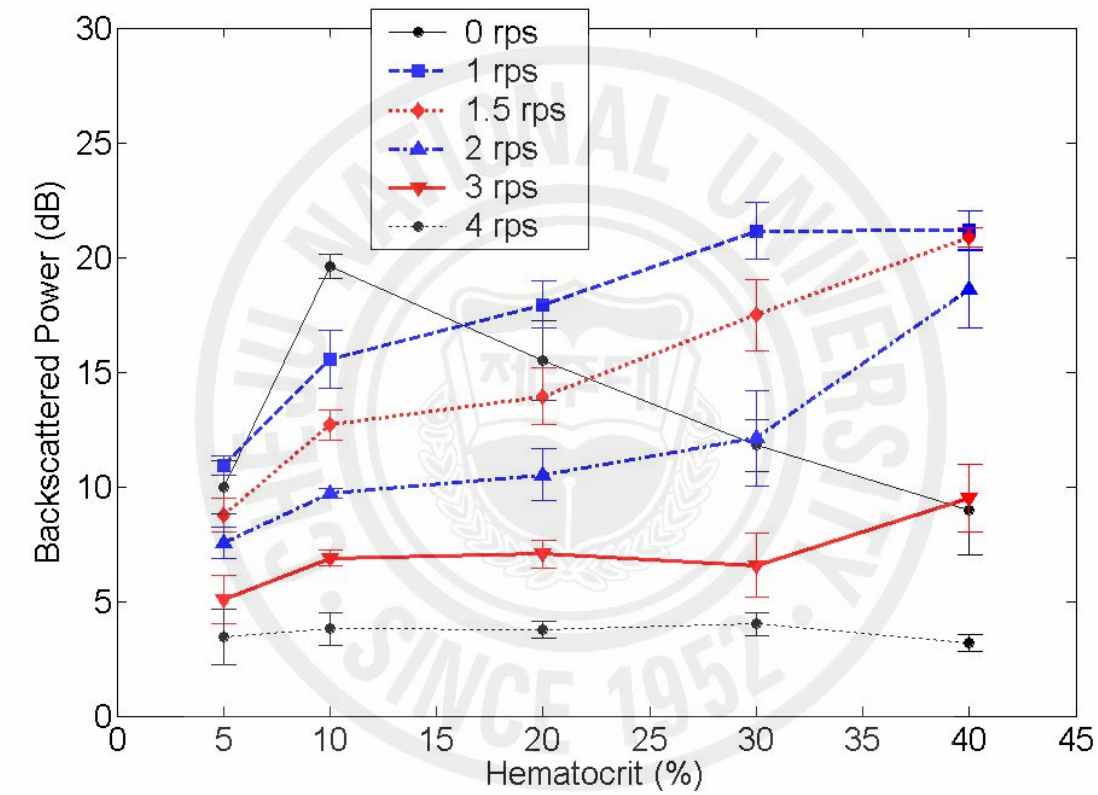

Fig. 26. Backscattered power as a function of hematocrit at stirring rate range between 0 and 4 rps. Each plot represents the mean ± S.D. (n=6).

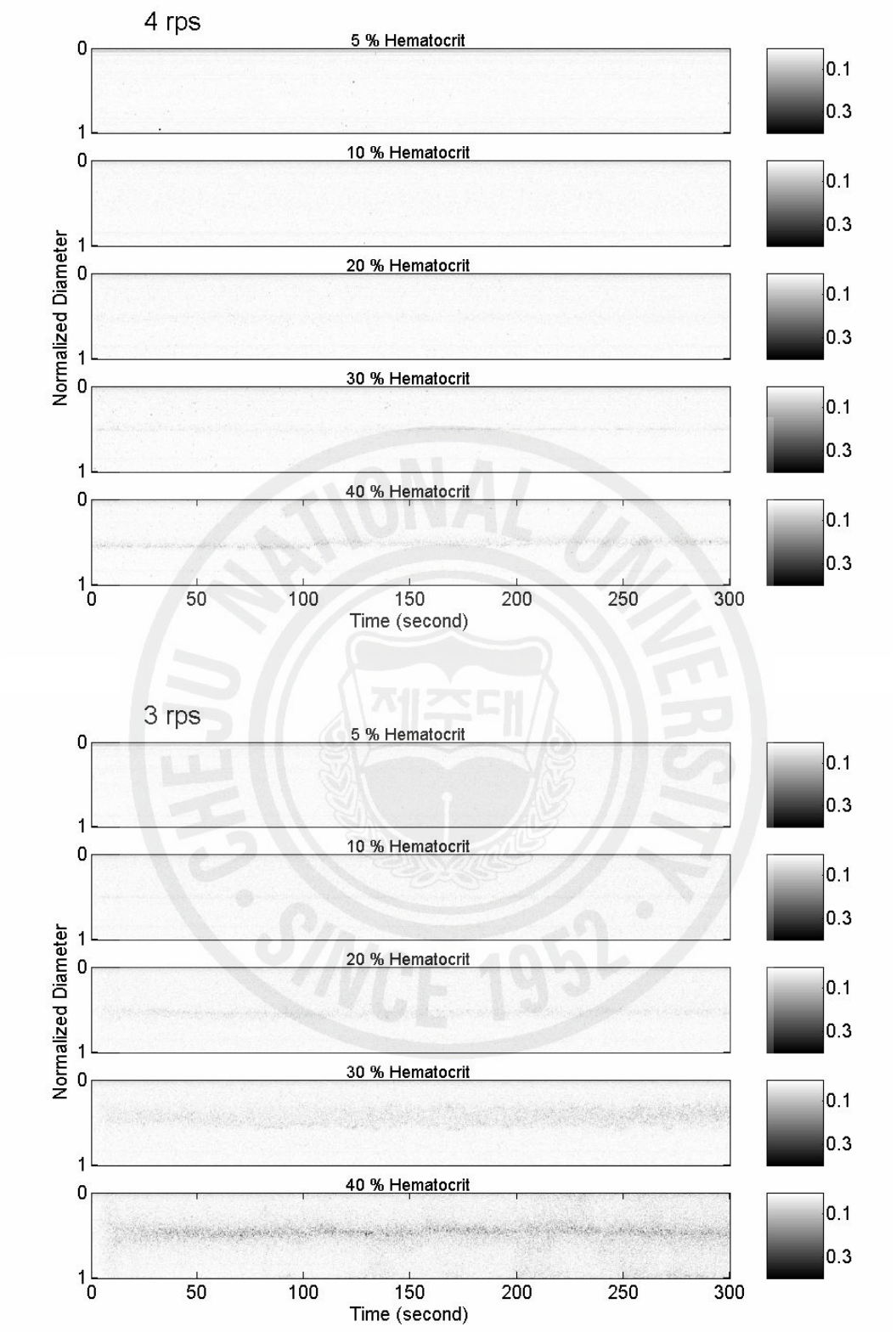

Fig. 27 (a). Typical echo imges from rat RBCs in 0.75 % PVP 360 solution at various hematocrit with stirring rates of 4 and 3 rps. Each image consists of 600 RF signal lines for 5 minutes. The gray scale corresponds to the enveloped amplitude of RF signal.

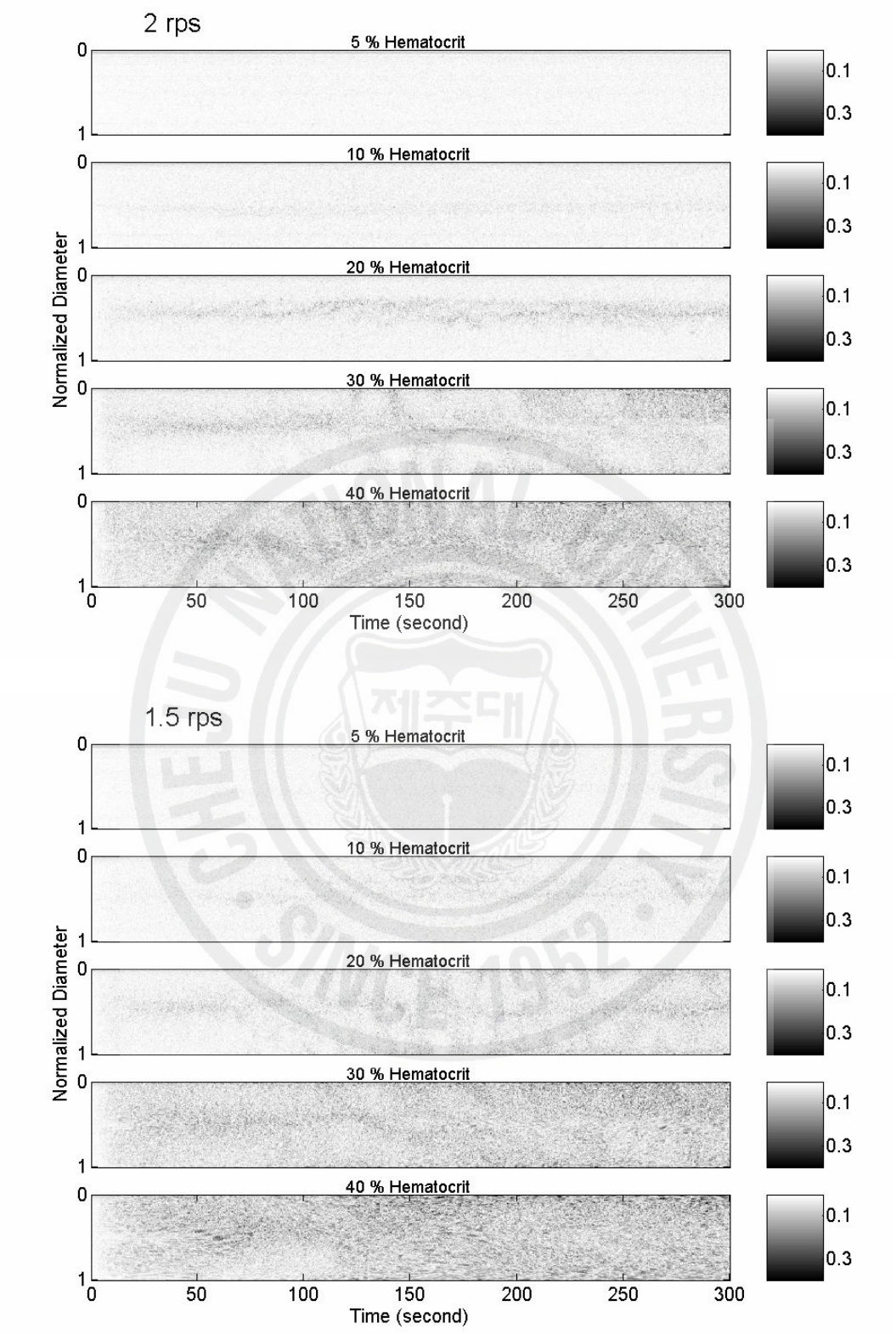

Fig. 27 (b). Typical echo imges from rat RBCs in 0.75 % PVP 360 solution at various hematocrit with stirring rates of 2 and 1.5 rps. Each image consists of 600 RF signal lines for 5 minutes. The gray scale corresponds to the enveloped amplitude of RF signal.

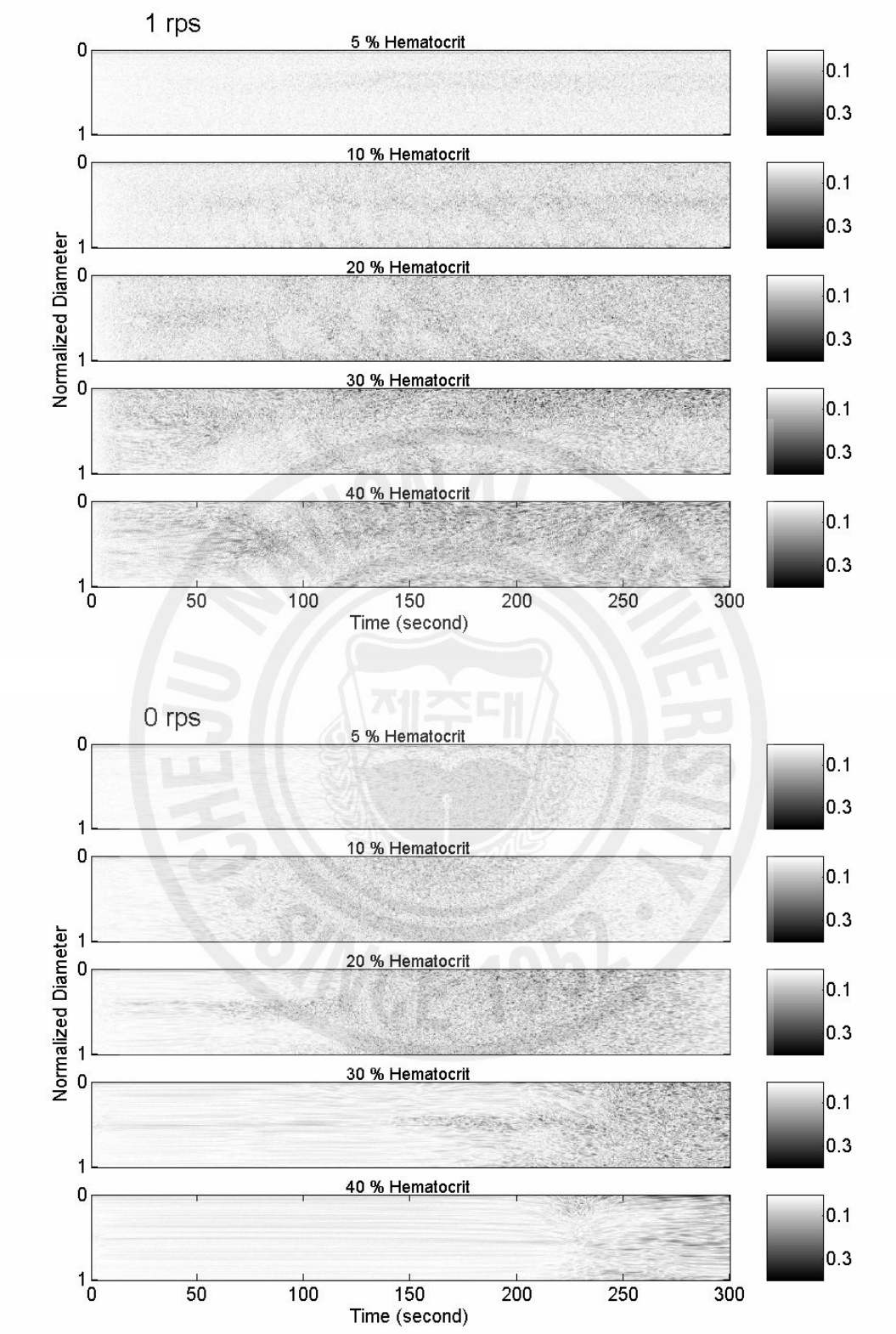

Fig. 27 (c). Typical echo imges from rat RBCs in 0.75 % PVP 360 solution at various hematocrit with stirring rates of 1 and 0 rps. Each image consists of 600 RF signal lines for 5 minutes. The gray scale corresponds to the enveloped amplitude of RF signal.

4.4. Discussion

Until now, most studies of RBC aggregation by ultrasound have been performed in a mock flow loop, since the shear rate could be well defined and easily controlled using this flow system and flow disturbance that may affect the scattering from blood could also be avoided (Shung et al. 1984). However this system requires large volume of blood sample and complex experimental setup to ensure proper flow condition (Shehada et al. 1994; Cloutier et al. 2004). As a simple alternative method, a mixing chamber sheared by rotational flow has been employed to study RBC aggregation by several investigators (Yuan and Shung 1988; Fatkin et al. 1997; Wang and Shung 2001; Rastegar et al. 2003). According to the report by Shung et al. (1984), the major drawbacks of this arrangement were that the shear rate is unknown and the stirring bar would cause the flow disturbance. Nonetheless, they suggested that the results obtained with this arrangement are still valuable if a general relationship between them and those for conduit flow can be established because this arrangement is considerably simpler and the required amount of blood is more reasonable for measurements on human blood. More recently, the same arrangement was successfully applied to examine the backscatter of whole blood and RBC suspension as a function of hematocrit ranging from 3 to 50 % at two spinning rate of 200 and 300 revolution per minutes (rpm) (Wang and Shung 2001). There were also two applications to investigate the pathogenesis of spontaneous echocardiographic contrast in a mixing chamber under rotational flow, where they well demonstrated the effects of plasma factors and antithrombotic therapy on RBC aggregation using echocardiographic images (Fatkin et al. 1997; Rastegar et al. 2003). In addition, the present chapter as well as the previous chapter (Nam et al. 2006) showed that the rotational shearing system could be well applicable to study RBC aggregation.

According to the previous report (Yuan and Shung 1988a), the bovine RBCs in whole

blood could be considered as small scatterers like RBCs in saline suspension due to their very low aggregability. Since rat RBCs have a similar aggregation level to bovine RBCs (Windberger et al. 2003), the scattering peak at 13-20 % hematocrit should be observed theoretically. However, the result at 4 rps in Fig. 23 shows no difference in the baseline powers among five hematocrit levels of 5 to 40 %. This phenomenon was also observed at stasis up to 2 minutes. We assume that this may be different from the well-known nonlinear function of the backscattering from RBC suspension with hematocrit, showing a scattering peak around 13-20 % hematocrit, because rat blood may include small portion of RBC aggregates. In this case, the baseline power may be decided by the compound interaction of the nonlinear function of the backscattering and the hematocrit dependency of RBC aggregation. In addition, the differences in RBC origin and shearing system should also be considered. The same baseline level of the backscattered power among 4 rps, 1 rps and stasis indicates that the effect of flow turbulence on our flow system is negligible or the 5 MHz transducer is less sensitive to flow turbulence. Therefore, we did not take account of the effect of flow disturbance in the result analysis.

Kim et al. (1989) showed that the echo intensity from human static blood is varied inversely with hematocrit range of 15 to 60 %, where blood was sheared by oscillatory flow in a distensible horizontal tube. They suggested two possible explanations for the inverse correlation between the rate of aggregate formation and hematocrit; the decrease in the total amount of fibrinogen as hematocrit increases and the greater freedom of motion of RBCs at lower hematocrit levels. This phenomenon is agreed with our result in Fig. 23 (b) and (d) that shows the maximal power buildup at 10 % hematocrit. By replacing the plasma with 0.75 % PVP 360 solution as an aggregating media, the backscattered power was remarkably increased up to 25 dB so that the hematocrit dependency of RBC aggregation was observed more strikingly at hematocrit range of 10 to 40 %. Kitamura et al. (1995) also showed that hematocrit affected the rate of aggregate formation whereas fibrinogen controlled aggregate size. Their result is in

agreement with our result and the report by Kim et al. (1989).

Doppler backscattered power from porcine whole blood was measured in a closed steady flow loop model at mean shear rate of 8.5 to 51 s^{-1} (Allard et al. 1996). They showed that the power increased in proportion to hematocrit from 5 to 40 %. This phenomenon is similar to the present result from autologous plasma shown in Fig. 23 (c), even though the difference in dB is very small below 1 dB. That was more clearly demonstrated by replacing the plasma with 0.75 % PVP 360 solution [Fig. 24 (a)-(e)]. At stirring rate of 1 to 3 rps, it should be noted that the relative power variations between 40 % and the lower hematocrit levels were gradually reduced by lowering stirring rate, which were more prominent when the power variation at 30 % hematocrit was compared with that at 40 % hematocrit, showing almost same level at 1 rps. This consistent change from 3 to 1 rps seems to correlate to the inverse relationship between hematocrit and the backscattered power at static condition in Fig. 24 (f). Lim et al. (1997) suggested that collision rate of RBCs under flowing condition may be mainly dependent on shear rate because of the relatively negligible influence of Brownian motion, whereas that may be subject to freedom of motion at stasis (Kim et al. 1989). This assumption seems to well explain the complicated relationship on RBC aggregation between hematocrit and shear rate. In that sense, Fig. 24 - 26 provide a good evidence for the rationale.

The previous report by Kim et al. (1989) also showed the direct correlation between hematocrit and RBC aggregation at shearing condition. However, the report by Kim et al. (1989) was performed at only two hematocrits of 30 and 43 % and the shear rate range from 20 to 125 s^{-1} in their report was not ideal one to study RBC aggregation because shear rate above 20 s^{-1} may disrupt a major portion of aggregates (Yuan and Shung 1988a). Wang and Shung (2001) reported that the scattering peak appeared at 20 to 30 % hematocrit when the whole blood was sheared in a mixing chamber at two spinning rate of 200 and 300 rpm. It is assumed that the discrepancy between this result and others may be caused by the difference of the

shearing system.

Fig. 23 (d) shows the power decrease at hematocrit of 30 and 40 % for 1 minute after a sudden flow stoppage. This phenomenon may result from RBC disaggregation due to the repulsive force by the higher negative charge on rat RBC surface (Baskurt et al. 1997). More studies are needed to prove the validity.

In Fig. 27, the echogenic contrast between the dark zone and the surrounding region may be explained by the distribution of RBC rouleaux caused by radial variation of shear rate. The flow velocity in a cylindrical chamber varies from center to the tube wall along the radial direction. The shear rate at the far point from the center is higher than at the center, so that low shear rate around the tube center may cause higher RBC aggregation. These echo images show that ultrasound is much superior to optical technique in that it can penetrate light opaque structures like blood.

Based on the previous reports and our results determined by ultrasonic measurement, it suggested that the extent and rate of aggregate formation increases in proportion to hematocrit (range of 10 to 40 %) at higher shear rate but in inverse proportion to hematocrit at very low shear rate or at stasis. On the other hand, the experimental results using optical technique have shown that RBC aggregation increased in proportion to hematocrit at static condition (Donner et al. 1988; Deng et al. 1994). The discrepancy between the two methods may result in the differences of shearing system and wave source for RBC scattering. More researches are necessary to make clear this uncertainty.

4.5. Conclusions

The experimental setup using rotational flow and rat RBC suspension in aggregating media is simple and requires relatively small amount of blood so that it may be useful to study the pathophysiological roles and the mechanisms of RBC aggregation. The present study demonstrated that the relationship between hematocrit and rat RBC aggregation is varied by shear rate. However, an extended study is needed to clarify our result in human blood.

Chapter 5

INHIBITORY EFFECT OF DIDS ON RBC AGGREGATION DETERMINED BY ULTRASONIC BACKSCATTER

5.1. Introduction

The rheological property of Blood is complex and mainly determined by hematocrit, RBC aggregation, deformability, and viscosity. Among them, RBC aggregation is one of the important hemorheological determinants that may cause problems at the level of microcirculation (Puniyani et al. 1991; Lipowsky 2005). Pathologically, hyperaggregation may reduce capillary perfusion and oxygen transfer to tissues and result in ischemia, local metabolic acidosis, degeneration of vascular wall, and tissue infarction (Soutani et al. 1995). Therefore, it is increasingly recognized that drugs that influence cardiovascular outcomes act not only on atheromatous plaques and adjacent thrombi, but also on the microcirculation, via reduction of RBC aggregation and of whole blood viscosity. Those kinds of pharmacological approaches to the elevated RBC aggregation have been a subject of investigation in recent years.

Lovastatin (Martinez et al. 1996), ticlopidine (Hayakawa and Kuzuya 1991), quinapril (Korbut et al. 2003), troxerutine (Durussel et al. 1998), and dipyridamole (Bozzo et al. 1996) are known to decrease elevated RBC aggregation. The action mechanisms of these drugs are still unknown, but it can be assumed that the degradation of fibrinogen, RBC deformation, and the attachment of drugs to RBC membrane are possible reasons. Aspirin has been intensively studied as an anti-platelet agent, but its effect on RBC aggregation has not been well studied. Bozzo et al (1996) and Korbut et al. (2003) reported that treatment with aspirin *in vitro* and *in vivo* significantly increased RBC aggregability. They suggested that aspirin was probably bound

to RBC membrane, thereby modifying their electrical charges that would account for the increase in RBC aggregation. On the other hand, Fatkin et al. (1997) reported an inconsistent result with the above studies that aspirin did not affect RBC aggregation.

In spite of these devoted studies, there is still an unresolved problem in the methodology to measure RBC aggregation. To fully understand the relationship between RBC aggregation and drugs, the application of a flow system appears to be extremely important. Most of the measurements employed in the previous studies to assess the effects of drugs on RBC aggregation are often carried out under static conditions by photometry, which may provide limited information or sometimes result in a discrepancy among the experiments. Ultrasound techniques allow this limitation to be overcome by exposing the blood under flow conditions. To evaluate the effects of drugs on RBC aggregation, we used our simplified method in Chapter 4 based on ultrasound measurement and rotational flow system.

5.2. Materials and Methods

The procedures to obtain rat blood and the post-processs to prepare the RBC suspension were the same as described in Chapter 4. The same ultrasound measurement setup was used in this chapter. RBC suspension of 10 % hematocrit in 0.75 % PVP 360 PBS solution (pH 7.4) was used for the experiments. That is because the result in Chapter 4 indicated that the rate of aggregate formation is the fastest at 10 % hematocrit and, by using the RBC suspension with low hematocrit, rat blood can be saved. For the inhibition experiments, the 4,4,-diisothiocyanatostilbene-2,2'-disulfonic acid (DIDS) disodium salt (Invitrogen, USA) was used as an aggregating inhibitor, which is known to cause RBC shape alterations by inducing echinocytosis (Blank et al. 1994) and to inhibit anion transport in a similar way to dipyridamole (Falke and Chan 1986). DIDS was dissolved in dimethylsulfoxide (DMSO) and diluted to 0.2, 2

and 20 mM. Four μl of each DIDS solution was added into 4 ml of 10 % RBC suspension (finally 0.2, 2, and 20 μM). Then, the RBC suspension with DIDS was incubated for 30 minutes at 37 ℃ before measuring the backscattered signals. RBC aggregation was induced at stirring rate of 1 rps and under static condition.

Student's t-test was employed to determine the statistical significance, and $p < 0.05$ or $p < 0.01$ was considered to be statistically significant.

5.3. Results and Discussion

The inhibitory effect of DIDS on RBC aggregation was determined by ultrasound backscattering measurement. At the stirring rate of 1 rps, the backscattered power from both normal and DIDS-treated RBC suspension rapidly increased for the first 30 seconds and then reached a steady state (Fig. 28). The backscattered power decreased with increasing DIDS concentration. The backscattered power level from 0.2 μM DIDS-treated RBC suspension was slightly lower than that from the normal group. Fig. 29 shows the mean backscattered power that was calculated by averaging the values for 3-5 minutes in Fig. 28. In all DIDS-treated groups, the mean backscattered power significantly decreased in comparison with normal group, which clearly showed a dose-dependent response. When the flow was suddenly stopped (Fig. 30), the power gradually increased over 2 minutes. The variation of backscattered power was inversely proportionate to the DIDS concentration, which was similar to the result at 1 rps condition. Especially, at the highest concentration of 20 μM DIDS, there was no variation for 2 minutes after treatment of DIDS. Fig. 31 shows the slopes that were calculated from the time-backscattered power graph in Fig. 30. The significant differences were observed at 2 and 20 μM DIDS-treated groups compared with normal group. DMSO did not affect the ultrasonic backscatter from RBC samples so that we could rule out the unexpected effect of the solvent on

RBC aggregation.

In conclusion, we explored an alternative measuring method for RBC aggregation that is convenient and useful to determine the effect of drugs on RBC aggregation. The mean backscattered power under flowing condition and the temporal slope of backscattered power curve at stasis are thought to be proper indexes comparing the relative levels of RBC aggregation.

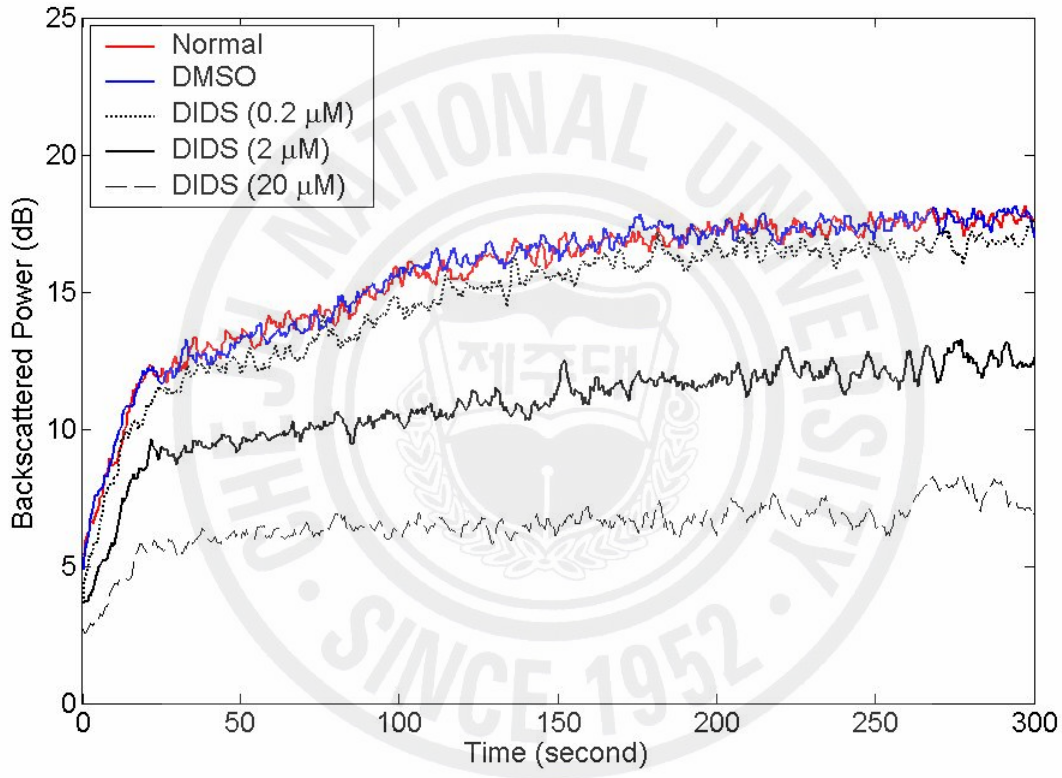

Fig. 28. The variation of backscattered power as a function of time from rat RBC suspension in 0.75 % PVP 360 solution. Zero time indicates the switching point from 4 rps to 1 rps. For each curve, averaging was performed over 6 experiments.

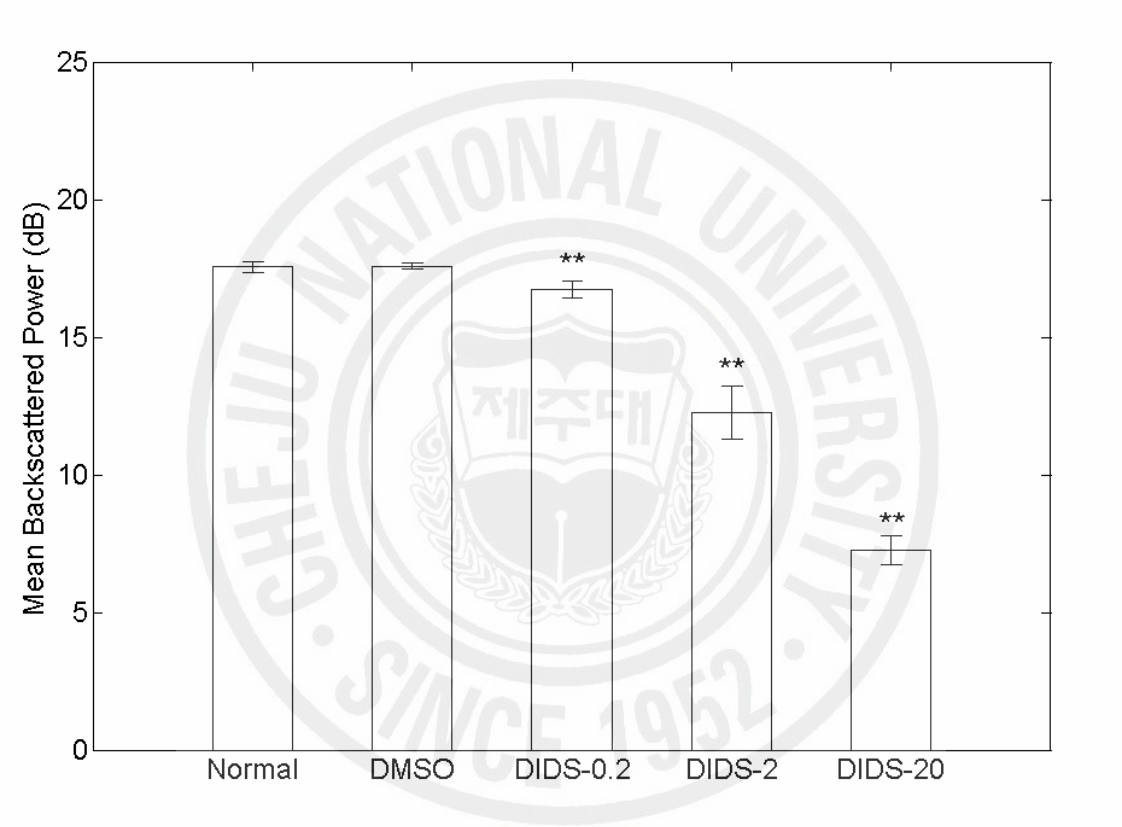

Fig. 29. Mean backscattered power obtained by averaging of last 2 minutes data in Fig. 28. Each value represents the mean ± S.E. (n=6). **p<0.01 versus normal group.

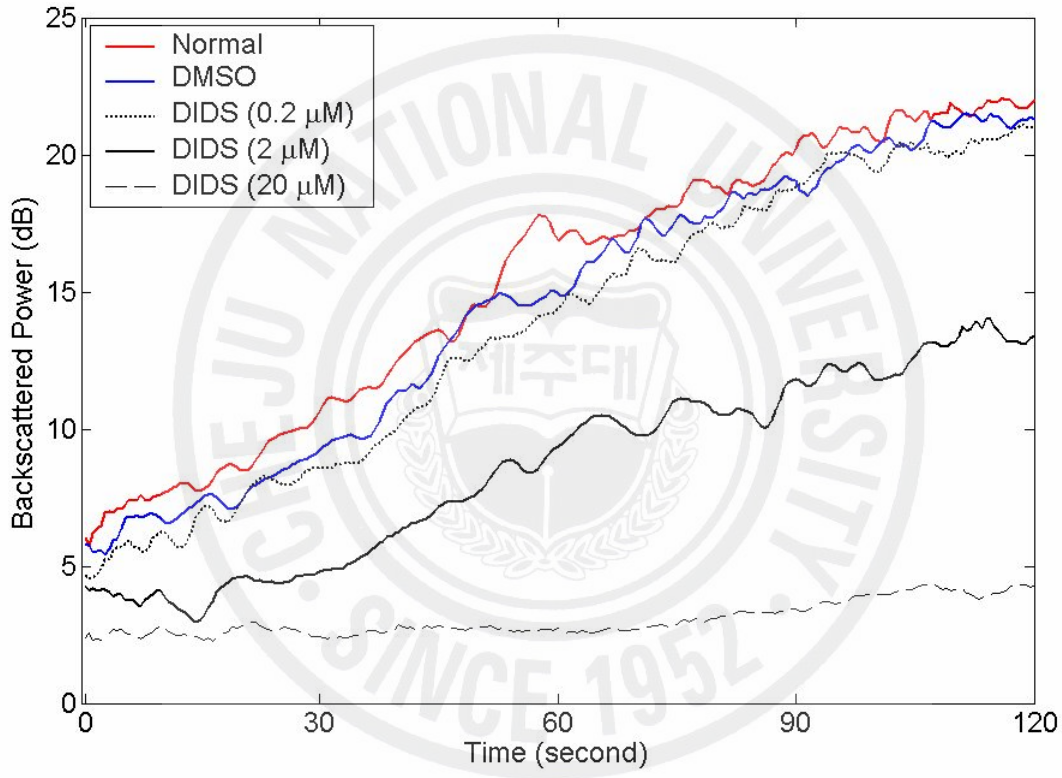

Fig. 30. The variation of backscattered power as a function of time from rat RBC suspension in 0.75 % PVP 360 solution. Zero time indicates the switching point from 4 rps to 0 rps. For each curve, averaging was performed over 6 experiments.

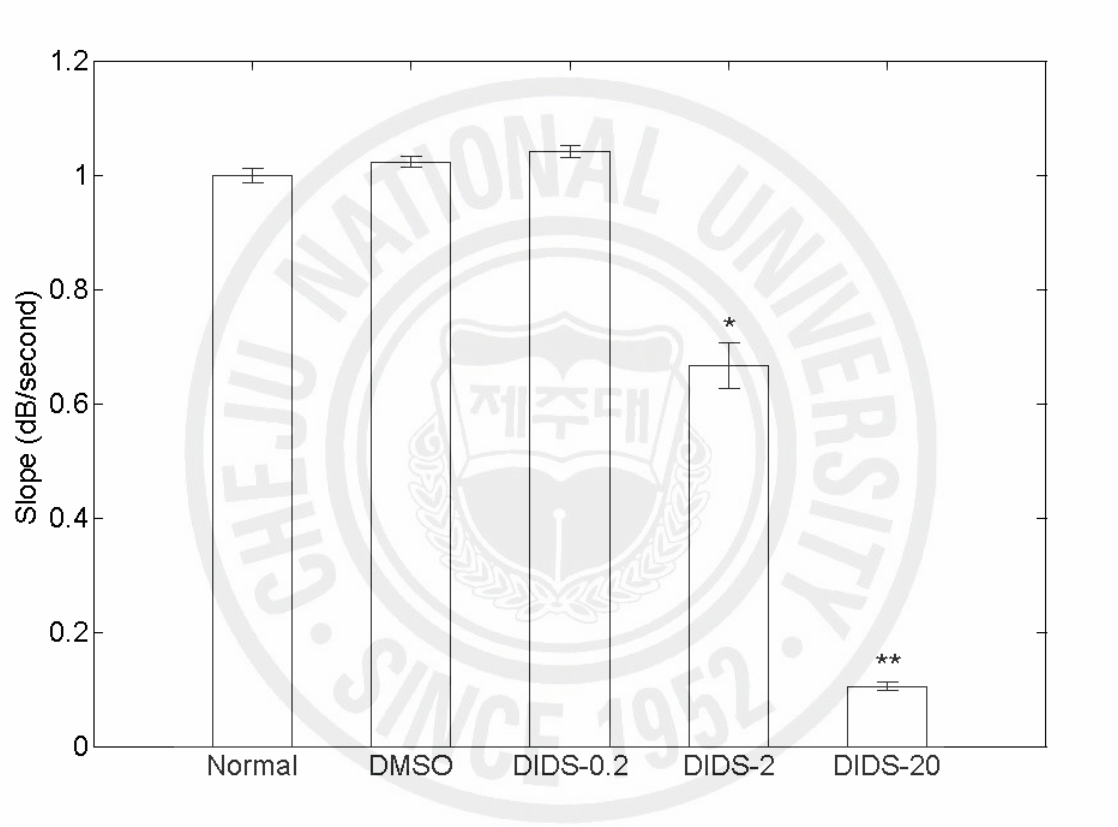

Fig. 31. Slopes of the backscattered power buildup in Fig. 30. Each value represents the mean ± S.E. (n=6). *p<0.05 and **p<0.01 versus normal group.

Chapter 6

CONCLUSIONS

In this research, the influences of hemodynamics and hematocrit on RBC aggregation have been investigated by ultrasonic measurements. A mock flow loop with an eccentric stenosis was employed to examine the effects of flow turbulence, shear rate, and flow acceleration on the backscattering characteristics from whole blood. A modified measurement system that requires smaller amount of blood was developed and verified. Using this simplified method, the studies were extended to measure the RBC aggregation of three mammalian species and hematocrit dependency of RBC aggregation, in addition to its pharmacological applications.

The principle idea for the stenotic model was to characterize the echogenic variation upstream and downstream that reflects spatial and temporal distribution of RBC aggregates around a stenosis. On the measurements from post-stenotic site, the spatial and cyclic variation of echogenicity may indicate the compound effects of flow turbulence, acceleration, and shear rate. The sudden increase of the echogenic variation 3D downstream from the stenosis is thought to be due to flow turbulence. The migration of bright parabolic profile during systole of every pulsatile cycle may indicate the formation of RBC aggregation by flow acceleration, which may be another evidence that flow acceleration is an important factor to form RBC aggregation in flowing conditions. On the other hand, the echogenic variations at pre-stenotic site were differentiated from the previous studies dealing with blood flows downstream. The disturbance of blood flow and RBC aggregation upstream was induced by the weak backward flow upstream of a stenosis. The reconstructed 3-dimensional images manifest the ‘bright ring’ phenomenon and the parabolic profile, which may be attributed to complicated hemodynamics including shear rate and flow acceleration.

Using the rotational shearing system and a pulse-echo setup with a 5 MHz transducer, the ultrasonic backscatter from RBC aggregation was successfully measured, which might practically be useful to repeat the experiments for statistical analysis using blood of small animals or human. The result from three mammalian species of human, horse, and rat has assured the usefulness of this measurement setup in comparison with the previous photometric measurements. Ultrasonic backscatter from rat RBCs in autologous plasma and in aggregating media was measured as a function of hematocrit as well as shear rate. Although the intact rat blood has poor RBC aggregability, it was overcome by replacing its plasma with a higher molecular weight polymer solution. The experimental results showed that the nonlinear relationship between hematocrit and ultrasonic backscatter is subject to shear rate, which may provide a unified insight to hematocrit dependency of RBC aggregation in flowing and static conditions. The usefulness of the measurement setup was also well verified by the dose-dependent study using aggregation inhibitor, which may be applicable to the screening method to examine the effect of drugs on RBC aggregation.

BIBLIOGRAPHY

Ahmed S. An experimental investigation of pulsatile flow through a smooth constriction. Exper Therm Fluid Sci 1998;17:309-318.

Allard L, Cloutier G, Durand L-G. Effect of the insonification angle on the Doppler backscattered power under red blood cell aggregation conditions. IEEE Trans Ultrason Ferroelet Freq Contr 1996;43:211-219.

Andrews FM, Korenek NL, Sanders WL, Hamlin RL. Viscosity and rheologic properties of blood from clinically normal horses. Am J Vet Res 1992;53:966-970.

Angelsen BA. A theoretical study of the scattering of ultrasound from blood. IEEE Trans Biomed Eng 1980;27:61-67.

Armstrong JK, Meiselman HJ, Fisher TC. Evidence against macromolecular "bridging" as the mechanism of red blood cell aggregation induced by nonionic polymers. Biorheology 1999;36:433-437.

Asada Y, Sumiyoshi A. Histopathology of thrombotic vascular diseases. Nippon Rinsho 1999;57:1555-1560.

Bascom PAJ, Cobbold RSC. On a fractal packing approach for understanding ultrasonic backscattering from blood. J Acoust Soc Am 1995;98:3040-3049.

Bascom PAJ, Johnston KW, Cobbold RSC, Ojha M. Relation of the flow field distal to a moderate stenosis to the Doppler power. Ultrasound Med Biol 1997;23:25-39.

Baskurt OK, Bor-Kucukatay M, Yalcin O, Meiselman HJ, Armstrong JK. Standard aggregating media to test the "aggregability" of rat red blood cells. Clin Hemorheol Microcirc 2000;22:161-166.

Baskurt OK, Farley RA, Meiselman HJ. Erythrocyte aggregation tendency and cellular properties in horse, human, and rat: A comparative study. Am J Physiol 1997;273:H2604-

H2612.

Baskurt OK, Meiselman HJ. Blood rheology and hemodynmics. Semin Thromb Hemost 2003;29:435-450.

Baskurt OK, Temiz A, Meiselman HJ. Red blood cell aggregation in experimental sepsis. J Lab Clin Med 1997;130:183-190.

Baumler H, Donath E, Krabi A, Knippel W, Budde A, Kiesewetter H. Eletrophoresis of human red blood cells and platelets. Evidence for depletion of dextran. Biorheology 1996;33:333-351.

Baumler H, Neu B, Donath E, Kiesewetter H. Basic phenomena of red blood cell rouleaux formation. Biorheology 1999;36:439-442.

Berger NE, Lucas RJ, Twersky V. Polydisperse scattering theory and comparisons with data for red blood cells. J Acoust Soc Am 1991;89:1394-1401.

Berger SA, Jou L-D. Flows in stenotic vessels. Annu Rev Fluid Mech 2000;32:347-382.

Blank ME, Hoefner DM, Diedrich DF. Morphology and volume alterations of human erythrocytes caused by the anion transporter inhibitors, DIDS and p-azidobenzylphlorizin. Biochim Biophys Acta 1994;1192:223-233.

Boynard M, Leliere JC. Size determination of red blood cell aggregates induced by dextran using ultrasound backscattering phenomenon. Biorheology 1990;27:39-46.

Bozzo J, Hernandez MR, Del Giorgio A, Ordinas A. Red blood cell aggregability is increased by aspirin and flow stress, whereas dipyridamole induces cell shape alterations: measurements by digital image analysis. Eur J Clin Invest 1996;26:747-754.

Brooks DE, Russell G, Janzen G, Janzen J. Mechanisms of erythrocyte aggregation. In Erythrocyte Mechanics and Blood Flow. Cokelet GR, Meiselman HJ, Brooks DE, editors. Liss AR, Inc., New York. 119-140.

Cao P-J, Paeng D-G, Shung KK. The 'black hole' phenomenon in ultrasonic backscattering

measurement under pulsatile flow with porcine whole blood in a rigid tube. Biorheology 2001;38:15-26.

Chabanel A, Horellou MH, Conard J, Samama MM. Red blood cell aggregability in patients with a history of leg vein thrombosis: influence of post-thrombotic treatment. Br J Haematol 1994;88:174-179.

Chen S, Barshtein G, Gavish B, Mahler Y, Yedgar S. Monitoring of red blood cell aggregability in a flow-chamber by computerized image analysis. Clin Hemorheol 1994;14:497-508.

Chien S. Electrochemical interactions and energy balance in red blood cell aggregation. In Topics in Bioelectrochemistry and Bioenergetics. John Wiley & Sons, Chichester, New York, Brisbane, Toronto. 73-112.

Cloutier G, Allard L, Durand L-G. Changes in ultrasonic Doppler backscattered power downstream of concentric and eccentric stenosis under pulsatile flow. Ultrasound Med Biol 1995;21:59-70.

Cloutier G, Allard L, Durand L-G. Characterization of blood flow turbulence with pulsed-wave and power Doppler ultrasound imaging. J Biomech Eng 1996;118:318-325.

Cloutier G, Daronatand M, Savery D, Garcia D, Durand LG, Foster FS. Non-Gaussian statistics and temporal variations of the ultrasound signal backscattered by blood at frequencies between 10 and 58 MHz. J Acoust Soc Am 2004;116:566-577.

Cloutier G, Qin Z, Garcia D, Soulez G, Oliva V, Durand L-G. Assessment of arterial stenosis in a flow model with power Doppler angiography: accuracy and observations on blood echogenicity. Ultrasound Med Biol 2000;26:1489-1501.

Cloutier G, Savery MDD, Garcia D, Durand L-G, Foster FS. Non-Gaussian statistics and temporal variations of the ultrasound signal backscattered by blood at frequencies between 10 and 58 MHz. J Acoust Soc Am 2004;116:566-577.

Davies PF, Remuzzi A, Gordon EJ, Dewey CF Jr, Gimbrone MA Jr. Turbulent fluid shear stress

induces vascular endothelial cell turnover in vitro. Proc Natl Acad Sci 1986;83:2114-2117.

Deng LH, Barbenel JC, Lowe GDO. Influence of hematocrit on erythrocyte aggregation kinetics for suspensions of red blood cells in autologous plasma. Biorheology 1994;31:193-205.

Donath E, Kuzmin P, Krabi A, Voigt A. Electrokinetics of structured interfaces with polymer depletion-a theoretical study. Coll Polym Sci 1993;271:930-939.

Donner M, Siadat M, Stoltz JF. Erythrocyte aggregation: approach by light scattering determination. Biorheology 1988;25:367-375.

Durussel JJ, Berthault MF, Guiffant G, Dufaux J. Effects of red blood cell hyperaggregation on the rat microcirculation blood flow. Acta Physiol Scand 1998;163:25-32.

Evans E, Berk D, Leung A, Mohandas N. Detachment of agglutinin-bonded red blood cells. Biophys J 1991;59:849-860.

Fabry TL. Mechanism of erythrocyte aggregation and sedimentation. Blood 1987;70:1572-1576.

Falke JJ, Chan SI. Molecular mechanisms of Band 3 inhibitors. 2 Channel blockers. Biochemistry 1986;25:7895-7898.

Fatkin D, Loupas T, Low J, Feneley M, Inhibition of red cell aggregation prevents spontaneous echocardiographic contrast formation in human blood, Circulation 1997;96:889-896.

Fish P. Physics and instrumentation of diagnostic medical ultrasound. Chichester, NY: John Wiley and Sons, 1990:143-164.

Fontaine I. Bertrand M, Cloutier G. A system-based approach to modeling the ultrasound signal backscattered by red blood cells. Biophys J 1999;77:2387-2399.

Hadengue A, Razavian SM, Del Pino M, Simon A. Levenson J. Influence of sialic acid on erythrocyte aggregation in hypercholesterolemia. Thromb Haemost 1996;76:944-949.

Hayakawa M, Kuzuya F. Effects of ticlopidine on erythrocyte aggregation in thrombotic disorders. Angiology 1991;42:747-753.

Johnn H, Phipps C, Gascoyne S, Hawkey C, Rampling MW. A comparison of the viscometric

properties of the blood from a wide range of mammals. Clin Hemorheol 1992;12:639-647.

Johnson PC, Dickson CS, Garrett KO, Sheppeck RA, Bentz ML. The effect of microvascular anastomosis configuration on initial platelet desposition. Plast Reconstr Surg 1993;91:522-527.

Khan MM, Puniyani RR, Huilgol NG, Hussain MA, Ranade GG.. Hemorheological profiles in cancer patients. Clin Hemorheol 1995;15:37-44.

Kim SY, Miller IF, Sigel B, Consigny PM, Justin J. Ultrasonic evaluation of erythrocyte aggregation dynamics. Biorheology 1989;26:723-736.

Kitamura H, Sigel B, Machi J. Roles of hematocrit and fibrinogen in red cell aggregation determined by ultrasonic scattering properties. Utrasound Med Biol 1995;21:827-832.

Klose HJ, Volger E, Brechtelsbauer H, Heinich L, Schmid-Schonbein H. Microrheology and light transmission of blood. I. The photometric effects of red cell aggregation and red cell orientation. Pfluegers Arch 1972;333:126-139.

Korbut RA, Madej J, Adamek-Guzik T, Korbut R. Secretory dysfunction of vascular endothelium limits the effect of angiotensin converting enzyme inhibitor quinapril on aggregation of erythrocytes in experimental hypertension. J Physiol Pharmacol 2003;54:397-408.

Ku DN, Giddens DP, Downing JM. Pulsatile flow and atherosclerosis in the human carotid bifurcation. Arteriosclerosis 1985;5:293-302.

Lacombe C, Lelievre JC. Interpretation of rheograms for assessing RBC aggregation and deformability. Clin Hemorheol 1987;7:47-61.

Lim B, Bascom PAJ, Cobbold RSC. Simulation of red blood cell aggregation in shear flow. Biorheology 1997;34:423-441

Lipowsky HH. Microvascular rheology and hemodynamics. Microcirculation 2005;12:5-15.

Lockwood GR, Ryan LK, Hunt JW, Foster FS. Measurement of the ultrasonic properties of

vascular tissues and blood from 35-65 MHz. Ultrasound Med Biol 1991;17:653-666.

Lowe GDO. Topics in preventive cardiology. The impact of fibrinogen on arterial disease. 1st edition, Lowe GDO ed., The Netherlands, Excerpta Medica, 1-32.

Lucas RJ, Twersky V. Inversion of ultrasonic scattering data for red blood cell suspensions under different flow conditions. J Acoust Soc Am 1987;82:794-799.

Mallinger F, Drikakis D. Laminar-to-turbulent transition in pulsatile flow through a stenosis. Biorheology 2002;39:437-441.

Martinez M, Vaya A, Marti R, Gil L, Lluch I, Carmena R, Aznar J. Effect of HMG-CoA reductase inhibitors on red blood cell membrane lipids and haemorheological parameters, in patients affected by familial hypercholesterolemia. Haemostasis 1996;26:171-176.

Maruvada S, Shung KK, Wang S-H. High-frequency backscatter and attenuation measurements of porcine erythrocyte suspensions between 30-90 MHz. Ultrasound Med Biol 2002;28:1081-1088.

Mittal R, Simmons SP, Udaykumar HS. Application of large-eddy simulation to the study of pulsatile flow in a modeled arterial stenosis. ASME J Biomech Eng 2001;123:325-331.

Mo LYL, Cobbold RSC. A unified approach to modeling the backscattered Doppler ultrasound form blood. IEEE Trans Biomed Eng 1992;39:450-461.

Mo LYL, Kuo IY, Shung KK, Ceresne L, Cobbold RSC. Ultrasound scattering from blood with hematocrits up to 100 %. IEEE Trans Biomed Eng 1994;41:91-95.

Murata T, Secomb TW. Effects of aggregation on the flow properties of red blood cell suspensions in narrow vertical tubes. Biorheology 1989;26:247-259.

Nam K-H, Paeng D-G, Choi MJ. Ultrasound backscattering from erythrocyte aggregation of human, horse and rat blood under rotational flow in a cylindrical chamber. J Acoust Soc Kor 2006;25:159-165.

Nash GB, Wenby RB, Sowemimo-Coker SO, Meiselman HJ. Influence of cellular properties on

red cell aggregation. Clin Hemorheol 1987;7:93-108.

Neu B, Meiselman HJ. Depletion-mediated red blood cell aggregation in polymer solutions. Biophys J 2002;83:2482-2490.

Neumann FJ, Katus HA, Hoberg E, Roebruck P, Braun M, Haupt HM, Tillmanns H, Kubler W. Increased plasma viscosity and erythrocyte aggregation: indicators of an unfavourable clinical outcome in patients with unstable angina pectoris. Br Heart J 1991;66:425-430.

Ohta K, Gotoh F, Tomita M, Tanahashi N, Kobari M, Shinohara T, Tereyama Y, Mihara B. Takeda H. Animal species differences in erythrocyte aggregability. Am J Physiol 1992;262(Heart. Circ. Physiol.):H1009-H1012.

Okumura M, Fujinaga T, Yamashita K, Tsunoda N, Mizuno S. Isolation, characterization, and quantitative analysis of ceruloplasmin from horses. Am J Vet Res 1991;52:1979-1985.

Paeng D-G, Cao P-J, Choi MJ, Shung KK. Ultrasonic backscatter response to blood flow disturbance by a severe eccentric stenosis. Key Eng Mater 2004a;270-273:2036-2041.

Paeng D-G, Cao P-J, Shung KK. Doppler power variation from porcine blood under steady and pulsatile flow. Ultrasound Med Biol 2001;27:1245-1254.

Paeng D-G, Chiao RY, Shung KK. Echogenicity variations from porcine blood I: The "bright collapsing ring" under pulsatile flow. Ultrasound Med Biol 2004b;30:45-55.

Paeng D-G, Chiao RY, Shung KK. Echogenicity variations from porcine blood II: The "bright ring" under oscillatory flow. Ultrasound Med Biol 2004c;30:815-825.

Paeng D-G, Kim BS, Choi MJ, Chiao RY, Shung KK. In vivo observation of blood echogenicity variation during a cardiac cycle on human carotid arteries. Proc IEEE Ultrason Symp 2003; 847-850.

Paeng D-G, Shung KK. Cyclic and radial variation of the doppler power from porcine whole blood. IEEE Trans Ultrason Ferroelec Freq Control 2003;50:614-622.

Poggi M, Palareti G, Biagi R, Legnani C, Parenti M, Babini AC, Baraldi L, Coccheri S.

Prolonged very low calorie diet in highly obese subjects reduces plasma viscosity and red cell aggregation but not fibrinogen. Int J Obes Relat Metab Disord 1994;18:490-496.

Popel AS, Johnson PC, Kameneva MV, Wild MA. Capacity for red blood cell aggregation is higher in athletic mammalian species than in sedentary species. J Appl Physiol 1994;77:1790-1794.

Potron G, Nguyen P, Pignon B. Fibrinogen, arterial risk factor, in clinical practice. Clin Hemorheol 1994;14:739-767.

Puniyani RR, Ajmani R, Kale PA. Risk factors evaluation in some cardiovascular diseases. J Biomed Eng 1991;13:441-443.

Rampling MW, Meiselman HJ, Neu B, Baskurt OK. Influence of cell-specific factors on red blood cell aggregation. Biorheology 2004;41:91-112.

Rampling MW, Whittingstall P, Linderkamp O. The effects of fibrinogen and its plasmin degradation products on the rheology of erythrocyte suspensions. Clin Hemorheol 1984;4:533-543.

Rastegar R, Harnick DJ, Weidemann P, Fuster V, Coller B, Badimon JJ, Chesebro J, Goldman ME. Spontaneous echo contrast videodensity is flow-related and is dependent on the relative concentrations of fibrinogen and red blood cells. J Am Coll Cardiol 2003;41:603-610.

Razavian SM, Del Pino M, Simon A. Levenson J. Increase in erythrocyte disaggregation shear stress in hypertension. Hypertension 1992;20:247-252.

Roelofsen B, Van Meer G, Op Den Kamp JAF. The lipids of red cell membranes. Scand J Clin Lab Invest 1981;41:111-115.

Samsel RW, Perelson AS. Kinetics of rouleau formation. II. Reversible reactions. Biophys J 1984;45:805-824.

Schmid-Schobein H. Volger E. Red-cell aggregation and red-cell deformability in diabetes.

Diabetes 1976;25:897-902.

Schneck DJ. On the development of a rheological constitutive equation for whole blood. College Eng Virginia Polytechnic Institute (Technical Report Number VPI-E-88-14) 1-17.

Shehada REN, Cobbold RSC, Mo LYL. Aggregation effects in whole blood: Influence of time and shear rate measured using ultrasound. Biorheology 1994;31:115-135.

Shiga T, Imaizumi K, Harada N, Sekiya M. Kinetics of rouleaux formation using TV image analyzer. I. Human erythrocytes. Am J Physiol 1983;245:H252-H258.

Shung KK, Cloutier G, Lim CC. The effects of hematocrit, shear rate, and turbulence on ultrasonic Doppler spectrum from blood. IEEE Trans Biomed Eng 1992;39:462-469.

Shung KK, Paeng D-G. Ultrasound: an unexplored tool for blood flow visualization and hemodynamic measurements. Jpn J Appl Phys 2003;42:2901-2908.

Shung KK, Siegelmann RA, Reid JM. Ultrasonic scattering by blood. IEEE Trans Biomedi Eng 1976;23:460-467.

Shung KK, Thieme GA. Ultrasonic scattering in biological tissues. CRC Press, Boca Raton, Ann Arbor, London, Tokyo. 1993.

Shung KK, Yuan YW, Fei DY, Tarbell JM. Effect of flow disturbance on ultrasonic backscatter from blood. J Acoust Soc Am 1984;75:1265-1272.

Sigel B, Coelho JCU, Spigos DG, Flanigan DP, Schuler JJ, Kasprisin D, Nyhus LM, Capek V. Ultrasonography of blood during stasis and coagulation. Invest Radiol 1981;16:71-76.

Sigel B, Machi J, Beitler JC, Justin JR. Red cell aggregation as a cause of blood-flow echogenicity. Radiology 1983;148:799-802.

Soutani M, Suzuki Y, Tateishi N, Maeda N. Quantitative evaluation of flow dynamics of erythrocytes in microvessels: influence of erythrocyte aggregation. Am J Physiol 1995;268:H1959-H1965.

Stein PD, Sabbah HN. Measured turbulence and its effect on thrombus formation. Circ Res

1974;35:608-614.

Twersky V. Acoustical bulk parameters in distributions of pair-correlated scatterers. J Acoust Soc Am 1978;64:1710-1719.

Twersky V. Low-frequency scattering by correlated distributions of randomly oriented particles. J Acoust Soc Am 1987;81:1609-1618.

Twersky V. Transparency of pair-correlated, random distributions of small scatterers, with applications of the cornea. J Opt Soc Am 1975;64:524-530.

Van Oss CJ, Arnold K, Coakley WT. Depletion flocculation and depletion stabilization of erythrocytes. Cell Biophys 1990;17:1-10.

Wang SH, Shung KK. In vivo measurements of ultrasonic backscattering in blood. IEEE Trans Ultrason Ferroelet Freq Contr 2001;48:425-431.

Weng X, Cloutier G, Beaulieu R, Roederer GO. Influence of acute-phase proteins on erythrocyte aggregation. Am J Physiol 1996a;271:H2346-H2352.

Weng X, Cloutier G, Pibarot P, Durand L-G. Comparison and simulation of different levels of erythrocyte aggregation with pig, horse, sheep, calf, and normal human blood. Biorheology 1996b;33:365-377.

Windberger U, Bartholovitsch A, Plasenzotti R, Korak KJ, Heinze G. Whole blood viscosity, plasma viscosity and erythrocyte aggregation in nine mammalian species: reference values and comparison of data. Exp Physiol 2003;88:431-440.

Womersley JR. Method for the calculation of velocity, rate of flow and viscous drag in arteries when the pressure gradient is known. J physiol 1955;127:553-563.

Yellin EL. Laminar-turbulent transition process in pulsatile flow. Circ Res 1966;19:791-804.

Yuan YW, Shung KK. Echogenicity of whole blood. J Ultrasound Med 1989;8:425-434.

Yuan YW, Shung KK. Ultrasonic backscatter from flowing whole blood I: dependence on shear rate and hematocrit. J Acoust Soc Am 1988a;84:52-58.

Yuan YW, Shung KK. Ultrasonic backscatter from flowing whole blood II: dependence on frequency and fibrinogen concentration. J Acoust Soc Am 1988b;84:1195-1200.

Zilberman L, Roqowski O, Rozenblat M, Shapira I, Serov J, Halpern P, Dotan I, Arber N, Berliner S. Inflammation-related erythrocyte aggregation in patients with inflammatory bowel disease. Dig Dis Sci 2005;50:677-683.

APPENDIX

Calculation of Flow Parameters

Reynolds number (*Re*) and Womersley number (α) are defined as following,

$$R_e = \frac{2a\rho V}{\mu}$$

$$\alpha = a\left(\frac{\omega}{\nu}\right)^{\frac{1}{2}},$$

where μ is the coefficient of viscosity of the fluid, a is the internal radius of the tube, ρ is the density of the fluid, V is the mean velocity of flow, and ω is the angular frequency. μ/ρ is called kinematic viscosity, and is designated by ν.

The flow velocity (V) and flow rate (Q) can be solved by,

$$V(t,r) = \mathrm{Re}\left\{\frac{-ja^2A}{\mu\alpha^2}\left[1-\frac{J_0(j^{3/2}\alpha\frac{r}{a})}{J_0(j^{3/2}\alpha)}\right]e^{j\omega t}\right\}$$

$$Q(t) = \mathrm{Re}\left\{\frac{-j\pi a^2A}{\omega\rho}\left[1-\frac{2J_1(j^{3/2}\alpha)}{j^{3/2}\alpha J_0(j^{3/2}\alpha)}\right]e^{j\omega t}\right\},$$

where J_0 and J_1 are the Bessel functions of order zero and one, respectively. Re is the real part of complex number.

SUMMARY (in KOREAN)

혈액에 의한 초음파 산란은 적혈구에 의해서 주로 일어나며 적혈구 응집은 혈액으로부터의 후방산란을 증가시키는 주된 요인으로 알려져 있다. 본 논문에서는 협착을 부착한 인공 혈액 순환계와 회전 흐름계를 이용하여 초음파 후방산란에 미치는 혈류역학과 적혈구 용적비율의 영향을 연구하였다.

박동 흐름 하에서 적혈구 응집현상은 비틀림율, 난류 그리고 가속과 같은 혈류역학적인 파라메타에 크게 의존하는 것으로 알려져 있다. 인공 혈액 순환계에 편심협착을 제작하여 부착하고 돼지 혈액을 이용하여 적혈구 응집과 초음파 반향에 미치는 이들 세가지 파라메타의 영향을 GE LOGIQ 700 장비를 이용하여 측정하였다. 수축기의 혈류가 가속하는 시기에 편심협착의 하류에서 고반향성의 포물선 모양이 관찰되었으며 이는 혈류의 가속에 의해서 적혈구 룰로가 유발될 수 있다는 가설에 대한 좋은 증거라고 할 수 있다. 협착 하류에서의 블랙홀 현상과 국소적인 초음파 반향 증가는 난류와 비틀림율의 복합적인 효과에 기인하는 것으로 여겨진다. 한편, 편심협착의 상류에서도 혈류의 교란에 의한 초음파 반향과 적혈구 룰로의 변화가 관찰되었다. 이완기에 튜브의 종단면으로 고반향성의 포물선 모양과 와류 현상이, 횡단면으로는 백색환 현상으로 관찰되었다. 이러한 영상은 이미지 편집 프로그램을 통하여 삼차원 동영상으로 재구성할 수 있었으며 그 결과 박동 흐름 시 편심협착 상류에서 적혈구 룰로의 동적인 변화를 잘 보여줄 수 있었다.

혈액을 담은 원통형 용기 내에서 자석교반기를 이용하여 혈액의 흐름을 제어하였고 이를 이용하여 사람, 말, 그리고 흰쥐 혈액에서의 적혈구 응집을 연구하였다. 혈액으로부터의 초음파 후방산란 파워는 5 MHz 집속형 초음파 변환기에 펄스를 가하고 되돌아온 반향 신호를 측정하여 계산하였다. 실험결과, 이들 포유류 중에서 적혈구 응집 경향이 말에서 가장 크고, 사람이 중간, 그리고 흰쥐에서 가장 낮게 측정되었다. 사람과 말 혈액에서의 초음파 후방산란은 자석교반기의 회전 속도 증가에 따라 감소하였으나, 흰쥐의 혈액에서는 어떠한 변화도 관찰되지 않았다. 갑작스럽게 혈액의 흐름을 멈추었을 때, 사람과 말

혈액으로부터의 후방산란 파워는 서서히 증가하는 경향을 보였다. 그러나 흰쥐 혈액에서는 이러한 응집 경향이 보이지 않았다. 반향 신호에 포락선을 적용한 이미지는 원통형 용기 내에서의 적혈구 응집의 시간적인 변화와 지름 방향의 공간적인 변화를 잘 보여주었다. 포유동물 종의 차이에 따른 이러한 연구는 적혈구 응집의 기전을 이해하는데 유용하리라고 사료된다.

혈장 또는 PVP 360 용액 내의 흰쥐 적혈구에 의한 초음파의 반향을 적혈구 용적비율과 비틀림율을 변화시켜가면서 측정하였다. 흰쥐 혈액으로부터의 후방산란 변화는 흰쥐 혈액 내에서 적혈구의 낮은 응집력 때문에 측정하는데 한계가 있었다. 적혈구의 응집 정도를 증가시키기 위해서 흰쥐 혈장을 PVP 360 용액으로 대체하여 실험하였다. 회전 흐름 하에서 후방산란은 급속히 증가하여 30 초 이내에 정상상태에 도달하였다. 정상상태에서의 평균 후방산란 파워는 적혈구 용적비율 10 - 40 % 사이에서 비례하여 증가하였다. 그러나 흐름을 갑작스럽게 멈춘 경우에 후방산란 파워는 최고치까지 서서히 증가하였고, 증가 속도는 적혈구 용적비율과 비선형적인 관계를 보였다. 간단한 흐름 장치와 응집을 유발하는 혈장 대체물을 이용한 소량의 적혈구 시료를 이용하여 적혈구 응집에 대한 적혈구 용적비율과 비틀림율 의존성을 잘 설명할 수 있었다.

끝으로, 위에서 제안한 간편한 방법이 적혈구 응집에 미치는 약물의 영향을 연구하기에 적절한 연구법임을 제안하였다. 전혈을 대신하여 PVP 360 용액에 흰쥐 적혈구를 현탁시켜서 적혈구 용적비율을 10 %로 만들고 이를 이용하여 실험하였다. 적혈구 응집 저해제를 적용했을 때, 정체 시와 흐르는 혈액 모두에서 용량의존적인 응집 저해를 보였다. 이러한 결과는 본 연구에서 제안한 적혈구 응집 측정 방법이 약물과 적혈구 응집의 상관관계를 연구하는데 유용하다는 것을 보여주며, 또한, 적혈구 응집의 병태생리학적인 역할과 발생기전을 밝히는데 도움을 줄 수 있으리라고 사료된다.

Key words: 적혈구 응집, 혈류 가속, 난류, 적혈구 용적율, 비틀림율, 초음파 후방산란.

ACKNOWLEDGEMENTS (in KOREAN)

감사의 글

조그마한 결실이지만 마무리하는 시점에서 되돌아보니 참으로 많은 분들께서 도움을 주셨습니다. 부족하나마 감사의 글로써 마음을 전합니다.

학위과정 시작에서부터 지금에 이르기까지 학문의 방향을 깨우쳐 주시고 성심껏 지도해 주신 팽동국 교수님의 끊임없는 관심과 커다란 가르침에 무한한 감사를 드립니다. 격려와 조언을 아끼지 않으셨고 연구에 정진할 수 있도록 나아갈 길을 밝혀 주신 최민주 교수님께 머리 숙여 감사를 올립니다. 바쁘신 중에도 본 논문을 세심하고 정성스럽게 심사해 주신 이광만 교수님, 박전홍 교수님, 김영리 교수님께 감사 드립니다. 아울러 연구에 정진할 수 있도록 배려해주신 약리학 교실의 강희경 교수님과 유은숙 교수님, 그리고 해양과학대학의 조일형 교수님, 이종현 교수님, 김준영 교수님께 감사를 표합니다.

해양정보시스템 연구실의 복태훈, 고혁준, 변승우, 한정희, 김정훈, 구태희, 잉, 마노 그리고 의공학 연구실의 강관석, 레디 모두에게 특별한 고마움을 전하며 원하는 일들을 꼭 이루기를 기원합니다. 약리학 연구실의 살림을 이끌어 가며 바쁜 중에도 여러모로 도움을 준 이혜자, 강경진 외에 대학원생들께도 고마움을 전합니다.

의공학 협동과정의 이경성 교수님, 박경규 선생님, 홍인실 선생님, 양정화 선생님, 김진아 선생님, 문상돈 선생님, 문일남 선생님께 감사의 마음을 전하며 좋은 결실 맺기를 기원합니다.

마지막으로 철없는 늦깎이 학생을 헌신적으로 뒷바라지해주고 또한 연구의 토론 상대자가 되어주었던 아내 유은숙과 나의 아들 우준이에게 사랑하는 마음을 전하며 이 논문을 바칩니다.